

Tuning Particle Interactions Using Tethered Ligands and Receptors

By

NATHAN WILLIAM MOORE

B.S. Chemical Engineering (University of Washington, Seattle) 2002

B.S. Technical Communication (University of Washington, Seattle) 2002

DISSERTATION

Submitted in partial satisfaction of the requirements for the degree of

DOCTOR OF PHILOSOPHY

in

Chemical Engineering

in the

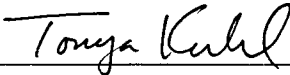
OFFICE OF GRADUATE STUDIES

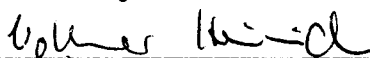
of the

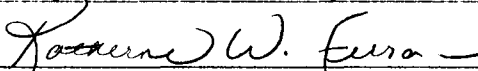
UNIVERSITY OF CALIFORNIA

DAVIS

Approved:







Committee in Charge

2006

UMI Number: 3250837

INFORMATION TO USERS

The quality of this reproduction is dependent upon the quality of the copy submitted. Broken or indistinct print, colored or poor quality illustrations and photographs, print bleed-through, substandard margins, and improper alignment can adversely affect reproduction.

In the unlikely event that the author did not send a complete manuscript and there are missing pages, these will be noted. Also, if unauthorized copyright material had to be removed, a note will indicate the deletion.

UMI[®]

UMI Microform 3250837

Copyright 2007 by ProQuest Information and Learning Company.

All rights reserved. This microform edition is protected against unauthorized copying under Title 17, United States Code.

ProQuest Information and Learning Company
300 North Zeeb Road
P.O. Box 1346
Ann Arbor, MI 48106-1346

Contents

Front Matter

Abstract	v
Figures	vi
Tables	viii
Publications	ix
Curriculum vitae	x
Acknowledgements	xiv

Overview 1

Chapter 1: The Role Of Flexible Tethers In Multiple Ligand-Receptor Bond Formation between Curved Surfaces 2

1.1 Abstract	2
1.2 Introduction	3
1.3 Single Bond Formation: Critical Binding Ranges	5
1.4 Multiple Bond Formation at Curved Interfaces	12
1.5 Bridging Dynamics and Surface Approach	16
1.6 Methods for Evaluating the Analytical Solutions	19
1.6.1 Independent Numerical Solutions	19
1.6.2 Experimental Measurements	20
1.7 Results & Discussion	24
1.7.1 Experimental Validation	24
1.7.2 Scaling Behavior of The Bridging Force	28
1.7.3 The Model as a Predictive Tool for Drug Targeting	32
1.8 Conclusions	34
1.9 Appendix 1-A: Bridging Angle Inconsequential to Normal Force	35
1.10 Appendix 1-B: Exact Analytical Solution for the Bridging Force Validates Scaling Behavior	36
1.11 Acknowledgements	37
1.12 References & Footnotes	38

Chapter 2: Bimodal Polymer Mushrooms: Compressive Forces and Specificity toward Receptor Surfaces 45

2.1 Abstract	45
2.2 Introduction	46
2.3 Materials	48
2.4 Methods	49

2.4.1	<i>Bimodal Architectures</i>	49
2.4.2	<i>Substrate Preparation</i>	51
2.4.3	<i>Receptor Architecture</i>	52
2.4.4	<i>Force-Distance Measurements</i>	53
2.4.5	<i>Capture Distance Measurements</i>	54
2.4.6	<i>Statistical Methods</i>	55
2.4.7	<i>Flow Adhesion Assay</i>	56
2.5	Results and Discussion	57
2.6	Conclusions	67
2.7	Acknowledgements	68
2.8	References & Footnotes	68

Chapter 3: Weak Ligand-Receptor Interactions Probed with an Automated Surface

	Forces Apparatus	72
3.1	Abstract	72
3.2	Introduction	73
3.3	Methods	75
3.3.1	<i>Materials</i>	75
3.3.2	<i>Preparation of Functionalized Bilayers</i>	75
3.3.3	<i>Computer-assisted Force-Distance Measurements</i>	78
3.3.4	<i>Statistical Methods</i>	82
3.4	Results and Discussion	82
3.4.1	<i>Force-Distance Profiles</i>	82
3.4.2	<i>Bond Rupture Forces</i>	86
3.4.3	<i>Repeated Compression and Withdrawal</i>	90
3.4.4	<i>Extraction of Bridging Forces from the Force Profiles</i>	95
3.4.5	<i>Thermodynamic Model for the Bridging Force</i>	97
3.4.6	<i>Kinetic Model for the Bridging Force</i>	102
3.5	Conclusions	111
3.5	Appendix 3-A: Survey of Ligand-Receptor Bond Energies and Molecules Selected for Force Spectroscopy	112
3.6	Appendix 3-B: Analytical Solution For the Capture Distance	115
3.7	Appendix 3-C: Measuring Interaction Radii with a CCD	115
3.8	Appendix 3-D: Analytical Solutions for Jump Out Distance	116
3.9	Appendix 3-E: Polydispersity Effects	118
3.10	Acknowledgements	121
3.11	References	121

Chapter 4: Synthesis of a Reversible Streptavidin Binder for Biomimetic Assemblies
129

4.1 Abstract	129
4.2 Introduction	129
4.3 Materials	131
4.4 Synthesis of HABA-PEG-DSPE 10	132
4.4.1 <i>Organic-Phase Synthesis</i>	133
4.4.2 <i>Aqueous-Phase Synthesis</i>	134
4.5 Characterization	134
4.5.1 <i>MALDI</i>	134
4.5.2 <i>¹H-NMR</i>	135
4.5.3 <i>Absorption Spectroscopy</i>	135
4.5.4 <i>Vesicle Preparation</i>	136
4.6 Results & Discussion	136
4.7 Conclusions	141
4.8 Acknowledgments	142
4.9 References	142

Abstract

Ligands mounted to particle surfaces via flexible tethers represent a growing class of molecules used to engineer adhesion in biosensing, drug targeting, and self-assembling nanostructures. In this work we show that the combination of lock-and-key specificity and the tether dynamics cooperate to allow the interaction between a tethered ligand and receptor to be easily tuned. In this way, the adhesion between surfaces decorated by herein-called “entropical forests” can be described by a set of practical, back-of-the-envelope relations that accurately predict the rate, range, and strength of adhesion. Over a wide parameter space, the relations agree well with direct measurements of the attractive cross-bridging forces and the repulsive polymer steric forces when strongly-binding biotin/streptavidin is used as a model ligand-receptor pair in the Surface Forces Apparatus. A more general theoretical framework is also developed to relate key properties of single tethered ligand-receptor interactions to multiple bond formation between curved surfaces in both static and dynamic conditions. This framework, along with the development of a high-resolution, automated Surface Forces Apparatus, has enabled some of the first direct force measurements of the decohesion of a low-affinity ligand-receptor bond. These results provide rare information on the kinetics of tethered ligand-receptor interactions. Implications are presented for the design of targeted drug carriers and self-assembling nanostructures, as well as for understanding bridging forces in colloidal and biological systems.

Figures

<u>#</u>	<u>Page</u>	<u>Abbreviated caption</u>
1-1	3	Depiction of two particles bridged by tethered ligand / receptor bonds.
1-2	7	Probability of a single PEG ₂₀₀₀ tether binding as a function of its extension for various ligand-receptor bond energies.
1-3	25	Comparison of <i>a priori</i> predictions of the maximum expected bridging force and measurements with the Surface Forces Apparatus for biotin/streptavidin ligand/receptors mounted on two tether lengths.
1-4	28	Dynamic approach of surfaces bound by PEG ₂₀₀₀ tethers.
1-5	29	Maximum bridging force between approaching surfaces decorated with ligated PEG ₂₀₀₀ as a function of the surface separation.
1-6	32	Effect of surface curvature on the force between two surfaces bridged by tethered ligand/receptors.
1-7	33	Examples of tuning the interaction profile to optimize adhesion for drug targeting or nanoassembly.
2-1	52	Schematic of the experiments in the SFA and chemical structures of PEG-lipids used in these studies.
2-2	58	Examples of force vs. distance profiles for a bimodal mixture of grafted PEG ligated with biotin interacting with a streptavidin-coated membrane.
2-3	59	Example of a force vs. distance profile for the compression of a non-ligated, bimodal mixture of grafted PEG interacting with a streptavidin-coated membrane.
2-4	60	Compression of the bimodal polymer mixture compared to the monomodal mixture after subtraction of electrostatic repulsion.
3-1	77	Schematic of the experiments in the SFA and chemical structure of the HABA-PEG-DSPE conjugate.
3-2	83	Example force profiles measured during surface approach.
3-3	85	Example force profiles measured during surface withdrawal.

3-4	91	Measured decohesion force as a function of the number of times surfaces had contacted.
3-5	94	Example fit to the force measured during surface approach as a function of the cycle number.
3-6	97	Bridging forces extracted from the force profiles.
3-7	100	Hypothesized tether configurations.
3-8	107	Probability of a single tether forming a cross-bridge.
3-9	109	Kinetic parameters of the tethered HABA-streptavidin interactions.
3-10	114	Distribution of biologically occurring ligand-receptor bond energies.
3-11	119	Ensemble-averaged probability of cross-bridge formation between plane-parallel interfaces bearing PEG-ligand / receptor architectures for various levels of polydispersity.
3-12	120	Ensemble-averaged bridging force for monodisperse and polydisperse PEG2000 tethers wielding HABA.
4-1s*	133	Reaction mechanism and pathways used for organic phase synthesis.
4-1	138	MALDI spectra of products separated from organic (A) and aqueous (B) syntheses of HABA-PEG-DSPE 11.
4-2	139	600 MHz ¹ H 2D DQF-COSY spectra of the aromatic/NH region of the reactants and products.
4-3	141	Fluorescence micrographs of vesicles functionalized with the sterically stabilizing HABA conjugate.

* scheme

Tables

<u>#</u>	<u>Page</u>	<u>Abbreviated caption</u>
1-1	10	Some ligands and receptors of interest for drug targeting and other biophysical research.
1-2	11	Some tethers of interest for drug targeting and other biophysical research.
1-3	23	Parameters used in calculating numerical results.
1-4	27	Measured and predicted ensemble capture distances and predicted single-tether binding ranges for PEG tethers of different lengths.
2-1	50	Properties of the PEG chains studied.
2-2	50	Molar compositions of the polymer-anchoring lipid leaflets.
2-3	62	Parameters fit to eq.2-1 for compression of the non-ligated polymer layers.
2-4	64	Measured properties of bond formation and rupture for the biotinylated architectures.
3-1	78	Procedural Parameters used in the SFA studies.
3-2	105	Predicted lifetimes of bonds stressed by PEG2000 tethers.
3-3	113	Selected ligands and receptors studied with Dynamic Force Spectroscopy and associated dissociation constants and bond energies.

Publications

- Moore, N.W. and T.L. Kuhl. *The Role of Flexible Tethers in Multiple Ligand-Receptor Bond Formation between Curved Surfaces*. 2006. *Biophys. J.*, 91(5):1675–1687.
- Moore, N.W. and T.L. Kuhl. *Bimodal Polymer Brushes: Compression and Specificity towards Receptor Surfaces*. 2006. *Langmuir*, In press.
- Moore, N.W. and T.L. Kuhl. *Weak Ligand-Receptor Interactions Probed with an Automated Surface Forces Apparatus*. In preparation.
- Moore, N.W., A.D. Delacruz, K.S. Lancaster, T. Diekmann, and T.L.Kuhl. *Synthesis of a Reversible Streptavidin Binder for Biomimetic Assemblies*. Submitted to *Aus. J. Chem.*
- Moore, N.W. and T.L. Kuhl. *Controlled Self-Assembly*. In *CRC Materials Processing Handbook*. J.R. Groza, J.F. Shackelford, E.J. Lavernia, and M.T. Powers, eds. CRC Press, Boca Raton., In press.
- Barber, S.M, P.J. Costanzo, N.W. Moore, T.E. Patten, K.S. Lancaster, C.B. Lebrilla, and T.L. Kuhl. *Bilateral, Difunctional Nanosphere Aggregates and Their Assembly Mediated by Polymer Chains*. 2006. *J.Phys.Chem.A*, 110(13), 4538–4542.

Curriculum vitae

Honors & Awards

- 2006. UC Davis Summer Graduate Student Research Award, Engineering
- 2004. Fellow, Professors for the Future, UC Davis
- 2004. UC Davis Summer Graduate Student Research Award, Engineering
- 2004. Citizen of the Year, Department of Chemical Engineering, UC Davis
- 2002. Distinction in Chemical Engineering, University of Washington
- 2001. Lee Prock Award in Technical Communication
- 2001. DOE Energy Research Undergraduate Laboratory Fellowship (ERULF)
- 2001. NSF Award for Success in Computer Science, Engineering, and Mathematics
- 2000. NSF Award for Success in Computer Science, Engineering, and Mathematics

Invited Seminars

Tuning Particle Interactions Using Tethered Ligands: From the Nanoscale to the Bioscale and Beyond—Pacific Northwest National Laboratory, Richland, WA, Aug. 24, 2005.

Engineering Adhesion Using Tethered Ligands. Dept. of Chemistry, Univ. of Washington, July 16th, 2004.

Presentations & Posters

Moore, N.W. and T.L. Kuhl. *A Model for Polymer Functionalization of Drug Delivery Vehicles: Maximizing Adhesion While Confronting Endothelial Glycocalyx*—AIChE National Meeting (Biomimetics II: Drug Delivery), San Francisco, Nov.16, 2006.

Moore, N.W. and T.L. Kuhl. *Discrete Binding Ranges of Ligated Biopolymers End-Grafted to an Interface: A Theoretical Study*—AIChE National Meeting (Biological Polymers), San Francisco, Nov.13, 2006.

Moore, N.W. and T.L. Kuhl. *Colloidal Bridging Forces from Multiple Tethered Ligand-Receptor Bonds*—AIChE National Meeting (Biomolecules at Interfaces IV), San Francisco, Nov.16, 2006.

Moore, N.W. and T.L. Kuhl. *Tuning Adhesion Using Tethered Ligand/Receptor Architectures*—ACS National Conference, Colloids & Interfaces, Membranes at Interfaces, San Francisco, Sept.13, 2006.

Engineering Interparticle Adhesion Using Tethered Ligand-Receptor Interactions—poster & presentation, NSF Engineering Research Center for Particle Science and Technology at the University of Florida, Gainesville, Jan.29, 2005.

Effect of Chain Architecture on Multiple Ligand-Bond Formation—poster presented at California Institute for Quantitative Biomedical Research, May 7, 2005, and AIChE National Conference, San Francisco Hilton, Nov. 2003.

Ink Drop Coalescence: Making Faster Inkjet Printers—presented at AIChE, Puget Sound Chapter, May 8, 2001.

Chernobyl & Nuclear Energy—presented to over 40 high school classes in Washington State through the UW Science Outreach Program, 1998–2000.

Undergraduate Projects Mentored

“Design of a Parallel Plate Flow Chamber for Characterization of Biomimetic Architectures.” Tammy Chan and Eunis Ngor., Jan.–June 2006.

“Statistical Analysis of Functionalized Particles Sheared Under Flow.” Bertha Kuo, Sept.2005–present.

“A FECO Modeling Tool for the Surface Forces Apparatus.” Kaki Cheung (co-supervised w/ J. Southworth and D. Mulder), Jan. 2004–June 2005.

“Adhesion of Functionalized Particles to Tethered Ligands Under Shear Flow.” Danny Nou, Sept. 2004–Aug. 2005.

“Synthesis and Characterization of Biotin Analogs with Lipopolymers.” Anthony Delacruz, June 2004–June 2005.

Preparation of Giant Unilamellar Vesicles Biofunctionalized with PEG Tethers and Characterization of Binding Specificity Under Flow.” Melodi King, June–Sept. 2004.

“Compression of PEG-PS Block Copolymers at the Air-Water Interface.” Momena Shemsu, May–Sept. 2004.

“A Simple Method for Producing Anisotropic Colloidal Particles.” Emily Conley, June–Sept. 2003.

Undergraduate Research Performed

"Equilibrium Surface Tension of Dyes Used in Inkjet Printers" with Prof. John C. Berg, Interfacial & Colloid Science Research Group, University of Washington Department of Chemical Engineering, Seattle, WA, 2000–2001.

"Encapsulation of Ammonium Nitrate and other Volatile Aerosols" with Dr. James Cowin, Chemical Structure & Dynamics Group, Environmental Molecular Sciences Laboratory, Pacific Northwest National Laboratory, Richland, WA, 2001.

“Teaching Mental Math to the Learning Disabled” with Elizabeth Haughton, Director, Haughton Learning Center, 1999–2002.

“Seismic Hazards Investigation in Puget Sound” with Professor Kenneth C. Creager, University of Washington Department of Geophysics, 1998.

Professional Activities

Attendee, Physics of Cellular Objects, Summer School in Cargese, France, Aug.12–28, 2006.

Attendee, Particle Science Winter School, NSF Engineering Research Center for Particle Science and Technology at the University of Florida, Gainesville, 2005.

Fellow, UC Davis Professors for the Future program, 2004–5.

President, Departmental Graduate Student Organization, 2004–5.

Mentor, McNair Scholars Program, UC Davis, 2003–4.

Representative, UC Davis Graduate Student Association, 2003–4.

Coordinated 7-seminar series on professional development for graduate students in the UC Davis College of Engineering, sponsored by the Department of Chemical Engineering & Materials Science, 2003–4.

Editor-in-Chief for Postcomm alumni magazine, published by the Univ. of Washington Department of Technical Communication, 2002.

Lecturer on Nuclear Engineering (presented to over 40 high school classes) and trainer for the Science Outreach Program, University of Washington, 1998–2000.

Member, American Institute of Chemical Engineers, since 1999.

Member, Biophysical Society, since 2005.

Instructional Workshops Delivered

Designing Effective Illustrations. UC Davis, April 28, 2005.

Designing Documents for Clarity and Visual Appeal. UC Davis, May 19, 2005.

Designing Effective Graphs. UC Davis, April 28, 2005.

Seminars Organized

Designing Effective Visuals—a series organized for the UC Davis Office of Graduate Studies, Spring 2005.

Fuel Cells: Laptops 2005--Autos 20??—Dr. Karl Kukkonen, UC Davis, 10/25/04.

The Engineer’s Guide to Writing—Kate Swoboda, UC Davis, 3/3/04.

Reading Scientific Papers Efficiently—Brian Higgins, UC Davis, Feb. 4, 2003.

Getting the Most Out of Grad School—Tonya Kuhl, UC Davis, 1/7/04.

Writing Your First Paper—Bruce Gates, UC Davis, 11/21/03.

Finding a Job After Grad School—Kathi Shull, et al, UC Davis, 11/03.

Choosing a Research Advisor—Panel discussion moderated by Nathan Moore, with Brian Higgins, Alan Jackman, and Tonya Kuhl, UC Davis, 10/13/03.

Teaching Experience

TA for Chemical Engineering Laboratory, UC Davis, Fall 2005.

TA for Mathematical Methods in Chemical Engineering, UC Davis, Fall 2004.

Certificate of Completion: UC Davis Seminar in College Teaching (20 hrs.)

Invited Lectures

An Introduction to the Surface Forces Apparatus. Dept. of Chemical Engineering & Materials Science, UC Davis, April 19th, 2006.

Designing Effective Tables & Graphs. School of Veterinary Medicine, UC Davis, Nov. 14th, 2005.

An Introduction to Error Analysis for Chemical Engineers. Dept. of Chemical Engineering & Materials Science, UC Davis, Oct. 4th, 2005.

Curriculum

Moore, N.W. *Designing Effective Visuals: A Guide for Graduate Students*. 51 pgs. 2005. Available online at <http://www.lulu.com/visuals>

Moore, N.W. *A Teacher's Guide to Mental Math* (2002), incl. four modules: *Subtraction* (2002), *Multiplication* (2001), *Addition* (2000), and *Place Value* (2000). Napa, CA: The Haughton Learning Center.

Science Journalism

Moore, Nathan. The Secret Life of Rocks: Scientists Find Life in the Hardest Places on Earth. *Northwest Science & Technology*, March 2003, p.47–50.

Moore, Nathan. PNNL Scientists Sniff Out the Source of Ozone. *Northwest Science & Technology*, April 2002, p.10.

Moore, Nathan. UO Professors Raise a Bumper Crop of Environmental Scientists. *Northwest Science & Technology*, September 2002, p.12–13.

Derelict Gear Removal in Puget Sound—fact sheet used by multiple Federal and Washington State agencies. Published by the Northwest Straits Marine Conservation Commission, 2002.

Acknowledgements

I wish to thank my committee, and especially my dissertation advisor, Dr. Tonya L. Kuhl, for their commitment to graduate education. Of my advisor I am particularly grateful for having been granted generous financial resources and intellectual freedom to pursue cutting edge science while developing professionally. Others who have graciously offered their mentorship include John C. Berg, James P. Cowin, and Elizabeth Haughton.

Those who have donated significant time towards this work are respectfully acknowledged through co-authorship of separate publications or at the end of each chapter. Though, I cannot thank enough Dennis J. Mulder for generously sharing his time in constructing and repairing electronics and in our collaboration to automate the Surface Forces Apparatus, and Carlos Marques for inspiring continuation of this work during my visit to the University of Strasbourg.

For financial support I wish to thank the National Science Foundation (Grants DMR-0606564 and NER DMII-0404457), the France-Berkeley Fund, the UC Davis Office of Graduate Studies, and the Professors for the Future program administered by the latter.

Last, many family and friends have provided wonderful personal support. I particularly wish to thank Chris Kuperstein for encouraging me to study technical communication at the University of Washington, the many Sacramento theater musicians for working with me “in the pit” during intense periods of this research, Joab Maldonado for co-establishing the NJ7 Art Centre in Davis, and those unnamed individuals who have provided generous financial gifts during my post-graduate education.

*Para Susan Redenbaugh,
por su amistad y amor.*

Overview

Chapter 1 develops a thermodynamic framework for predicting the strength, range, and rate of adhesion between particles bridged by many tethered ligands and receptors, and presents experimental justification for the scaling relations derived. By comparing direct force measurements of tethered ligand-receptor architectures of varying polymer composition, **Chapter 2** shows that the specific bridging and steric forces are uncorrelated in the parameter regime relative to drug targeting. Also presented are implications for the design of targeted liposomes and other particles conjoined by tethered ligands and receptors. **Chapter 3** presents rare direct force measurements of a weakly-binding ligand receptor pair. For this work, an automated Surface Forces Apparatus was constructed to enable high-resolution measurement. Additional theory is developed to relate these measurements to those presented in Chapters 1 and 2 and to explain the roles of tether polydispersity and lipid-membrane “bond” strength on the surface adhesion. **Chapter 4** provides a more complete record of the methods used in Chapter 3 but is otherwise not pivotal to the dissertation. Specifically, it describes the synthesis and characterization of a novel lipolymer-tethered ligand that binds to streptavidin with an affinity that more closely resembles that of biological ligands and receptors, which was used for the experiments reported in Chapter 3.

In all chapters, references to cited works and appendices refer to those listed at the end of each chapter.

Chapter 1: The Role Of Flexible Tethers In Multiple Ligand-Receptor Bond Formation between Curved Surfaces

Reproduced with permission from Moore, N.W. and T.L. Kuhl. The Role of Flexible Tethers in Multiple Ligand-Receptor Bond Formation between Curved Surfaces. 2006. Biophys. J., 91(5):1675–1687.. Copyright 2006 The Biophysical Society.

1.1 Abstract

Ligands mounted to surfaces via extensible tethers are present in nature and represent a growing class of molecules used to engineer adhesion in drug targeting, biosensing, self-assembling nanostructures, and in other biophysical research. Using a continuum approach with geometric and thermodynamic arguments we derive a number of analytical expressions that relate key properties of single tethered ligand / receptor interactions to multiple bond formation between curved surfaces. The theoretical predictions are in good agreement with measurements made with the Surface Forces Apparatus (SFA). We establish that, when ligated, many tethers commonly used in biophysical research exhibit a discrete binding range that can be accurately measured with force spectroscopy. The distribution of bound ligated tethers is independent of the surfaces' interaction radius, R . The bridging force scales linearly with R , the tether's effective spring constant and grafting density, and with the ligand-receptor bond energy when the surfaces are in direct contact. These results are contrasted to bridging forces that evolve between plane-parallel geometries. Last, we show how our simple analytical reductions can be used to predict adhesive forces for Stealth[®] Liposomes and other targeted and self-assembled nanoparticles.

1.2 Introduction

In this work we examine the adhesive forces between tethered ligand-receptor architectures. As an example, Fig.1-1 shows two surfaces—one anchoring extensible molecular tethers that each bear a ligand that can bind specifically to a dense field of receptors on the opposing surface. Such architectures are biomimetic and are used in targeting liposomes and other bioactive particles towards cell tissues (1, 2), in biofunctionalizing surfaces (3, 4), and in the self-assembly of colloidal- and nano-structures (i.e. refs (5, 6)).

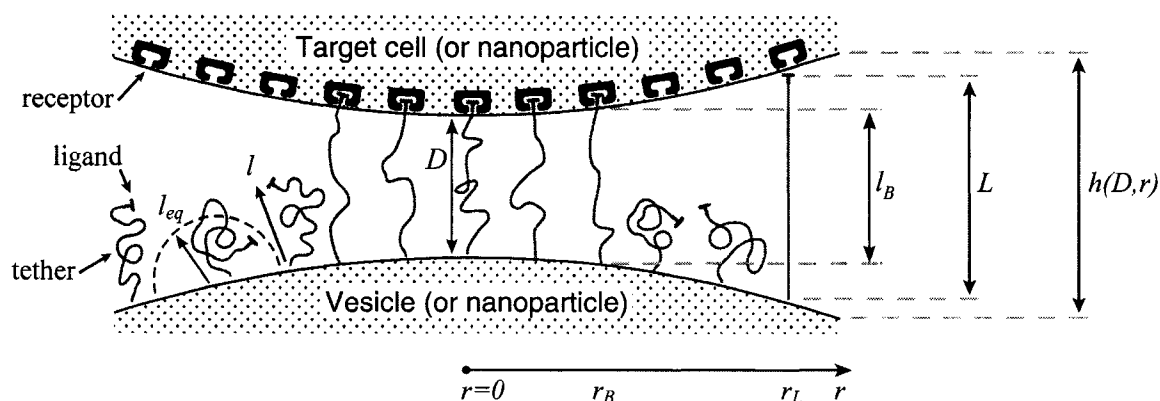


Figure 1-1. Depiction of two particles (i.e. cells, liposomes, or nanoparticles) bridged by tethered ligand / receptor bonds. The gap height, or surface separation, $h(D,r)$, is a function of the spheres' tip-to-tip distance (D) and the position along the lateral axis (r). The surface curvature limits how many particles may bridge the two surfaces. The relevant interaction area is constrained by the tether extension, or contour length (L), and the corresponding radial distance (r_L). The area containing bound tethers is geometrically limited by the effective binding range of an individual tether (l_B) and the corresponding radial distance (r_B). Ligands tethered to extensible molecules, such as polymers in good solvents, will stochastically sample many distances (l) away from their tether's anchor, which can be much farther away than the tether's time-average or equilibrium extension (l_{eq}) (16,17). These larger extensions produce the bridging forces that we model in this paper.

A wide range of tethers have been utilized in drug targeting and controlled nano-assembly, including the nonimmunogenic poly(ethylene glycol) (PEG) and other

synthetic polymers, and biologically harvested materials such as DNA strands, actin filaments, and fibronectin (7–12). Likewise, a wide range of biospecificities has been imparted to many of these tethers and their binding efficacy studied (13–15). What remains debated is the most efficacious structure for engineering adhesion between particles coated with tethered ligands / receptors.

The tethered ligand / receptor architectures that have been studied most are found in targeted Stealth[®] Liposomes. Like the stealth bomber, these drug-carrying vesicles are designed to evade the body's defenses—the immune system—and deliver their payload in a precisely targeted location, such as a cancer cell (1). They are armored by a forest of PEG chains, some of which bear target-specific ligands. These grafted polymer chains stochastically sample many chain conformations, which dramatically increases a tethered ligand's probability of finding its target compared to ligands mounted flush on a surface (16–20). The entropic motion of grafted chains also produces a spring-like force that pulls bridged surfaces together once the tethered ligand and receptor bind (18, 19, 21). This same entropic motion is responsible for repulsive steric forces as the grafted layer is compressed. The net achievement of these “entropical forests” is a long-range attraction and a shorter-range repulsion between surfaces they bridge. These forces may extend beyond the influence of attractive van der Waals or repulsive electrostatic forces and thus dictate the adhesive properties of surfaces, such as the distance at which bonds form and how strongly a liposome adheres to a target cell.

The tether's tug against the ligand-receptor bond reduces the bond lifetime (22), a phenomenon that has been examined through a variety of kinetic (18, 19, 21, 23), thermodynamic (23a–28), and mechanical (29) models. The *rupture* of single and

multiple tethered bonds has also been studied extensively through force microscopy (for a review see (30)). Unfortunately, it is very difficult to experimentally measure the *formation* of multiple molecular cross-bridges and to relate the measured adhesive properties to the properties of individual tethered ligand-receptor bonds. The most similar prior works have studied ensembles of grafted tethers using “adhesive dynamics”—a stochastic simulation method that tracks binding probabilities for each molecule and sums the forces on each bond to calculate the net adhesive force between two bridged bodies (31–36).

Here, we seek a continuum model to describe the interaction between individual tethered ligands / receptors and to relate those single-molecule properties to the adhesive strength, range of interaction, and speed of approach between surfaces bridged by many tethered ligands / receptors. This framework allows us to develop scaling laws that are useful for understanding multiple bond formation between tethered ligand-receptor architectures on curved surfaces. We demonstrate the predictive accuracy of our model by comparing it to measurements with the Surface Forces Apparatus. Last, we illustrate how our analytical solutions can be used to design “smart” biointerfaces for drug targeting, biosensing, and nano-assembly, using Stealth[®] Liposomes as an example.

1.3 Single Bond Formation: Critical Binding Ranges

Of fundamental importance to tethered ligand-receptor interactions is the question: at what distance will tethered ligands bind to receptors? Bonds formed when the tether is stretched beyond its equilibrium extension are antagonized by the tether’s contractile force and can dissociate if the entropic pull of the tether is sufficiently strong (18, 19, 22, 38). External forces, such as those applied in force microscopy, can also

increase the rate of bond dissociation (22, 38). However, in contrast to the bulk of experimental work where surfaces are separated (i.e., ref. 38), with *approaching* surfaces the apparent bond strength may appear to decrease with increased surface speed if bond formation is constrained by the time required for tethered ligands to diffuse towards receptors (16, 18, 19). In Section 1.5 we show quantitatively that this is not always an important constraint for modeling the adhesion of liposomes and larger particles, since diffusion of the kinds of small, high affinity ligands tethered by polymers used in drug targeting is often very rapid compared to the timescale of the entire adhesion event. Nonetheless, assuming that tethered ligands and receptors are in chemical equilibrium will reveal some useful scaling relations and provide explicit expressions for the *maximum* bridging force between surfaces bound by tethered ligands, as well as estimates of the adhesion timescale and fraction of bound tethers.

Moreira, et al. (18, 19) used a kinetic model to show that in the limit of chemical equilibrium, tethered ligands / receptors have the binding probability:

$$\phi(l) = \frac{e^{[W-U(l)]/k_B T}}{1 + e^{[W-U(l)]/k_B T}} \quad \text{Eq.1-1}$$

where W is the ligand-receptor bond dissociation energy and $U(l)$ is the energy required to stretch a tether a distance l away from its anchor. Fig.1-2 plots the probability of bond formation for PEG₂₀₀₀ tethers with various ligand-receptor dissociation energies. Each curve is sigmoidal, with a high probability of bond formation when $U(l) < W$ and a low probability of binding when $U(l) > W$. At the inflection point $U(l) = W$, the binding probability is 0.5.

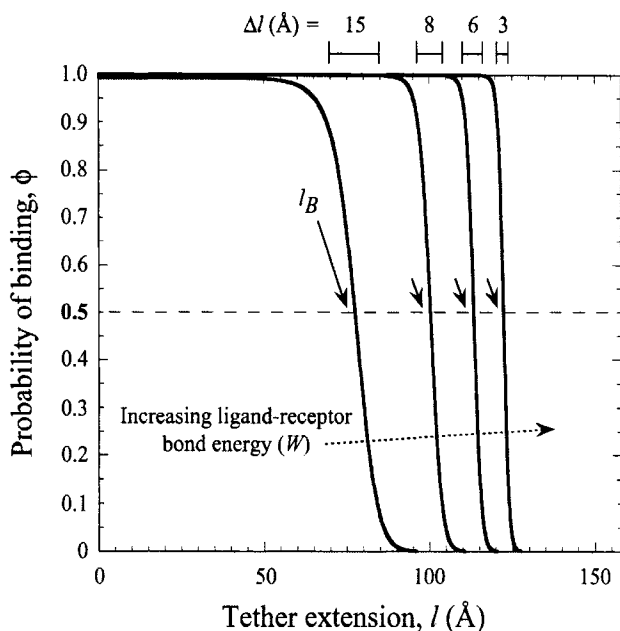


Figure 1-2. Probability of a single PEG₂₀₀₀ tether binding (Eq.1-1) as a function of its extension, l , for various ligand-receptor bond energies (left to right: $W=5, 15, 25, 35 k_B T$). Arrows mark each tether's binding range, l_B , defined as the tether extension at which $\phi = 0.5$, which coincides with each curve's inflection. Bonds form less frequently when the distance between the tether's anchor and the receptor is greater than l_B . This critical binding range becomes greater as the ligand-receptor bond energy increases, as the bond becomes more thermodynamically stable and can more easily resist the entropic pull of the tether. Brackets above the graph designate each curve's Δl , which estimates the range over which ϕ changes from 1 to 0. The fully extended tether length is $L=159\text{\AA}$ (length of abscissa). As W increases, $\Delta l/L$ decreases and ϕ more closely resembles a step function. If the receptor is moving towards the anchored tether, the general shape of the binding probability curves remains, although the inflection point (l_B) will be decreased by an amount that depends on the approach velocity (18, 19).

As seen in Fig.1-2, the interval in l over which the binding probability changes from 1 to 0, Δl , is a small fraction of the tether length, L . In such cases, there is a sharply defined extension, l_B , below which nearly all tethers bind and beyond which the binding probability is essentially zero. Mathematically,

$$\phi(l) \approx \begin{cases} 1, & l \leq l_B \\ 0, & l > l_B \end{cases} \quad \text{Eq.1-2}$$

We call this critical extension, l_B , the tether's binding range, corresponding to the inflection of each curve in Fig.1-2. For tethers with a harmonic stretching potential, $U(l) = (k/2)(l - l_{eq})^2$, where k is an effective tether spring constant, and so the critical binding range is $l_B = l_{eq} + (2W/k)^{1/2}$ and $\Delta l = 3k_B T / (kW)^{1/2}$ (39). Eq.1-2 also describes well the binding probability of tethered ligands when surfaces approach quickly compared to the bond formation timescale (of the order $\sim 1 \mu\text{s}$ for PEG tethers)(16). In that case, the binding probability curve still approximates a step function, but the critical binding range decreases by an amount that depends on the approach speed (18, 19). Thus, in settings far from equilibrium, l_B can be interpreted as the *maximum* effective binding range.

The question is: do biological tethers (and synthetic tethers) in common use have a sharply defined binding range when interacting with biological receptors? To answer this broad question, we first determine typical bond energies (W) for biospecific interactions. Table 1-1 compares the bond energies of ligand-receptor pairs commonly used in drug targeting and other biophysical research (13, 14). Although this list is not exhaustive, an attempt has been made to represent a variety of molecular classes. With the exception of a single nucleotide bond, all the biospecific interactions listed in Table

1-1 have a bond energy of $W > 5 k_B T$ and most have $W > 15 k_B T$. In fact, of the 2,276 biological ligand-receptor complexes currently listed in the PDBbind database v.2004 (41, 42), we calculate an average bond energy of $W = 14.7 k_B T$ (monomodal with standard deviation $4.9 k_B T$) (43). The strongest biological noncovalent interaction is between biotin and avidin ($W = 35 k_B T$).

To survey characteristic values for tether stiffness, Table 1-2 compares the lengths (L) and effective spring constants (k) of tethers that have been used in drug targeting, controlled self-assembly, and elsewhere (7). Importantly, a calculation of $\Delta l/L$ is listed using the characteristic value of $W = 15 k_B T$ that was determined from Table 1-1. In all cases, Δl is a small fraction of L ; thus, tethers listed in Table 1-2 are expected to exhibit a discrete binding range when bearing “typical” biospecific ligands, such as those listed in Table 1-1. In some cases, $\Delta l \ll L$ and we expect a binding probability curve much steeper than those shown in Fig.1-2, and thus an even more distinct binding range.

Table 1-1. Some ligands and receptors of interest for drug targeting and other biophysical research.

Ligand	Receptor	Bond energy $W / k_B T$ *	Dissociation constant K_d (M)*	Ligand MW (D)	Ref.
folic acid	folate receptor	21–25	$10^{-9} - 10^{-11}$	441	(68, 69)
sialyl Lewis X [†]	L-selectin	18–24	$2 \times 10^{-8} - 4 \times 10^{-11}$	120,000	(70–72)
PSGL1	P-selectin	17	5.5×10^{-8}	120,000	(72, 73)
adenine (A)	thymine (T)	2.3	1×10^{-1}	135	(74)
RGD peptide	integrin $\alpha_{IIb}\beta_3$	14	1×10^{-6}	770	(75)
fibrinogen	integrin $\alpha_{IIb}\beta_3$	16	1×10^{-7}	N/A	(75)
145-2C11 mAb (antibody)	CD3	16	7×10^{-8}	N/A	(76, 77)
fluorescein	anti-fluorescein	19–21	$0.75 - 8.9 \times 10^{-9}$	380	(78)
human serum albumin (HSA)	anti-HSA	14 [‡]	8.3×10^{-7}	66,500	(79)
serine endopeptidases (various)	protein inhibitor	18–29	$1.5 \times 10^{-8} - 2.5 \times 10^{-13}$	N/A	(77)
“typical” antibody	“typical” antigen	18	10^{-8}	>100,000	(22, 73)
biotin	avidin	35	1.0×10^{-15}	244	(80)
biotin analogues (various)	streptavidin	5–30	$1.0 \times 10^{-2} - 5 \times 10^{-8}$	214–258	(80, 81)

* When only one of W or K_d was reported, the other was estimated (43). [†]Modified PSGL-1 ligand. [‡] Estimated as $W = (\text{rupture force}) \times (\text{effective rupture length})$ (22).

Table 1-2. Some tethers of interest for drug targeting and other biophysical research.

Tether	Spring constant., k (mN/m)	Length, L^\dagger	Binding interval, Δl (nm) [‡]	$\Delta l/L$	Ref.
DNA	$10^{-5} - 10^{-4}$	20 μm	70	0.0035	(82)
* RNA	0.1	320 nm	6.1	0.019	(83)
* dextran (polysaccharide)	5.1	0.4–1.6 μm	0.7	0.0004–0.002	(84)
* xanthan (polysaccharide)	93	~1 μm	0.2	0.0002	(85)
* cellulose (carboxymethylated)	1–30	0.1–1.2 μm	2	0.001–0.02	(85)
neutrophil microvilli	0.15–1.3	0.2–1.6 μm	1.2–3.0	0.006–0.002	(86)
lamellar bodies (lung surfactant complex)	0.0125	8 μm	14	0.0018	(87)
PEG ₂₀₀₀	1.0	15.9 nm	3.7	0.23	¶
PEG ₃₃₀₀	0.57	23.2 nm	4.4	0.19	¶
PEG ₆₂₆₀	0.27	49.7 nm	7.0	0.14	¶
poly(styrene)	0.1–2	10–1000 nm	1–4	0.04–0.10	¶
* poly(vinyl alcohol)	1.0	50–1000 nm	1.6	0.002–0.03	(88)
* poly(methylacrylic acid)	1.1	20–120 nm	1.0	0.05–0.005	(89)
* poly(NIPAM)	1.8	100–1600 nm	1.0	0.0007–0.01	(90)

* An effective molecular stiffness was estimated from the slope of reported force-distance curves in the low-force regime. [†] “Contour length” or fully-stretched extension. [‡]Estimated for a characteristic value of $W=15 k_B T$ (c.f. Table 1-1). ¶ (43); for comparison, see refs. (91–93).

1.4 Multiple Bond Formation at Curved Interfaces

In the rest of this paper we relate the properties of single tethered ligand-receptor interactions to what may be observed when many such molecules decorate curved surfaces (i.e. Fig.1-1). We seek to answer: how many bonds will form at a given surface separation, what will be the bridging force between the two surfaces, and what is the timescale of the adhesion event? Our analysis assumes that anchoring surfaces are non-deformable as the conventional first step in quantifying the interactions of deformable solids (44).

When tethered ligand-receptor pairs are evenly spread across two opposing curved surfaces, geometry dictates the maximum number of tethers that may bind:

$$N_{total} = 2\pi R L \sigma \quad \text{Eq.1-3}$$

where R is the effective interaction radius of the surfaces (45), L is the tether's fully extended length or contour length, and σ is the tether surface grafting density (46). Eq.1-3 assumes the surfaces are touching (see Fig.1-1). It is exact provided $R \gg L$, and is still correct to a factor less than 10 when $R = L$. Examples of when Eq.1-3 is accurate include the adhesion of two cells ($R = 10 \mu\text{m}$, $L \sim 1 \mu\text{m}$) (Table 1-2), the binding of a targeted liposome onto a cell surface ($R = 38\text{--}100 \text{ nm}$, $L = 16 \text{ nm}$)(47), and the cross-linking of nanoparticles via adsorbed polymer ($R = 100 \text{ nm}$, $L = 21 \text{ nm}$)(5). Using Eq.1-3, a 100-nm Stealth[®] liposome with $\sigma=10^5$ tethers/ μm^2 of PEG₂₀₀₀ (1) may form a maximum of ~1,000 bonds to a cell, while the folate-targeted liposomes used by Reddy, et al. ($R=50 \text{ nm}$, $L=27 \text{ nm}$, $\sigma\sim 10^3$ tethers/ μm^2) (48) would be expected to form at most ~10 bonds per liposome. We postulate that in both cases these are enough bonds to render continuum models insightful.

The number of tethers that can form bonds depends not only on the tether / ligand / receptor properties but also on the surface curvature. Tethers near the interaction center will be closest to the receptor surface and thus more likely to form bonds, while those away from the center will be more highly stretched and thus less frequently bound. As we have shown that most tethers of interest exhibit a discrete binding range (Eq.1-2), we can simplify the analysis considerably. Using geometric arguments, the number of tethers bridging two curved equilibrated surfaces may be readily estimated:

$$N_{bound} = 2\pi R\sigma (l_B - D) \quad \text{Eq.1-4}$$

for $D \leq l_B$ and $R \gg L$. Thus, the number of tethers that can bind depends intimately on l_B . Further, by comparing to the total number of tethers in the interaction area (Eq.1-3), the fraction of chains bound is

$$\Phi = N_{bound} / N_{total} = (l_B - D) / L \quad \text{Eq.1-5}$$

Thus, the fraction of bound chains is independent of the size of the interaction area. Although simple in form, Eq.1-5 makes a remarkably accurate calculation of Φ compared to our numerical solutions for complimentary surfaces decorated with multiple PEG tethers (identical within $\pm 1\%$ over the entire range, $0 < D < L$ for $5k_B T < W < 35k_B T$). For approaching surfaces, Eqs.1-4 and 1-5 estimate *maximum* expected values, since l_B decreases with increased approach speed (18, 19).

With justification for treating binding ranges of single tethers as discrete when *multiple* tethers are present, we now develop an analytical solution for the maximum bridging force between two curved, approaching surfaces. Our derivation centers on developing appropriate expressions for the component of the interfacial energy, $E(D)$, per unit area that develops from multiple tethered ligand / receptor bond formation

between two plane-parallel surfaces. As detailed in Appendix 1-A, the many angles at which tethers bind have little effect on the bridging force normal to the plane of interaction. By our definition, individual tethers at equilibrium exhibit significant binding probabilities when $0 < l < l_B$. Thus, we set $\phi = 1$ (maximum) for $0 < l < l_B$, which restricts the validity of the result to $0 < D < l_B$. (We will address the possibility of nondiscrete binding ranges in Section 5.1). Last, we assume a constant grafting density, σ (46). Then for the plane-parallel geometry, the component of the interfacial energy per unit area that arises from the bridging force is:

$$E(D) = -\sigma \int_{l_B}^D f(l) dl \quad \text{Eq.1-6}$$

We employ two models for the stretching force, $f(l) = dU(l)/dl$. In the first we treat each tether as a Hookian (harmonic) spring. Although ideal springs do not exist in nature, this simplification is useful because spring models are often used to approximate a single molecule's actual mechanical behavior (29, 49). For example, single-molecule force spectroscopy has been used to measure effective spring constants for a number of tether molecules (e.g., Table 1-2) (51). Moreover, because the spring model is one of the simplest models for polymer stretching, it will make the scaling behavior of the bridging force more apparent.

The maximum (or equilibrium) bridging force between two surfaces is calculated using the Derjaguin approximation, which has been shown to be valid for any type of force provided $R \gg D$ (51). For the spring model the result is:

$$F_{bridging}(D) = -\pi R k \sigma (l_B - D)(D + l_B - 2l_{eq}) \quad \text{Eq.1-7}$$

Eq.1-7 shows that the maximum bridging force for spring-like tethers bridging approaching surfaces scales linearly with the interaction radius (R), tether spring constant (k), and tether grafting density (σ) (46). This scaling behavior for tethered ligand-receptor interactions is also validated in Appendix 1-B without using the Derjaguin approximation. Using Eq.1-7 with our analytical estimate for l_B suggests that the bridging force scales linearly with the ligand-receptor bond energy (W) over the entire regime $0 < D < L$ when $W \gg kL^2/k_B T$, which for freely-jointed polymers (i.e. PEG) requires $W \gg (3/2)(N^{2/5} - 1)^2 k_B T$ (51), or when $D \leq l_{eq}$ requires simply $W \gg (3/2)k_B T$ for any polymer length. This latter constraint is typically met in drug targeting; thus, we might anticipate $F_{bridging} \propto W$ when liposomes are attached to target cells.

The second model we employ for the polymer stretching force is the “worm-like chain” (WLC) model, which is known to more accurately describe the stretching potential of many bio- and synthetic polymers at long extension, as it accounts for finite chain length (29). In the WLC model, the force required to stretch a single tether is:

$$f(l) = (k_B T / l_p) \left[(1/4)(1 - l/L)^{-2} + l/L - 1/4 \right] \quad \text{Eq.1-8}$$

where l_p is the tether’s persistence length, which characterizes the chain’s resistance to bending stress between adjacent mers. Applying the same assumptions used to derive Eq.1-7 except using the WLC model (Eq.1-8) estimates the maximum (or equilibrium) bridging force for an entire ensemble of flexible tethers between two curved, approaching surfaces:

$$F_{bridging} = -(\pi R \sigma k_B T / 2l_p) \left[(l_B - D) / (l_B - L)(L - D) \right] \\ \times \left[3L + 2Dl_B (l_B + D) / L - (2l_B + D)(l_B + 2D) \right] \quad \text{Eq.1-9}$$

As with the spring model, the WLC model predicts that the bridging force will scale linearly with the interaction radius (R) and tether grafting density (σ), and will vanish as $D \rightarrow l_B$. The stiffness of individual chains is manifest in the bridging force as an inverse proportionality to the persistence length (l_p) in Eq.1-9.

1.5 Bridging Dynamics and Surface Approach

The preceding analysis is useful for calculating the maximum effective binding range of an individual tether (via Eq.1-1), the maximum number and fraction of bound tethers (Eqs.1-4 and 1-5), and the maximum bridging force (Eqs.1-7 and 1-9). However, these expressions can represent not just maximal values but exact values when the surface speed is slow enough that tethered ligands and receptors can be assumed to be in a state of chemical equilibrium. Although a detailed kinetic analysis is beyond the scope of this paper, identifying the conditions in which tethered ligands and receptors anchored to curved surfaces are expected to be in chemical equilibrium clarifies the applicability of our model and provides useful information about the dynamics of surface approach.

For ligands tethered to immobile surfaces, the average rate of bond formation to opposing receptors depends on the intrinsic kinetics of ligand-receptor bond formation and on the effective diffusion rate of the ligated tether. The distal end of a grafted polymer chain in good solvent has the characteristic diffusion time, $\tau(l) = 1.43\tau_z \text{Exp}(U(l))/U(l)$ (18, 19). The chain relaxation time used here is the “Zimm time”, $\tau_z = \mu l_{eq}^3 / k_B T$, which takes into account hydrodynamic drag of the chain as it moves thermally (37). As an example, a characteristic value for this diffusion time for a single, ligated PEG₂₀₀₀ tether in water opposing a receptor less than 100Å away is τ_z

$\approx 1 \mu\text{s}$. Because this timescale is much longer than that of intrinsic ligand-receptor bond formation (in the nanosecond range), bond formation with ligated PEG—and with less flexible tethers—can be assumed to be diffusion limited. In such cases, surfaces that move slowly compared to the tether diffusion timescale will have equilibrium bond kinetics and equilibrium adhesion forces.

To estimate the surface approach timescale, we note that the adhesion begins near the surface separation $D \approx l_B$, where tethers grafted near the contact center are first able to form stable cross-bridges (Fig.1). These bound tethers begin tugging the surfaces together, bringing more tethers into range until the surfaces are an equilibrium distance apart, $D_{eq} < l_B$. The characteristic time for the surfaces to move across this distance is then:

$$\tau_{adhesion} = (l_B - D_{eq}) / \langle dD/dt \rangle \quad \text{Eq.1-10}$$

where $\langle dD/dt \rangle$ is a representative speed of the surfaces' approach. To calculate the approach speed, we use the thin film assumption (52) to write the force balance:

$$F_{intersurface} + F_{cantilever} + F_{hydrodynamic} = 0 \quad \text{Eq.1-11}$$

$F_{intersurface}$ is the bridging force plus any nonspecific intersurface forces. $F_{cantilever}$ is the force of an external cantilever mounting one surface, as would be present in a force microscopy experiment. It has previously been shown that when $R \gg L$ the hydrodynamic force is dominated by the force required to squeeze out fluid from between the two surfaces, viz.,

$$F_{hydrodynamic} = 6\pi\mu R_G R_H (dD/dt) / (D - SP) \quad \text{Eq.1-12}$$

where $R_G = (R_1 R_2)^{1/2}$ and $R_H = 2(1/R_1 + 1/R_2)^{-1}$ are the geometric and hyperbolic radii, respectively, μ is the fluid viscosity, and SP is the distance that the hydrodynamic slip

plane extends from the surface (from $D = 0$) (52). We simplify with $R_1 = R_2$ so that $R_G R_H = R$. Then from Eqs.1-11 and 1-12, the approach velocity is

$$dD/dt = [F_{intersurface}(D) + F_{cantilever}(D)](D - SP) / 6\pi\mu R^2 \quad \text{Eq.1-13}$$

It is insightful to simplify Eq.1-13 as follows. First, $F_{cantilever}$ is typically much smaller than $F_{intersurface}$ during surface movement in force microscopy, and is zero in the context of liposomal targeting *in vivo*. Second, the bridging force typically dominates over the nonspecific forces except at short distances, and so $F_{intersurface} \approx F_{bridging}$. With these simplifications we can use Eqs.1-7 and 1-11 to derive the maximum surface approach speed:

$$|dD/dt| \leq (k\sigma / 6\mu R) [(D - SP)(l_B - D)(D + l_B - 2l_{eq})] \quad \text{Eq.1-14}$$

By comparing Eq.1-14 to Eq.1-10 we can identify the following scaling relation:

$$\tau_{adhesion} \propto \mu R / k\sigma \quad \text{Eq.1-15}$$

We can use this scaling relation to estimate the minimum adhesive timescale for particles of different sizes, for example. For an SFA experiment that mimics architectures commonly used in drug targeting (1), the adhesion timescale is of the order of 1s for $R \sim 1\text{cm}$. For a self-similar liposomal architecture with $R = 50\text{ nm}$, Eq.1-15 estimates $\tau_{adhesion} \geq 5\mu\text{s}$. In both cases, $\tau_{adhesion}$ is longer than the $1\mu\text{s}$ sampling time typical for PEG₂₀₀₀ chains extended below $l < 100\text{\AA}$ where surface movement is fastest, and is significantly larger than the polymer's intrinsic relaxation (Zimm) time of 9 ns. This observation substantiates our assumption of chemical equilibrium between PEG-anchored ligands and receptors for the drug targeting applications with which this paper is primarily concerned.

1.6 Methods for Evaluating the Analytical Solutions

1.6.1 Independent Numerical Solutions

To evaluate our analytical reductions, we also calculated more exact expressions for the bridging force as follows. As discussed previously, the bridging force for an ensemble of tethered ligands spread between two curved surfaces depends on the surface geometry and on properties of the ligand, receptor, and tether. Tethers near the interaction center ($r = 0$) will be less stretched than tethers near the periphery of interaction (see Fig.1-1). Thus, the contractile force of a tether, $f(h)$, depends on the gap height, h . Because a stretched tether opposes bond formation, the probability that a given tether will bind, $\phi(h)$, also depends on the gap height. Thus, calculating the total bridging force between two curved surfaces requires an integral over the entire interaction area:

$$F_{\text{bridging}}(D) = \int_{r=0}^{r=r_L} 2\pi r \sigma f(h) \cdot \phi(h) \cdot \mathcal{A}(h) dr \quad \text{Eq.1-16}$$

where $\mathcal{A}(h)$ is a mathematical operator that accounts for tethers binding to receptors at different angles and r_L is the radius of the interaction area corresponding to a gap height of $h(D, r_L) = L$ (Fig.1-1). For two curved surfaces, the gap height is

$$h(D, r) = D + R - (R^2 - r^2)^{1/2} \quad \text{Eq.1-17}$$

where D is the nominal surface separation (tip to tip), R is the effective interaction radius (45), and r is the lateral distance from the center of the interaction area (see Fig.1-1). To compute this force for PEG tethers, we have interpolated stretching force profiles from Monte Carlo simulations reported elsewhere for various PEG lengths (16). To compute

the *local* binding probability of a single tether, $\phi(h)$, we replace l with the gap height, h , in Eq.1-1:

$$\phi(h) = e^{[W-U(h)]/k_B T} / \left(1 + e^{[W-U(h)]/k_B T} \right) \quad \text{Eq.1-18}$$

Appendix 1-A provides a detailed derivation of $\alpha(h)$ for two spherical particles bridged by tethered ligands. In scenarios relevant to drug targeting, $\alpha(h)$ ranges between 1 and 1.15, and thus serves as only a small correction to Eq.1-16 that we account for in our numerical results.

1.6.2 Experimental Measurements

To further validate our model, we compare it to measured adhesive forces between membranes functionalized with tethered ligands and receptors, measured with the Surface Forces Apparatus (SFA) as reported elsewhere (16, 17; Kuhl, T.L. S. Zalipsky, and J.Y. Wong, unpublished data). The SFA technique is one of the most powerful tools available for determining the force–distance relationship between weakly interacting surfaces (49). In short, two molecularly smooth mica surfaces were coated with lipid membranes anchoring a known fraction of ligated PEG_x, where the subscript ‘x’ is the average polymer molecular weight. This coating was made using Langmuir Blodgetty, which allowed the tether grafting density to be controlled for each sample. Biotin (to oppose streptavidin receptors) was the chosen ligand because of its typical molecular weight and extensive characterization (c.f. Table 1-1)(54). A dense field of streptavidin receptors (>79% coverage) (55) was presented on the opposing membrane. One surface was mounted on a double cantilever spring; its measured displacement is proportionate to the intersurface force. Simultaneously, the intersurface spacing, D , was

controlled and measured with angstrom precision using white-light interferometry (56). For dynamic measurements, a camera recorded the interferogram (52).

In comparing to these experiments, we added to our model nonspecific interactions between biological surfaces as follows: 1) van der Waals attraction between lipid membranes calculated using a non-retarded Hamaker constant typical for membranes (57); 2) electrostatic repulsion calculated numerically by solving the nonlinear Poisson-Boltzmann equation for membranes characteristic in drug targeting research (58); and 3) polymer steric repulsion calculated using Dolan and Edwards theory for grafted polymer mushrooms (59) These three nonspecific forces were added to the specific bridging force (Eqs.1-7 or 1-14) for direct comparison to both static and dynamic measurements with the SFA. For $D < l_{eq}$ it was also necessary to add $\pi Rk\sigma (D - l_{eq})^2$ so that polymeric compression was not accounted for twice when summing Dolan and Edwards theory to either of Eqs.1-7 or 1-14.

The predicted forces were also used to estimate the ensemble capture distance, $D_B \approx l_B$, which is the farthest separation at which two surfaces experience net attraction. In surface force measurements, the capture distance is an artifact of the experiment (the distance at which the slope of the net intersurface force profile equals the spring constant of the cantilever ($k_{cantilever}$) that holds one surface (60). Yet because it is easily quantifiable, D_B serves as a useful third validation of our adhesion model. More specifically, the predicted capture distances were calculated by solving for the farthest distance at which

$$\frac{\partial F_{intersurface}(D)}{\partial D} = k_{cantilever} \quad \text{Eq.1-18b}$$

where $F_{intersurface}$ represents the predicted force profile (Eq.1-16 plus values for the nonspecific forces described above).

Input parameters for the numerical (and analytical) solutions were chosen to match experimental variables (Table 1-3). Except where noted, all results are *a priori* estimates, not data fits. The three molecular weights of PEG correspond to lengths that have been commonly used for drug targeting *in vivo* (47). Likewise, the tether grafting density of $\sim 10^5$ tethers/ μm^2 is typical for drug targeting (47). This grafting density is also on par with reported expressions of folate receptors on tumor cells (34, 61), and only one order of magnitude greater than estimated cell surface densities of integrin receptors (33).

Table 1-3. Parameters used in calculating numerical results (except where specified). Values with uncertainties indicate experimentally measured values, which were used in the model when comparing to experimental data.

	Symbol	Value(s)	Units	Ref.
<i>Tether (PEG) Properties</i>				
molecular weight	PEG _x	2000, 3300, 6260	g/mol	
number of mers	<i>N</i>	45, 75, 142*		
length (full extension)	<i>L</i>	159, 262, 497* [†]	Å	
tether resting extension	<i>l_{eq}</i>	42.8, 58.4, 87.9* [‡]	Å	(16)
length per mer	<i>a</i>	3.5 [§]	Å	
grafting density	<i>σ</i>	(1.17±0.03)×10 ⁵	tethers/μm ²	
ligand-receptor bond energy	<i>W</i>	5–35	<i>k_BT</i>	
<i>Surface Properties</i>				
Hamaker constant		3.0 × 10 ⁻²¹	J	(58)
surface charge densities (grafting surface / receptor surface)		-0.0186 / -0.01	C/m ²	(94)
interaction radius	<i>R</i>	0.1–3.0, 1.48±0.05	cm	
slip plane	<i>P</i>	0, 158	Å	
cantilever spring constant	<i>k_{cantilever}</i>	100–300, 236±18	N/m	
<i>Environmental properties</i>				
Temperature	<i>T</i>	25.0±0.2	°C	
pH		7.2±0.1		
ionic concentration		0.50±0.01	mM	
Viscosity	<i>μ</i>	8.9 × 10 ⁻⁴	kg m ⁻¹ s ⁻¹	
Dielectric constant		78		

* Corresponding to the three polymer molecular weights listed above. [†] $L = a \times N$ (50). [‡]Calculated from Monte Carlo data (16). [§]Coincidentally about the same length as an amino acid in a polypeptide (95). ||Kuhl, T.L. S. Zalipsky, and J.Y. Wong, unpublished data

1.7 Results & Discussion

1.7.1 Experimental Validation

It is nontrivial to measure bridging forces directly because mechanical instabilities that are present in all force spectroscopy create regions of distances where the surfaces move quickly and equilibrium forces cannot be measured (60). Therefore, to validate our model we rely on a combination of measurements of static forces, capture distances, and the speed of surface approach.

Figs. 1-3A and 1-3B compare the measured intersurface forces to those predicted *a priori* for two tether lengths (PEG₆₂₆₀ and PEG₂₀₀₀, respectively), using the spring model (Eq.1-7) for the specific bridging force. The model correctly identifies the capture distances (D_B), adhesive minima, and equilibrium resting positions (D_{eq}) to within experimental error ($\pm 0.1 D/L$). From these figures we see that the model predictions are numerically accurate to better than an order of magnitude. It should be emphasized that the solutions shown in Fig.1-3 were not “fit” to the experimental data. Instead, these calculations were made *a priori* using the parameters in Table 1-3. Further, the predicted force profiles are based on the *maximum* bridging force expected. With these views, we find that the model agrees remarkably well with the experimental data.

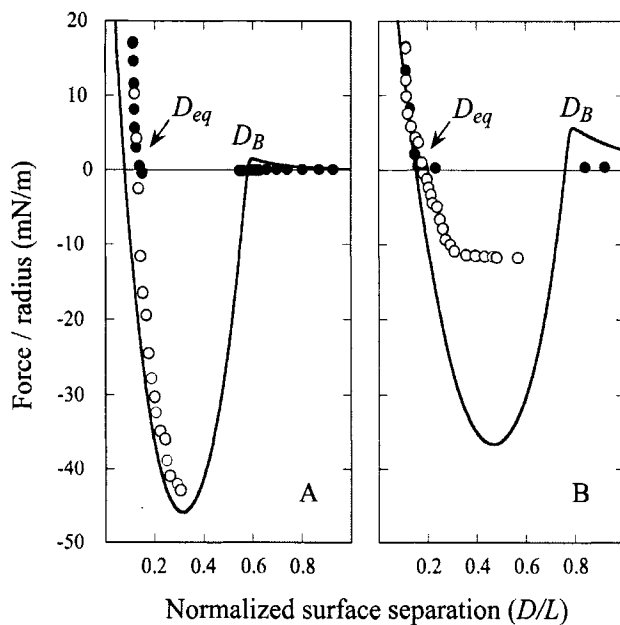


Figure 1-3. Comparison of *a priori* predictions of the maximum expected bridging force (lines) and measurements with the Surface Forces Apparatus (SFA) for biotin/streptavidin ligand/receptors ($W=35 k_B T$) mounted on two tether lengths: A) PEG₆₂₆₀ and B) PEG₂₀₀₀ (Kuhl, T.L. S. Zalipsky, and J.Y. Wong, unpublished data). Forces were measured between unperturbed surfaces as they approached (solid circles) and during withdrawal after surfaces had been pressed into adhesive contact (open circles). Discontinuities in the measured data exist from instabilities in the cantilever spring that support one of the functionalized surfaces. The *a priori* model correctly identifies the capture distances (D_B) and equilibrium resting positions (D_{eq}) to within experimental error ($\pm 0.1 D/L$), and forces to within less than a factor of three.

Differences between the predicted and measured forces arise from two primary sources. First, what is common to both Figs. 1-3A and 1-3B is that the long-range steric repulsion is overestimated by the Dolan and Edwards theory. In fact, reliable force laws for grafted polymer mushrooms are only well established for polymer compression ($D < l_{eq}$) (59). However, this has little effect on either the capture distances (D_B) or the majority of the force profile because the polymer bridging force dominates when $D < D_B$.

Second, the measured bridging force for the PEG₂₀₀₀ tethers (Fig.1-3B) is underestimated by about a factor of three. It has been shown that lipid anchors can be the

weakest “bond” between membranes bridged by polymers (62). In short, the energy required to extract a phosphatidylethanolamine from a lipid membrane ranges from 10–25 $k_B T$ (62–66), which is significantly less than the biotin-streptavidin bond energy (35 $k_B T$). Thus, it is likely that the uprooting of lipid anchors—which may also depend on the tether spring constant or kinetics—decreases the bridging force in these experiments. For example, shorter polymer chains are stiffer and would apply more force to the lipid-membrane “bond” and rupture them more quickly (22, 37). However, this effect is most significant in *separating* surfaces (62), and does not invalidate our *a priori* model’s general agreement with the SFA data.

The ensemble capture distances (D_B) measured with the SFA were found to agree with our model’s predictions, as shown in Table 1-4. Within experimental error, the ensemble capture distances were also identical to the predicted binding ranges of individual tethers (l_B). However, comparing the predicted capture distances to the predicted binding ranges shows that the two are not numerically equivalent. That is, l_B is a property of a single tether—the inflection point in Fig.1-2—while D_B is a property of an ensemble and of the measuring method. In fact, using our numerics we estimate the total fraction of bound chains required to pull these surfaces in these experiments together as $\Phi(D_B) \approx 0.001$ (Kuhl, T.L. S. Zalipsky, and J.Y. Wong, unpublished data). In contrast, l_B is defined by $\phi(l) = 0.5$. Although the two quantities are not strictly synonymous, our numerical model predicts that D_B is a reasonable estimate of l_B when l_B is discrete (viz., when $\Delta l/L$ is small), and that the same capture distances would be measured for a broad range of cantilever spring constants (1–100 mN/m) and interaction

radii (1 μ m–10 cm). Consequently, the SFA measurements provide direct evidence of tethers exhibiting discrete binding ranges.

Table 1-4. Measured and predicted ensemble capture distances and predicted single-tether binding ranges for PEG tethers of different lengths. Ligand / receptor was biotin / streptavidin ($W=35 k_B T$). The ensemble capture distance is the farthest range at which two surfaces are observed to experience bridging, and hence depends on the measurement method. In contrast, the theoretical binding range of *single* tethers depends only on the properties of the tether and ligand/receptor.

Tether	Ensemble capture distance (D_B), Å		Single-tether binding range (l_B), Å
	Measured*	Predicted [†]	Predicted [‡]
PEG ₂₀₀₀	129±10	127	122
PEG ₃₃₀₀	176±20	187	181
PEG ₆₂₆₀	275±25	294	284

* With SFA as reported elsewhere (16). [†]Eq.1-18b. [‡]From Eq.1-1; i.e., inflection points in Fig.1-2.

As a third verification, we report the dynamic approach of two surfaces identical to those shown in Fig.1-3B. The results are shown in Fig.1-4 along with the prediction based on the dynamic model (Eq.1-13). Again, the model's prediction is an *a priori* estimate, not a data fit. With this view, we find the agreement to be excellent. As predicted by Eq.1-13, the surface separation varies sigmoidally with time. By fitting the data to a three-parameter logistical model, we measure $\tau_{adhesion} = 0.88 \pm 0.06$ s, in reasonable agreement with the predicted $\tau_{adhesion} = 0.3$ s. It was also found numerically that moving the hydrodynamic slip plane to be coincident with the tether's equilibrium extension ($SP = l_{eq}$) increased the adhesive timescale by less than 5% compared to when

$SP = 0$. Thus, although the value of the slip plane affects the equilibrium resting position (D_{eq}), it should have little effect on the adhesion dynamics in these scenarios.

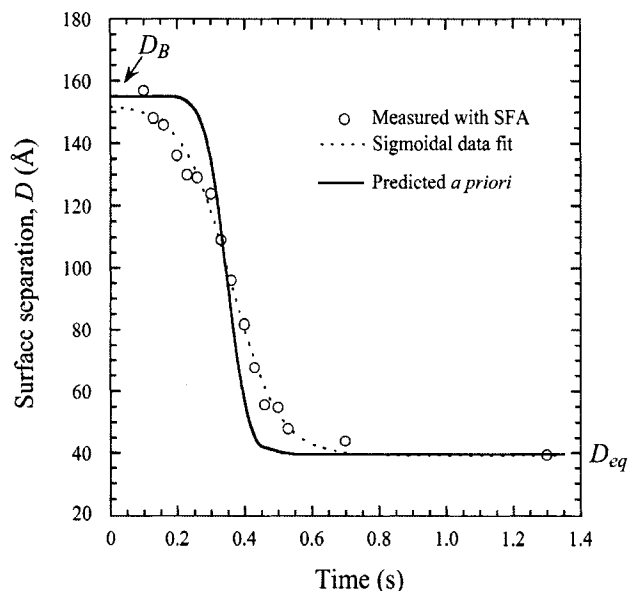


Figure 1-4. Dynamic approach of surfaces bound by PEG₂₀₀₀ tethers. The ligand and receptor were biotin and streptavidin ($W=35 k_B T$). Measurements with SFA (circles) follow the prediction of Eq.1-13 (solid line). Fitting the measured data to a three-parameter logistic model (dashed line) (96) calculates the measured $\tau_{adhesion} = 0.88 \pm 0.06$ s, in reasonable agreement with the *a priori* model's predicted of $\tau_{adhesion} = 0.30$ s.

1.7.2 Scaling Behavior of the Bridging Force

Fig.1-5 demonstrates a calculation of the bridging force for PEG₂₀₀₀ tethers. Plotted are both the full numerical solution (Eq.1-16) and the two analytical solutions (spring model, Eq.1-7; WLC model, Eq.1-9). The spring model was fit to the numerical solution by varying only the PEG tether's effective spring constant, k . Reasonable agreement was found for $k=2.6 \pm 0.6$ mN/m, which is in reasonable agreement with the $k = 1.0$ mN/m predicted for PEG₂₀₀₀ chains (51). For high ligand / receptor bond energies (here $W \geq 15 k_B T$) the WLC model gives better overall agreement. The latter yields a

persistence length of $l_p = 5.71 \pm 0.01 \text{ \AA}$, just longer than the 3.5 \AA mer length, and close to the $l_p = 4.75 \text{ \AA}$ determined from fitting Monte Carlo data reported elsewhere for single chains (16). In addition, bridging forces predicted by the numerical solutions scale linearly with the interaction radius, R , as predicted by Eqs.1-7 and 1-9.

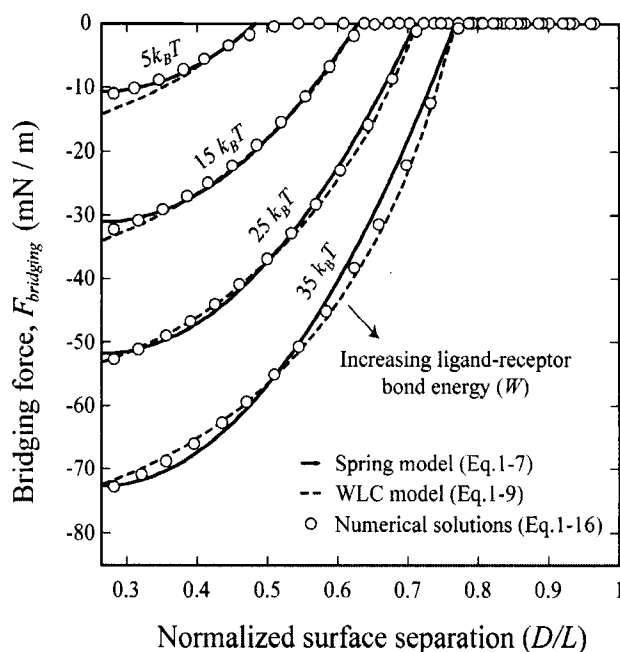


Figure 1-5. Maximum bridging force between approaching surfaces decorated with ligated PEG₂₀₀₀ as a function of the surface separation (normalized as D/L over the range $l_{eq} < D < L$, where l_{eq} is the tether's equilibrium extension and L is the tether's contour length). Ligand-receptor bond energies were (left to right): 5, 15, 25, and 35 $k_B T$, as marked. The spring model (Eq.1-7, solid lines) was fit to exact numerical solutions (Eq.1-16, circles) by varying only the tether spring constant, k . Best agreement was found for $k = 2.6 \pm 0.6 \text{ mN/m}$. For $W \geq 15 k_B T$, better agreement was achieved by modeling PEG tethers as worm-like chains (Eq.1-9, dashed lines), giving a persistence length of $5.71 \pm 0.01 \text{ \AA}$. All solutions converge to zero near the critical binding ranges (left to right, $l_B = 77, 100, 113, 122 \text{ \AA}$), and reach maximum force at $D \leq l_{eq}$ (far left). There the bridging force increases linearly with W , as predicted by the spring model.

Differences in these force profiles stem from differences in mathematical form.

For example, the analytical solutions assume that no tethers bind beyond $D > l_B$ (c.f.

Fig.1-2); thus, both slightly underestimate the bridging force at these long extensions. For smaller distances (i.e. $D \approx l_{eq}$), the poorer agreement of the WLC model to the numerical solution with lower bond energies (i.e. $W = 5 k_B T$) partly arises from assuming all tethers bind in the direction of the surface normal (Appendix 1-A), and it is perhaps an empirical coincidence that the spring model is less sensitive to this simplification, giving differences that are $\leq 6\%$. The numerical solutions correctly converge to zero force as $D \rightarrow l_B$, reflecting the distance at which most receptors are beyond the stable binding range of tethers, as predicted by Eqs.1-7 and 1-14. Both the spring model and the numerical solutions reach maximum force at $D = l_{eq}$, where as predicted the bridging force increases linearly with increased ligand-receptor bond energy, W ($R^2=0.9998$; note even spacing of vertical intercepts in Fig.1-5). Qualitatively, this is because more tethers are able to form stable cross-bridges at larger gap heights near the edge of the interaction area.

It should be noted that the forces plotted in Fig.1-5 represent the *maximum* bridging forces that may be achieved with these molecular architectures, as discussed previously. Kinetic constraints or the uprooting of lipid anchors may create binding probabilities for individual tethers that are functions of time, viz., $\phi(l,t) < 1$ for $l \leq l_B$, or that are more complicated functions of the tether extension than expressed by Eq.1-1. While these effects decrease the magnitude of the bridging force, they are not expected to change its scaling with respect to k , σ , or R , since Moreira et al. have shown that tethered ligands mounted to a movable surface still have discrete, albeit shortened, binding ranges (18, 19). Likewise, the scaling of the adhesive timescale (Eq.1-15) does not strictly require ligands and receptors to be in chemical equilibrium.

The force profiles shown in Fig.1-5 are distinct from what would be observed between two plane-parallel surfaces. As a shortcut, it may be tempting to model the interface as two flat surfaces (hereon “flat-flat”) on the grounds that $R \gg D$ in many applications, as discussed. However, at a flat-flat interface all tethers would have equal probability of binding to receptors. Fig.6 illustrates how this phenomenological difference creates a qualitatively different force-profile than our model for curved interfaces. As seen in Fig.1-6, the bridging force between curved interfaces is zero near l_B and reaches a maximum force at $D=l_{eq}$. In contrast, the bridging force between flat-flat interfaces increases sharply at l_B , then vanishes as $D \rightarrow l_{eq}$. These results are normalized by the number of tethers in the interaction area; hence, they are independent of R . Thus, although correct to an order of magnitude, modeling a curved interface as flat-flat will produce significant error in estimating individual bond forces when ligands are tethered. This finding may be significant for those doing force spectroscopy or flow cytometry. Instead, Eqs.1-7 and 1-9 provide simple yet accurate ways to predict equilibrium or maximum bridging forces while still accounting for the curvature of slowly adhering surfaces (46).

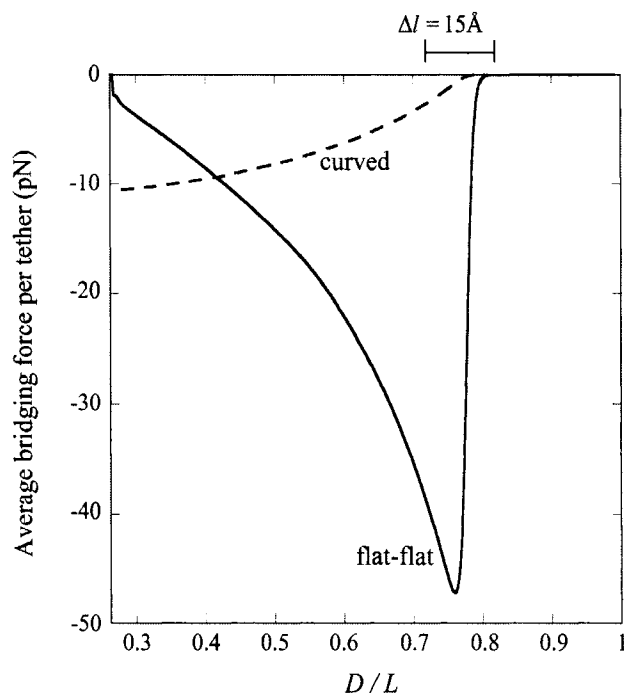


Figure 1-6. Effect of surface curvature on the force between two surfaces bridged by tethered ligand/receptors. The tether is PEG₂₀₀₀ with streptavidin / biotin ($W=35 k_B T$). The abscissa corresponds to $l_{eq} < D < L$. Shown is the average bridging force per tether calculated for two geometries: spherically curved interfaces (i.e. Fig.1-1, or equivalently, sphere-flat or cross-cylinder geometries (45); dashed line) and a plane-parallel, or “flat-flat” interface (solid line). Both are normalized by the number of tethers and therefore are independent of the size of the interaction area (or of the interaction radius for curved interfaces). The presence or absence of curvature at the interface creates phenomenologically different force profiles; i.e., curved interfaces have a bridging force that increases as $D \rightarrow l_{eq}$ and decreases as $D \rightarrow l_B$ (center of bracket), while the reverse is true for plane-parallel interfaces.

1.7.3 The Model as a Predictive Tool for Drug Targeting

We briefly demonstrate how the analytical solutions we have derived can be used to estimate the adhesive properties of targeted liposomes. Fig.1-7A shows the expected force profile for a “typical” liposome targeted with PEG₂₀₀₀ tethers (1) (parameters in Table 1-3). As shown in Fig.1-7A, a strong adhesion can be transformed into what is nearly a net repulsion by reducing the ligand-receptor bond energy (W) by less than one order of magnitude. Also, the capture distance (D_B) decreases with decreasing W . As

before, these forces represent the *maximum* adhesive forces expected. Anchor removal or impedance from glycocalyx or other membrane-bound molecules may reduce the attractive forces significantly.

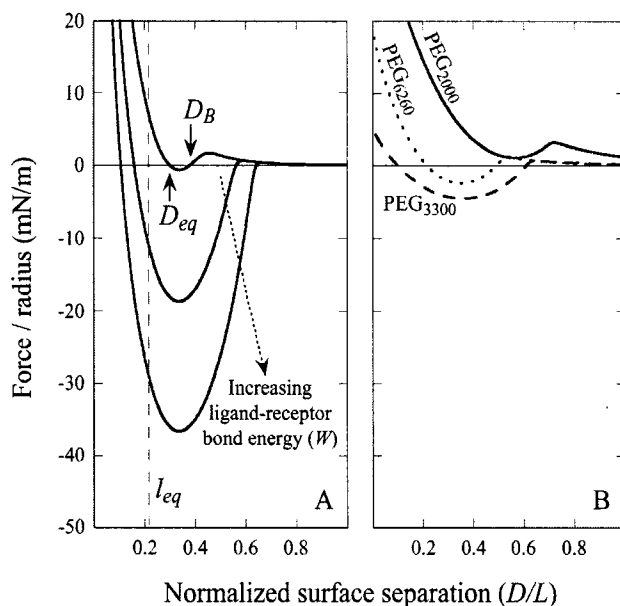


Figure 1-7. Examples of tuning the interaction profile to optimize adhesion for drug targeting or nanoassembly. A) Choosing ligand-receptors with different bond energies (top to bottom: $W=5$, 15 , and $25 k_B T$). Tethers are PEG₂₀₀₀; all other parameters are from Table 1-3. Increased bond energy increases the maximum number of bound tethers and hence the net adhesion. Too small of a W will result in an insufficient probability of ligand-receptor bond formation to produce a bridging attraction large enough to counteract the repulsive steric and electrostatic forces also present in adhesion. B) Parameters chosen to simulate folate targeting for a Stealth[®] Liposome. Choosing different lengths for the PEG tether suggests the existence of an optimum tether length for producing the strongest adhesion.

Fig.1-7B shows the predicted interaction profile for a folate-targeted liposome (for a review see (20)). The folic acid / folate receptor bond energy was fixed at $W=25 k_B T$ (Table 1-1), while the PEG tether length was varied. Grafting densities were $(1/l_{eq}^2) \times 90\%$ to model PEG chains in the slightly overlapping brush regime, which has been shown to be important in minimizing nonspecific adhesion between liposomes and

extracellular components (1). The characteristic surface density of folate receptors (2×10^{16} sites/m²) (67) was on the same order but always less than the density of ligands; thus, this number was used to calculate the number of cross-bridges formed. Also, the folic acid ligand has only twice the molecular weight of biotin (Table 1-1), which is small compared to the length of the shortest tether considered (159Å for PEG₂₀₀₀); consequently, its length does is assumed to not impact the results of the present calculation. As before, these are *a priori* estimates of the *maximum* adhesive force between such particles. Fig.7B suggests there may be an optimum tether length that capitalizes on the synergy between maximizing bond formation and minimizing steric repulsion. Perhaps not coincidentally, the strongest adhesion shown in Fig.7B occurs when the PEG tether has a molecular weight of 3400—the same tether some recommend for folate targeting *in vitro* (48, 61).

1.8 Conclusions

We have shown that tethers of practical interest in drug targeting and other biophysical research exhibit a critical binding range. This observation has allowed us to develop analytical predictions for the range, strength, and rate of adhesion between single tethered ligand-receptors and between surfaces they decorate. These metrics were accurately predicted in comparison to measurements made with the Surface Forces Apparatus and with independent numerical predictions. These relations should be useful for optimizing adhesion in drug targeting, biosensing, and nano-assembly, as well as for providing insight into bridging forces involved in biological adhesion.

1.9 Appendix 1-A: Bridging Angle Inconsequential to Normal Force

Cross-bridges formed at angles away from the surface normal are more highly stretched than bridges formed to a receptor that is directly above the tether's anchor point. Because tethers that are more highly stretched tend to form bonds less frequently, the angle (θ) at which a tether binds affects not only the force that bond exerts in the normal direction but also the probability of attachment. To correct for these effects, we derive a continuum expression for the angle operator $\mathcal{A}(h)$ in Eq.1-16.

If an individual spring-like tether has a contour length, L , much smaller than the particle radius ($L \ll R$), then the gap height, h , will appear constant within each tether's vicinity. A tether can form bonds at an arbitrary angle θ away from the surface normal by stretching a distance $l = h/\text{Cos}\theta$. Upon forming a cross-bridge, the normal component of the bridging force is

$$f_{\perp}(h) = f(h)\text{Cos}\theta = -k(h/\text{Cos}\theta - l_{eq})\text{Cos}\theta = -k(h - l_{eq}\text{Cos}\theta) \quad \text{Eq.1-19}$$

When $\theta = 0$, $f_{\perp}(h) = f(h) = -k(h - l_{eq})$, which is what we would calculate if we ignored angling effects. By comparing these two quantities, we can estimate the angle operator as

$$\mathcal{A}(h) = \frac{1 - (l_{eq}/h)\text{Cos}(\bar{\theta}(h))}{1 - (l_{eq}/h)} \geq 1 \quad \text{Eq.1-20}$$

where $\bar{\theta}(h)$ is the average angle that tethers bind for a given gap height, h . The angle operator $\mathcal{A}(h)$ is essentially a correction factor to the integrand in Eq.1-16. We compute the average binding angle using Boltzmann statistics, viz.,

$$\bar{\theta}(h) = \left(\int_0^{\theta_{\max}(h)} \theta P_{\theta} d\theta \right) / \left(\int_0^{\theta_{\max}(h)} P_{\theta} d\theta \right) \quad \text{Eq.1-21}$$

where P_{θ} is the probability of bond formation at a given angle and $\theta_{\max}(h) = \text{ArcCos}(h/L)$ is the maximum angle at which bridging can occur. An analytical solution for Eq.1-21 exists for tethers with a discrete binding range. A critical binding range (l_B) will correspond to a critical angle (θ_B) beyond which no binding occurs. The average binding angle then approaches

$$\bar{\theta}(h) \rightarrow \theta_B(h)/2 = \text{ArcCos}(h/l_B)/2 \quad \text{Eq.1-22}$$

For the ensemble, the error in ignoring angling effects is greatest when the surfaces are in contact (F_{bridging} underestimated by ~15% for $R \geq 10L$ and ~25% for $R=L$). This error reduces to zero when the surfaces are far apart. This behavior can be explained by noting that when the surface separation is near the binding range ($D \approx l_B$) only highly stretched tethers can bind. There $\bar{\theta}(h) \approx 0$ and hence $\angle(h) \approx 1$ (Eq.1-20). At closer distances, the error is still small because most of the tethers that are bound are away from the interaction center. It is these highly stretched tethers, which are more numerous, that constitute the bulk of the bridging force (37). Further, anchor diffusion tends to alleviate stresses on cross-bridges by moving anchors nearer receptors (25). Overall, the total bridging force normal to particle interfaces has little dependence on the angles at which tethers bind to receptor surfaces.

1.10 Appendix 1-B: Exact Analytical Solution for the Bridging Force Validates Scaling Behavior

To validate the scaling behavior of the bridging force between tethered ligand-receptor architectures (Eq.1-7), we have derived an analytical solution for the bridging

force (Eq.1-16) without using the Derjaguin approximation. As before, we set $\kappa = 1$, $\phi = 1$, and σ constant in the range $0 < r < r_B$, where r_B corresponds to $h(D, r_B) = l_B$. Then Eq.1-16 simplifies to:

$$F_{\text{bridging}}(D) = 2\pi\sigma \int_0^{r_B} r f(h) dr \quad \text{Eq.1-23}$$

where the gap height, h , is given by Eq.1-17. Then for harmonic tethers Eq.1-23 has the exact solution

$$F_{\text{bridging}}(D) = -2\pi k\sigma \left\{ (1/3) \left[\left(R(R + 2D - 2l_B) \right)^{3/2} - R^3 \right] \dots \right. \\ \left. \dots + (l_B - D)R^2 + (l_B - D)(D - l_{eq})R \right\} \quad \text{Eq.1-24}$$

Contrary to how it looks, Eq.1-24 is remarkably linear with respect to R over a tremendous range of R values. When $l_{eq} \leq 0.25l_B$, Eq.1-24 is linear in R over the range $l_B < R < 10^7 l_B$. And when $l_{eq} \leq 0.95l_B$, Eq.1-24 is linear in R over the range $l_B < R < 10^6 l_B$. In these regimes, this exact solution is numerically equivalent to the expression for the bridging force for spring-like tethers derived using the Derjaguin approximation (Eq.1-7) and exhibits the same scaling behavior.

1.11 Acknowledgements

We thank Carlos Marques for many useful discussions and for furnishing the Monte Carlo data, Elena E. Dormidontova for useful discussions, Alexis Grabbe for providing the electrostatics program, and Joyce C. Wong for assistance with sample preparation. This work was supported by NSF NER DMII-0404457, NSF DMR-0606564, and the France-Berkeley Fund.

1.12 References & Footnotes

1. Lasic, D. and F. Martin, eds. 1995. *Stealth Liposomes*. CRC Press, Boca Raton.
2. Ferrari, M. 2005. Cancer Nanotechnology: Opportunities and Challenges. *Nature Rev. Cancer* 5(3):161–171.
3. Tziampazis, E., J. Kohn, and P. Moghe. 2000. PEG-variant biomaterials as selectively adhesive protein templates: model surfaces for controlled cell adhesion and migration. *Biomaterials*. 21:511–520.
4. Dori, Y., H. Bianco-Peled, S.K. Satija, G.B. Fields, J.B. McCarthy, and M. Tirrell. 2000. Ligand accessibility as means to control cell response to bioactive bilayer membranes. *J. Biomed. Mater. Res. B*. 50(1):75–81.
5. Barber, S.M, P.J. Costanzo, N.W. Moore, T.E. Patten, K.S. Lancaster, C.B. Lebrilla, and T.L. Kuhl. 2006. Bilateral, Difunctional Nanosphere Aggregates and Their Assembly Mediated by Polymer Chains. *J. Phys. Chem. A*, 110(13):4538–4542.
6. Hiddessen, A.L., S.D. Rodgers, D.A. Weitz, and D.A. Hammer. 2000. Assembly of Binary Colloidal Structures via Specific Biological Adhesion. *Langmuir*, 16, 9744–9753.
7. Harris, J.M. and S. Zalipsky. 1997. *Poly(ethylene glycol): Chemistry and Biological Applications*. American Chemical Society: Washington D.C.
8. Photos, P.J., L. Bacakova, B. Discher, F.S. Bates, and D.E. Discher. 2003. Polymer vesicles in vivo: correlations with PEG molecular weight. *J. of Controlled Release*. 90:323–334.
9. Goubault, C., F. Leal-Calderon, J.-L. Viovy, and J. Bibette. 2005. Self-Assembled Magnetic Nanowires Made Irreversible by Polymer Bridging. *Langmuir*. 21(9):3726–3729.
10. Liu, A.P. and D.A. Fletcher. 2005. Photopatterning of Actin Filament Structures. *Nano Lett.* 5(4):625–628.
11. Li, Y., Y.D. Tseng, S.Y. Kwon, L. d’Espaux, J.S. Bunch, P.L. Mceuen, and D. Luo. 2004. Controlled assembly of dendrimer-like DNA. *Nat. Mater.* 3:38–42.
12. Meadows, P.Y. and G.C. Walker. 2005. Force Microscopy Studies of Fibronectin Adsorption and Subsequent Cellular Adhesion to Substrates with Well-Defined Surface Chemistries. *Langmuir*. 21:4096–4107.
13. Allen, T.M. 2002. Ligand-Targeted Therapeutics in Anticancer Therapy. *Nat. Rev. Cancer* 2(10):750–766.
14. Hashida, M, S. Kawakami, and F. Yamashita. 2005. Lipid carrier systems for targeted drug and gene delivery. *Chem. Pharm. Bull.* 53(8): 871–880.
15. Zlatanova, J. 2000. Single molecule force spectroscopy in biology using the atomic force microscope. *Prog. Biophys. Molec. Biol.* 74:37–61.
16. Jeppesen, C., J.Y. Wong, T.L. Kuhl, J.N. Israelachvili, N. Mullah, S. Zalipsky, and C.M. Marques. 2001. Impact of Polymer Tether Length on Multiple Ligand-Receptor

- Bond Formation. *Science*. 293:465–468.
17. Wong, J.Y., T.L. Kuhl, J.N. Israelachvili, N. Mullah, and S. Zalipsky. 1997. Direct Measurement of a Tethered Ligand-Receptor Interaction Potential. *Science* 275:820–822.
 18. Moreira, A.G. and Marques, C.M. 2004. The role of polymer spacers in specific adhesion. *J. Chem. Phys.* 120(13): 6229–6237.
 19. Moreira, A.G., C. Jeppesen, F. Tanaka, and C.M. Marques. 2003. Irreversible vs reversible bridging: when is kinetics relevant for adhesion? *Europhys. Lett.* 62(6):876–882.
 20. Hilgenbrink, A.R. and P.S. Low. 2005. Folate Receptor-Mediated Drug Targeting: From Therapeutics to Diagnostics. *J. Pharm. Sci.*, 94(10): 2135–2146.
 21. Sain, A. and M. Wortis. 2004. Influence of tether dynamics on forced Kramers escape from a kinetic trap. *Phys.Rev.E.* 70:031102.
 22. Bell, G.I. 1978. Models for the Specific Adhesion of Cells to Cells. *Science* 200: 618–627.
 23. Ratto, T.V., R.E. Rudd, K.C. Langry, R.L. Balhorn, and M.W. McElfresh. 2006. Nonlinearly Additive Forces in Multivalent Ligand Binding to a Single Protein Revealed with Force Spectroscopy. *Langmuir* 22: 1749–1757.
 - 23a. Carignano, M.A. and I. Szleifer. 2003. Controlling Surface Interactions with Grafted Polymers. *Interface Sci.* 11(2):187–197.
 24. Manghia, M. and M. Aubouy. 2003. Mobile polymer connectors. *Eur. Phys. J. E* 11:243–254.
 25. Weikl, T.R., and R. Lipowsky. 2001. Adhesion-induced phase behavior of multicomponent membranes. *Phys. Rev. E.* 64:0119031.
 26. Bruinsma, R., A. Behrisch, and E. Sackmann. 2000. Adhesive switching of membranes: Experiment and theory. *Phys. Rev. E.* 61(4):4253–4267.
 27. Lipowsky, R. 1996. Adhesion of Membranes via Anchored Stickers. *Phys. Rev. E.* 77(8):1652–1655.
 28. Zuckerman, D. 1995. Statistical Mechanics of Membrane Adhesion by Reversible Molecular Bonds. *Phys. Rev. Ltrs.* 74(19):3900–3903.
 29. Bao, G. 2002. Mechanics of Biomolecules. *J. Mech. Phys. Solids* 50:2237–2274.
 30. Leckband, D.E. and J. Israelachvili. 2001. Intermolecular Forces in Biology. *Quarterly Rev. Biophys.* 34(2):105–267.
 31. Chang, K.C. and D.A. Hammer. 1996. Influence of Direction and Type of Applied Force on the Detachment of Macromolecularly-Bound Particles from Surfaces. *Langmuir.* 12:2271–2282.
 32. English, T.J. and D.A. Hammer. 2004. Brownian Adhesive Dynamics (BRAD) for Simulating the Receptor-Mediated Binding of Viruses. *Biophys. J.* 86:3359–3372.
 33. Erdmann, T. and U.S. Schwarz. Stochastic dynamics of adhesion clusters under

- shared constant force and with rebinding. 2004. *J.Chem.Phys.* 121(18):8997–9017.
34. Ghaghada, K.B., J. Saul, J.V. Natarajan, R.V. Bellamkonda, and A.V. Annapragada. 2005. Folate targeting of drug carriers: A mathematical model. *J. Cont. Rel.* 104(1):113–128.
 35. Tees, D.F.J., J.T. Woodward, and D.A.Hammer. 2001. Reliability theory for receptor–ligand bond dissociation. *J. Chem. Phys.* 114(17):7483–7496.
 36. Vijayendran, R., D. Hammer, and D. Leckband. 1998. Simulations of the adhesion between molecularly bonded surfaces in direct force measurements. *J. Chem. Phys.* 108 (18):7783–7794.
 37. De Gennes, P. 1979. *Scaling concepts in Polymer Physics.* Cornell Univ. Press, Ithaca.
 38. Evans, E. 1999. Looking inside molecular bonds at biological interfaces with dynamic force spectroscopy. *Biophys. Chem.* 82(2–3):83–97.
 39. In general, $\Delta l = 4 k_B T / |f(l_B)|$, where $f(l) = dU(l) / dl$ is the monotonic stretching force for a single tether, which need not be Hookian. For dilute polymers in good solvents, it follows that $l_B \propto l_{eq} \left(1 + (2W/3k_B T)^{1/2}\right)$. Thus, for freely-jointed chains l_B scales linearly with l_{eq} , which we have verified with our independent numerical model ($R^2 \geq 0.996$ for all parameters in Table 1-3). This predicted scaling of l_B with respect to W agrees with reported Monte Carlo calculations of binding probability curves for multivalent ligands with energies totaling 8, 16, and 24 $k_B T$ for a fixed length of end-grafted PEG ($N = 64$)(40).
 40. Chen, C.-C. and E.E. Dormidontova. 2005. Architectural and Structural Optimization of the Protective Polymer Layer for Enhanced Targeting. *Langmuir* 21:5605–5615.
 41. Wang, R., X. Fang, Y. Lu, and S. Wang. 2004. The PDBbind Database: Collection of Binding Affinities for Protein-Ligand Complexes with Known Three-Dimensional Structures. *J. Med. Chem.* 47, 2977–2980.
 42. Wang, R., X. Fang, Y. Lu, C.-Y. Yang, and S. Wang. 2005. The PDBbind Database: Methodologies and Updates. *J. Med. Chem.* 48:4111–4119.
 43. The bond dissociation equilibrium constant and energy are related by $K_d = \exp(-W/k_B T)$ (22).
 44. Shull, K.R. 2002. Contact mechanics and the adhesion of soft solids. *Mat. Sci. Engr. R* 36(1):1–45.
 45. $R = R_1 R_2 / (R_1 + R_2)$ for two interacting spheres with radii R_1 and R_2 , respectively (54). For a sphere interacting with a flat surface, R reduces to the sphere radius. For liposomes ($R_1 \sim 100$ nm) targeting a cell ($R_2 \sim 10$ μ m), the interaction radius is $R = 99$ nm $\approx R_1$.
 46. Although here “grafting density” refers to the areal density of tethers, it can be replaced by the areal density of receptors without complication. Such a substitution would be appropriate if the receptors were the limiting reagent.

47. Lasic, D.D. and D. Needham. 1995. The “Stealth” Liposome: A Prototypical Biomaterial. *Chem. Rev.* 95(8):2601–2628.
48. Reddy, J.A., C. Abburi, H. Hofland, S.J. Howard, I. Vlahov, P. Wils, and C.P. Leamon. 2002. Folate-targeted, cationic liposome-mediated gene transfer into disseminated peritoneal tumors. *Gene Ther.* 9:1542–1550.
49. Lim, T.-C. 2003. Spring constant analogy for estimating stiffness of a single polyethylene molecule. *J. Math. Chem.* 34(3–4):151–161.
50. For dilute polymers in good solvents, $k \approx 3 k_B T / l_{eq}^2$ and $l_{eq} \approx a \times N^{3/5}$ or “Flory radius”; a = mer length, N = number of mers per tether) (37).
51. Derjaguin, B.V. 1934. Friction and adhesion. IV. The theory of adhesion of small particles. *Kolloid Zeits.* 69, 155–164.
52. Chan, D.Y.C. and R.G. Horn. 1985. The Drainage of Thin Liquid Films Between Solid Surfaces. *J. Chem. Phys.* 83:5311–5324.
53. Bongrand, P. 1999. Ligand–receptor interactions. *Rep. Prog. Phys.* 62:921–968.
54. Pincet, F. and J. Husson. 2005. The Solution to the Streptavidin-Biotin Paradox: The Influence of History on the Strength of Single Molecular Bonds. *Biophys. J.* 89: 4374–4381.
55. Sheth, S.R. and D. Leckband. 1997. Measurements of attractive forces between end-grafted poly(ethylene glycol) chains. *Proc. Natl. Acad. Sci. U.S.A.* 94:8399–8404.
56. Israelachvili, J.N. AND E. Gayle. 1978. Measurement of Forces between Two Mica Surfaces in Aqueous Electrolyte Solutions in the Range 0-100 nm. *J. Chem. Soc., Farad. Trans. 1*, 74:975–1001.
57. Israelachvili, J. N. *Intermolecular & Surface Forces*, 2e. Academic Press, San Diego: 1992.
58. Grabbe, A. 1993. Double Layer Interactions between Silylated Silica Surfaces. *Langmuir.* 9:797–801.
59. Efremova, N.V., B. Bondurant, D.F. O’Brien, and D.E. Leckband. 2000. Measurements of Interbilayer Forces and Protein Adsorption on Uncharged Lipid Bilayers Displaying Poly(ethylene glycol) Chains. *Biochemistry* 39:3441–3451.
60. Vinogradova, O.I. and R.G. Horn. 2001. Attractive Forces between Surfaces: What Can and Cannot Be Learned from a Jump-In Study with the Surface Forces Apparatus? *Langmuir* 17:1604–1607.
61. Gabizon, A., A.T. Horowitz, D. Goren, D. Tzemach, F. Mandelbaum-Shavit, M.M. Qazen, and Samuel Zalipsky. 1999. Targeting Folate Receptor with Folate Linked to Extremities of Poly(ethylene glycol)-Grafted Liposomes: In Vitro Studies. *Bioconj. Chem.* 10:289–298.
62. Wieland, J.A., A.A. Gewirth, and D.E. Leckband. 2005. Single-Molecule Measurements of the Impact of Lipid Phase Behavior on Anchor Strengths. *J. Phys. Chem. B.* 109:5985–5993.

63. Marrink, S.J., O.Berger, P. Tieleman, and F.Jähnig. 1998. Adhesion Forces of Lipids in a Phospholipid Membrane Studied by Molecular Dynamics Simulations. *Biophys.J.* 74:931–943.
64. Uster a, P.S., T.M. Allen, B.E. Daniel, C.J. Mendez, M.S. Newman, and G.Z. Zhu. 1996. Insertion of poly(ethylene glycol) derivatized phospholipid into preformed liposomes results in prolonged in vivo circulation time. *FEBS Lett.* 386(2–3):243–246.
65. Ashok, B., L. Arleth, R.P. Hjelm, I. Rubinstein, and H. Önyüksel. 2004. In Vitro Characterization of PEGylated Phospholipid Micelles for Improved Drug Solubilization: Effects of PEG Chain Length and PC Incorporation. *Pharm Sci.* 93(10):2476–2487.
66. Chen, T., L.R. Palmer, D.B. Fenske, A.M.I. Lam, K.F. Wong, and P.R. Cullis. 2004. Distal Cationic Poly(Ethylene Glycol) Lipid Conjugates in Large Unilamellar Vesicles Prepared by Extrusions Enhanced Liposomal Cellular Uptake. *J. Liposome Res.* 14(3&4): 155–173.
67. Lee, R.J. and P.S. Low. 1994. Delivery of Liposomes into Cultured KB Cells via Folate Receptor-mediated Endocytosis. *J.Biological Chemistry.* 269(5): 3198–3204.
68. Kamen, B.A., M.-T. Wang, A.J. Streckfuss, X. Peryea, and R.G.W. Anderson. 1988. Delivery of folates to the cytoplasm of MA104 cells is mediated by a surface membrane receptor that recycles. *J. Biol. Chem.* 263:13602–13609.
69. Lu, Y. and P.S. Low. 2002. Folate-mediated delivery of macromolecular anticancer therapeutic agents. *Adv. Drug Deliv. Rev.* 54:675–693.
70. Shao, J.Y. and R.M. Hochmuth. 1999. Mechanical Anchoring Strength of L-Selectin, b2 Integrins, and CD45 to Neutrophil Cytoskeleton and Membrane. *Biophys. J.* 77:587–596.
71. Evans, E. A. Leung, D. Hammer, and S. Simon. 2001. Chemically distinct transition states govern rapid dissociation of single L-selectin bonds under force. *Proc. Natl. Acad. Sci. U.S.A.* 98(7): 3784–3789.
72. Fritz, J., A.G. Katopodis, F. Kolbinger, and D. Anselmetti. 1998. Force-mediated kinetics of single P-selectin/ligand complexes observed by atomic force microscopy. *Proc. Natl. Acad. Sci. U.S.A.* 95: 12283–12288.
73. Isacke, C.M. and M.A. Horton. 2000. *Adhesion Molecule Facts Book.* Academic Press, San Diego.
74. Pincet, F., E. Perez, G. Bryant, L. Lebeau, C. Mioskowski. 1994. Long-Range Attraction Between Nucleotides with Short-Range Specificity: Direct Measurements. *Phys. Rev. Lett.* 73(20): 2780–2783.
75. Guttenberg, Z., A. R. Bausch, B. Hu, R. Bruinsma, L. Moroder, and E. Sackmann. 2000. Measuring Ligand-Receptor Unbinding Forces with Magnetic Beads: Molecular Leverage. *Langmuir* 16, 8984–8993.
76. Jost, C.R., J.A. Titus, I. Kurucz and D.M. Segal. 1996. A Single-chain Bispecific Fv2 Molecule Produced in Mammalian Cells Redirects Lysis Activated by CTL.

- Molec.Immun. 33(2):211–219.
77. Vajda, S., Z. Weng, R. Rosenfeld, and C. DeLisi. 1994. Effect of Conformational Flexibility and Solvation on Receptor-Ligand Binding Free Energies. *Biochem.* 33:13977–13988.
 78. Ros, R., F. Schwesinger, D. Anselmetti, M. Kubon, R. Schäfer, A. Plückthun, and L. Tiefenauer. 1998. Antigen binding forces of individually addressed single-chain Fv antibody molecules. *Proc. Natl. Acad. Sci. U.S.A.* 95:7402–7405.
 79. Hinterdorfer, P. W. Baumgartner, H.J. Gruber, K. Schilcher, and H. Schindler. 1996. Detection and localization of individual antibody-antigen recognition events by atomic force microscopy. *Proc. Natl. Acad. Sci. U.S.A.* 93:3477–3481.
 80. Torreggiani, A. and G. Fini. 1998. The Binding of Biotin Analogues by Streptavidin: A Raman Spectroscopic Study. *Biospectroscopy* 4(3):197–208.
 81. Leckband, D.E., Müller, W., F.J. Schmitt, and H. Ringsdorf. 1995. Molecular mechanisms determining the strength of receptor-mediated intermembrane adhesion. *Biophys.J.* 69:1162–1169.
 82. Chiou, C-H. and G.-B. Lee. 2005. A micromachined DNA manipulation platform for the stretching and rotation of a single DNA molecule. *J. Micromech. Microeng.* 15:109–117.
 83. Gerland, U., R. Bundschuh, and T. Hwa. 2003. Mechanically Probing the Folding Pathway of Single RNA Molecules. *Biophys. J.* 84: 2831–2840.
 84. Rief, M., F. Oesterhelt, B. Heymann, and H.E. Gaub. 1997. Single Molecule Force Spectroscopy on Polysaccharides by Atomic Force Microscopy. *Science* 275:1295–1297.
 85. Li H.B., M. Rief, F. Oesterhelt, and H.E. Gaub. 1998. Single-molecule force spectroscopy on xanthan by AFM. *Adv. Mater.* 10:316–319.
 86. Park, E.Y.H., M.J. Smith, E.S. Stropp, K.R. Snapp, J.A. DiVietro, W.F. Walker, D.W. Schmidtke, S.L. Diamond, and M.B. Lawrence. 2002. Comparison of PSGL-1 Microbead and Neutrophil Rolling: Microvillus Elongation Stabilizes P-Selectin Bond Clusters. *Biophys. J.* 82:1835–1847.
 87. Singer, W., M.Frick, T. Hallery, S. Bernet, M. Ritsch-Marte, and P. Dietly. 2003. Mechanical Forces Impeding Exocytotic Surfactant Release Revealed by Optical Tweezers. *Biophys. J.* 84: 1344–1351.
 88. Li H.B., Zhang W.K., Xu W.Q., and X. Zhang. 2000. Hydrogen bonding governs the elastic properties of poly(vinyl alcohol) in water: single-molecule force spectroscopic studies of PVA by AFM. *Macromolecules* 33:465–9.
 89. Ortiz C, and G. Hadziioannou. 1999. Entropic elasticity of single polymer chains of poly(methacrylic acid) measured by atomic force microscopy. *Macromolecules* 32:780–7.
 90. Zhang, W., S. Zou, C.Wang, and X. Zhang. 2000. Single Polymer Chain Elongation of Poly(N-isopropylacrylamide) and Poly(acrylamide) by Atomic Force Microscopy.

- J. Phys. Chem. B, 104:10258–10264.
91. Anne, A. C. Demaille, and J. Moiroux. 1999. Elastic Bounded Diffusion. Dynamics of Ferrocene-Labeled Poly(ethylene glycol) Chains Terminally Attached to the Outermost Monolayer of Successively Self-Assembled Monolayers of Immunoglobulins. *J. Am. Chem. Soc.*, 121:10379–10388.
 92. Maaloum, M. and A. Courvoisier. 1999. Elasticity of Single Polymer Chains. *Macromolecules*, 32, 4989–4992.
 93. Pedersen, J. S. and P. Schurtenberger. 1999. Static properties of polystyrene in semidilute solutions: A comparison of Monte Carlo simulation and small-angle neutron scattering results. *Europhys. Lett.* 45(6):666–672.
 94. Leckband, D.E., J.F.-J. Schmitt, J.N. Israelachvili, and W. Knoll. 1994. Direct Force Measurements of Specific and Nonspecific Protein Interactions. *Biochemistry* 33, 4611–4624.
 95. Kellermayer, M.S.Z., S.B. Smith, H.L. Granzier, and C. Bustamante. 1997. Folding-Unfolding Transitions in Single Titin Molecules Characterized with Laser Tweezers. *Science* 276:1112–1116.
 96. Ratkowsky, D.A. 1990. *Handbook of Nonlinear Regression Models*. Marcel Dekker, New York. Eq.5.3.1.

Chapter 2: Bimodal Polymer Mushrooms: Compressive Forces and Specificity toward Receptor Surfaces

Reproduced with permission from Moore, N.W. and T.L. Kuhl. Langmuir, 2006, 22(20):8485–8491. Copyright 2006 American Chemical Society.

2.1 Abstract

End-grafted poly(ethylene glycol) (or PEG) polymer chains are used to extend the in vivo circulation time of targeted liposomes and nanoparticles; however, the most efficacious structure for also imparting high target specificity remains unknown. Using the surface forces apparatus, we have measured the specific and nonspecific forces between bimodal mixtures of grafted polymer mushrooms and model receptor surfaces. Specifically, supported lipid membranes anchoring 2000- or 5000- Dalton (D) PEG with a controlled fraction of PEG-2000 bearing biotin ligands were compressed against opposing streptavidin surfaces. The presence of the longer 5,000 Da chain increased the steric repulsion of the bimodal mushroom layer and thus decreased the net adhesive force when shorter chains were ligated. However, the 5,000 Da chain did not detectably alter the distance where ligand-receptor binding occurs and adhesion begins. This latter result is in good agreement with theoretical predictions based on summing the repulsive steric and attractive bridging forces. Further, all ligated structures adhered to receptors under both static and dynamic fluid flow conditions. The dynamic movement of the flexible PEG tethers permitted ligand-receptor bonds to form far beyond the equilibrium edge of the bimodal mushroom layer. This work demonstrates that liposome targeting should be enhanced by grafting ligands to liposomes with a tether that has a contour length longer than the equilibrium height of the bimodal mushroom layer.

2.2 Introduction

A primary goal of drug targeting is to engineer drug delivery vehicles with high specificity, that is, with a high affinity for targets and a low affinity for nontargets. There are many surface functionalization strategies for imbuing liposomes (or nanoparticles) with a high affinity for various known targets, most notably by attaching specific ligands to the liposome surface^{1,2}. It has also been established that affinities for nontargets may be reduced by coating liposomes with grafted poly(ethylene glycol) (or PEG) polymer chains³. However, the dual goals of maximizing adhesion to targets and minimizing nonspecific adhesion may prescribe different polymer architectures, and the most efficacious structure for doing both remains unknown⁴. For example, a study by Blume et al. showed that liposomes had the greatest circulation time *in vivo* when the ligand was deeply buried in the polymer layer (close to the liposome bilayer), but that these architectures bound to targets less frequently⁵. Thus, a useful structure may be a bimodal mixture of grafted PEG chains: a fraction bearing ligands to target the liposome and a fraction without ligands to minimize adhesion to nontargets⁵⁻⁷. However, the ideal structure of such a bimodal coating of PEG remains debated. Specifically, should the ligated PEG chains be shorter than, longer than, or the same length as those PEG chains that do not bear ligands, and in what concentrations?

At issue is how these polymer architectures modulate the specific and nonspecific forces involved in targeting biological surfaces. In thermodynamic terms, PEG chains grafted at a spacing just less than their radius of gyration are in the mushroom phase⁸⁻¹⁰ and stochastically sample conformations that put their distal end much farther away than their equilibrium end-to-end distance¹¹⁻¹⁴. An approaching surface or protein confines these chains, producing an osmotic repulsion that inhibits adhesion or protein adsorption

and renders liposomes nonimmunogenic¹⁵⁻¹⁷. The conformational sampling / chain motion can also be harnessed to increase ligand accessibility for more effective targeting. Therefore, we are interested in defining the compressive steric forces in bimodal mushroom architectures and the impact of architecture on specific bridging forces.

Force laws for compressing polymers in the closely packed “brush” regime have been well characterized both experimentally and theoretically for both bimodal¹⁸⁻²⁴ and monomodal^{15,19,25-29} architectures. Likewise, force laws between more widely spaced polymer “mushrooms” that are monomodal have been studied experimentally^{22,30-34} and theoretically^{28,35-40}. There have also been theoretical descriptions for compressing polydisperse polymer mushrooms³² and brushes²⁴. However, quantitative experimental measurements and comparisons are limited, especially for short grafted chains as investigated here.

As for specificity, polymer chains bearing ligands are able to bind to complementary receptors on an opposing surface. Once bound, the entropic motion of individual tethers produces a spring-like force that attracts bridged surfaces^{12-14,41,42}, compressing the polymer layer until a mechanical equilibrium is reached^{6,28}. The net achievement of these “entropical forests” is then a long-range attraction and a shorter-range repulsion between surfaces they bridge. In many situations these forces extend beyond the influence of attractive van der Waals or repulsive electrostatic forces and thus dictate the adhesive properties^{11,28,43,44}. For example, it has been shown that grafting 2000-Dalton PEG prevents liposomes from attaching specifically to model targets when the ligand is hidden inside the polymer layer on a relatively short tether (10–12 Å)^{5,22}. Thus, successfully targeting these liposomes may require tethers that are considerably

longer. Likewise, Monte Carlo simulations with ligated PEG tethers of fixed length (64 mers) and variable lengths for neighboring, non-reactive PEG suggest the existence of an optimum ratio of lengths for polymers in the bimodal mixture, which in principle might also depend on their grafting density, ligand-ligand and ligand-polymer interactions, receptor concentration and accessibility, and other *in situ* conditions⁶. Thus, it remains to be determined how long the ligated tethers should be, how long the non-ligated chains should be, and in what concentrations. Also unresolved is the role that the longer, non-ligated chains in a bimodal architecture may have on the kinetics or strength of this specific bridging for polymer lengths of interest, for example, if neighboring chains may entangle⁴⁵ or sterically reduce the ligands' access to receptors.

To quantify the interactions of bimodal mixtures of PEG with receptor surfaces, we used the surface forces apparatus (SFA) with bimodal and monomodal mixtures of grafted polymers. In particular, we measured the forces induced against an opposing receptor surface during the surfaces' approach and separation. Both ligated and non-ligated polymer mixtures were studied to separate specific from non-specific forces. For the ligated architectures, we also quantified the capture distance where significant cross-bridge formation first occurred during the approach. With these measurements, our goal is to further elucidate molecular features of the polymer layer that are important for designing targeted liposomes.

2.3 Materials

Hereon the subscript in PEG_x refers to the chain molecular weight of a single component. PEG_x was purchased pre-conjugated to DSPE lipid and to the biotin ligand where indicated (Fig.1B). The following high purity lipids and lipid conjugates (>99%)

were purchased from Avanti Polar Lipids (APL; Alabaster, AL) and Northern Lipids (NL; Vancouver, British Columbia, Canada): dipalmitoylphosphatidylethanolamine (DPPE, Lot#160PE-81), dilauroylphosphatidylethanolamine (DLPE, Lot#120PE24), distearoylphosphatidylethanolamine (DSPE, Lot#180PE62), DSPE-poly(ethylene glycol)(PEG MW = 2000) (DSPE-PEG₂₀₀₀), DSPE-poly(ethylene glycol)(PEG MW = 2000)-biotin (DSPE-PEG₂₀₀₀-biotin, APL Lot#180PEPEG2Bio-14, NL Lot#AL11203601), and DSPE-poly(ethylene glycol)(MW5000) (DSPE-PEG₅₀₀₀, Lot#180PEG5PE-26). *N*-((6-(biotinoyl)amino)hexanoyl)-1,2-dihexadecanoyl-*sn*-glycero3-phosphoethanolamine, triethylammonium salt (biotin-X DHPE, Lot#45311) was purchased from Molecular Probes (Eugene, OR). Streptavidin was purchased from Pierce Biotechnology (Rockford, IL) (Lot#GC94900). Octadecyltrichlorosilane (OTS) and all salts were of high purity (>99.5%) and were purchased from Sigma-Aldrich (St. Louis, MO). Water was purified with a Millipore Milli-Q filtration system (Billerica, MA). HPLC grade methanol and chloroform were from Fisher Scientific (Pittsburgh, PA). 6- μ m streptavidin-coated silica microspheres were from Bang's Laboratories (Fishers, IN) (Lot#553313).

2.4 Methods

2.4.1 Bimodal Architectures

Various mixtures of two PEG chain lengths were studied—some with ligands, some without, and some longer than others—by incorporating them in defined ratios into supported lipid membranes. The properties of the polymer portion of the DSPE-PEG_x-biotin used are listed in Table 2-1. The compositions of the five polymer mixtures studied are listed in Table 2-2.

Table 2-1. Properties of the PEG chains studied.

Abbreviation	MW ^a	N ^b	L (Å) ^b	R_f (Å) ^b	τ_{zimm} (ns) ^c
2k	2000	45	159	35	9
5k	5000	113	397	60	46

^a molecular weights, excluding the DSPE or biotin portions of the conjugates used ^b The polymerization index (N) was used with the average length per mer ($a = 3.5$ Å) to estimate the chain length ($L = a \times N$) and Flory radius ($R_f = a \times N^{0.6}$) ¹⁰. For grafting densities greater than the overlap concentration, grafted polymer chains will tend to extend further away than R_f to decrease chain crowding and increase solvent contact. ^c The characteristic relaxation time of these polymers was estimated as $\tau_{zimm} \approx \mu R_f^3 / kT$, where μ is the solvent viscosity, k is the Boltzmann constant, and T is temperature ¹⁰.

Table 2-2. Molar compositions (%) of the polymer-anchoring lipid leaflets.

	architecture				
	5k-2kB	2k-2kB	2kB	5k-2k	2k
DSPE-PEG ₅₀₀₀	3%	---	---	3%	---
DSPE-PEG ₂₀₀₀	---	3%	---	2%	5%
DSPE-PEG ₂₀₀₀ -biotin	2%	2%	5%	---	---
DSPE	95%	95%	95%	95%	95%

In the 5k-2kB mixture, 60% of the grafted chains were 2.5 times longer than the chains that bore ligands. In the 2k-2kB mixture, all polymers were the same length, and again only 40% bore ligands. In the 2kB case, all polymers were the same length and all bore ligands. No ligands were present in the 5k-2k and 2k cases. In all cases, the fraction of lipids in the leaflet anchoring polymers totaled 5% so that the polymer layer remained

in the weakly-overlapping mushroom regime. The net surface grafting density of polymer was always $\sigma = 1.19 \times 10^5$ PEG chains per μm^2 to mimic typical grafting densities of targeted liposomes³⁰. To ensure statistical validity, each architecture was prepared between two and five times in independent experiments, with multiple measurements possible in different regions of each sample, as described below.

2.4.2 Substrate Preparation

Supported lipid bilayers were prepared by Langmuir-Blodgett (LB) deposition using a Wilhelmy trough (Nima Technology Ltd., Coventry, UK) as described elsewhere⁸. All preparations were carried out in a laminar flow box (Labconco, Kansas City, MO). Lipids were dissolved in 9:1 chloroform/methanol at a concentration of ~ 1 mg/mL. Fig.2-1 shows a schematic of the receptor and ligand surfaces constructed for this study. A close-packed, solid phase inner monolayer of DPPE ($\sim 43 \text{ \AA}^2$ per molecule, $\Pi = 40 \text{ mN/m}$) was deposited onto molecularly smooth, back-silvered mica substrates glued onto silica disks by pulling the substrates up through a compressed DPPE monolayer at the air-water interface. Afterward, the DPPE-coated mica substrates were allowed to air-dry overnight. For the tethered ligand surface, a mixture of DSPE, biotin-PEG_x-DSPE, and/or PEG_x-DSPE was then deposited by passing the DPPE coated substrates down through the monolayer film ($\sim 43 \text{ \AA}^2$ per molecule, $\Pi = 40 \text{ mN/m}$) to form the outer leaflet of the membrane. Subsequently, the membrane-coated surfaces were kept under water. All measurements were conducted in phosphate buffer containing 0.5 mM Na^+ at pH 7.2. The buffer was saturated with DSPE to prevent solubilization of the bilayer. Lateral diffusion of lipids was minimized by operating at $25 \pm 0.2 \text{ }^\circ\text{C}$, which is below the phase transition temperature of the lipid bilayers.

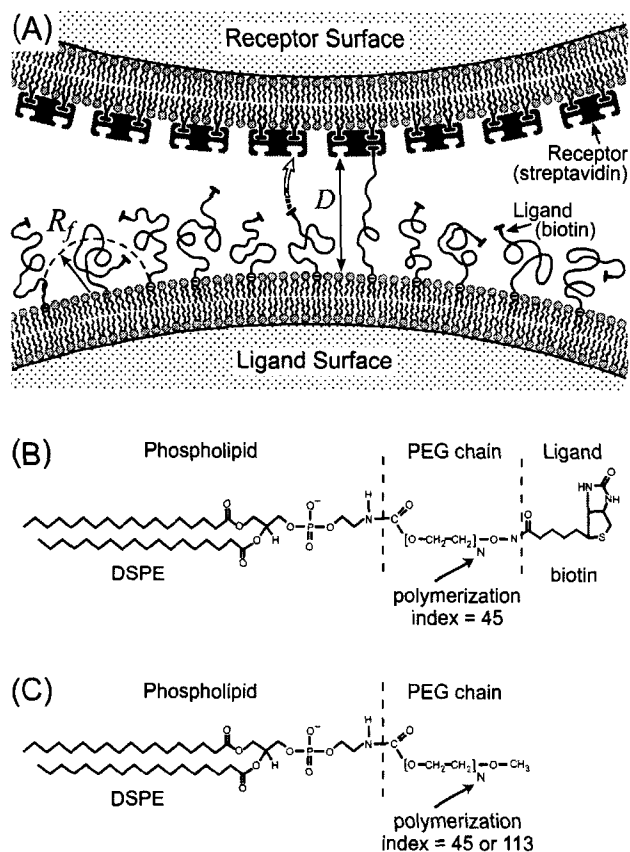


Figure 2-1. (A) Schematic of the experiments in the SFA. Shown as an example is a monomodal grafting of PEG ligated with biotin and positioned at a distance (D) from the receptor surface. Here the chains are grafted apart at a distance near their Flory radius (R_f). The receptor pockets of streptavidin are parallel to the upper supported membrane. The surface curvature is exaggerated for clarity (typically the interaction radius is ~ 1 cm). Shown also are the chemical structures of PEG-lipids used in these studies: (B) ligated 2kB and (C) non-ligated 2k and 5k.

2.4.3 Receptor Architecture

The high-affinity ligand-receptor pair biotin-streptavidin was utilized in these studies (binding energy of 88 kJ/mol or $\sim 35 kT$ per bond)⁴⁶⁻⁵¹. Although biotin and streptavidin are not cellular adhesion molecules, their high binding affinity is ideal for studies on the effect of flexible tethers in ligand-receptor binding and complementary adhesion, since the off-rate or back-reaction is minimized. Likewise, the small size of biotin (MW = 234 D) is less likely to perturb the sampling of the polymer chains.

Commonly used targeting ligands such as folic acid (MW = 441 D) or the GRGDSP motif of fibronectin (MW = 569 D) also have relatively low molecular weights and similar molecular dimensions⁵² (for more examples see Table 1-1).

The preparation of oriented monolayers of streptavidin has been described previously^{49,53}. Briefly, streptavidin was assembled by specific adsorption onto a supported lipid bilayer where the outer leaflet was a mixture of DLPE and 5 mol % DHPE-X-biotin, a lipid conjugate where biotin is coupled to DHPE via a thirteen-carbon spacer, ($\sim 43 \text{ \AA}$ per molecule, $\Pi = 35 \text{ mN/m}$). After deposition of the mixed DLPE:DHPE-X-biotin outer leaflet, the membrane was removed under water from the Wilhelmy trough and incubated with streptavidin at a concentration of 0.05 mg/mL in phosphate buffer for a minimum of 3 h. The coverage of streptavidin using this adsorption method has previously been determined to be $\sim 3600 \text{ \AA}^2$ per streptavidin, or 79% of the bilayer surface³¹. The receptor grafting density was comparable to the ligand grafting density, and comparable to reported expressions of folate receptors on tumor cells^{54,55}.

2.4.4 Force-Distance Measurements

The surface forces apparatus (SFA) technique has been used extensively to measure interaction forces between surfaces^{56,57}. Unlike the AFM technique, the SFA provides a definitive reference for the surface separation ($\pm 2 \text{ \AA}$) and quantitative information on the interactions of an entire ensemble of chains ($\sim 10^8$), ensuring statistical significance without the need for complicated analysis. A Mark II SFA was utilized in these studies. One surface was mounted on a fixed support, while the other was mounted on a double-cantilever spring, displaceable vertically by a micrometer screw (Fig.2-1A). The silver layer on each disk partially transmits light directed normally through the

surfaces but also constructively interferes such that distances between the surfaces can be measured by observation of the displacement of fringes of equal chromatic order (FECO) within a spectrometer⁵⁶⁻⁸. The uncertainty in measuring forces with this technique is typically $\pm 10\%$.

In the force-distance curves shown in this study, D is defined as the distance between the outer edge of the streptavidin receptor and the outer lipid leaflet on the opposing ligated surface as shown in Fig.2-1A. This reference frame was determined at the end of each experiment by draining the buffer from the SFA with the surfaces well separated. This process removes the outer monolayers of the assembled bilayers. After draining, the surfaces were brought into contact and the thickness change was measured with interferometry. Known thicknesses for DSPE, DLPE, and streptavidin allow the remainder to be ascribed to the PEG chains⁵³. The surfaces were then dried *in situ* with a stream of dry nitrogen or 0.2 μm -filtered air and subsequently treated with UV light to vaporize the DPPE monolayers remaining on each surface. The surfaces were then re-contacted and the polymer thickness recalculated independently.

2.4.5 Capture Distance Measurements

As in Chapter 1, we define the capture distance (D_B) as the distance during surface approach at which surfaces jump into contact. This mechanical instability occurs when the gradient of the interaction force exceeds the spring constant of the measuring spring in the SFA⁵⁹. It has been shown that D_B is a reasonable estimate of the extension at which cross-bridge formation becomes favorable for a single polymer tether^{12,43}. This is because for a single tether the transition from the bound to the unbound state occurs over a very small range in the surface separation ($\sim 3 \text{ \AA}$ for PEG₂₀₀₀ bearing biotin against

streptavidin, or $\sim 2\%$ of the tether length)¹². Thus, when many such molecules decorate curved surfaces, near the capture distance the attractive polymer bridging force increases extremely rapidly compared to the repulsive steric and electrostatic forces. Consequently, for the parameters of interest, the measurement of D_B does not depend strongly on either the cantilever spring constant or the interaction radius of the substrates⁴³. Conveniently, the capture distance should therefore represent the distance at which a targeted liposome or other particle will spontaneously adhere to its target.

Three nonidealities in the experiment were corrected for as follows. First, in a typical experiment the surfaces are approached stepwise with steps $\Delta D \approx 15$ Å. This means that on average the capture distance (D_B) would be overestimated by a value equal to $\Delta D/2$. Thus, $\Delta D/2$ was subtracted from the D_B measured for each case. Second, it would seem improbable for the capture distance to be greater than the polymer length (L). Thus, capture distances greater than $L + \Delta D/2$ were classified as outliers and ignored in computing statistical averages. As this tended to occur in the minority of measurements ($\sim 25\%$ of the time) and in seemingly random fashion, we attributed these occurrences to over-stepping of the surface separation, which was controlled manually by a simple on/off switch that actuated a motor on the SFA. Third, because surface damage may occur after the surfaces have contacted (due to pull-out of the lipid anchors), only capture distances from the first approaches were averaged.

2.4.6 Statistical Methods

Because our method only allows the polymer thickness to be measured once per sample, each architecture was prepared and characterized in 2–5 independent experiments, with multiple force measurements made in different regions of each sample,

and occasionally with different operators to reduce bias. Uncertainties in calculating capture distances were propagated in the usual way, and can be attributed to stepping the surface separation ($\pm 2\text{--}8 \text{ \AA}$), measuring the polymer layer thickness ($\pm 3\text{--}10 \text{ \AA}$), and other effects that produced random variation, such as is present in all experimental endeavors ($\pm 17\text{--}20 \text{ \AA}$, 95% CI calculated with Student's t distributions).

Before compression force profiles were fitted, electrostatic repulsion was subtracted by fitting data in the electrostatic regime ($D > 100 \text{ \AA}$) to: $F = (\pi R \sigma_e^2 / \epsilon \epsilon_0 \kappa) e^{-\kappa D}$, where σ_e is the surface charge density (assumed constant), κ^{-1} is the Debye length, ϵ is the permittivity, and ϵ_0 is the permittivity of a vacuum¹⁵. This expression adequately represented the electrostatic force to $\pm 0.5 \text{ mN/m}$, as compared to numerical solution of the nonlinear Poisson-Boltzmann equation using a computer program kindly provided by Alexis Grabbe⁶⁰. The semi-quantitative choice of cutoff distance ($D > 100 \text{ \AA}$) dominated the error in fitting, which we account for in the reported uncertainties. For the non-ligated surfaces, the uncertainty in measuring D ($\pm 4.1 \text{ \AA}$ and $\pm 6.5 \text{ \AA}$ for 5k-2k and 2k, respectively), which arose primarily from measuring the thickness of the polymer layers under compression, was also incorporated into reported uncertainties of fitted parameters.

2.4.7 Flow Adhesion Assay

To determine how the bimodal structure affects adhesion under flow (and to mimic targeted liposomes *in vivo*), the same architectures studied here were coated onto standard microscope slides hydrophobized with octadecyltrichlorosilane (OTS), incubated with 6- μm streptavidin-coated silica microspheres, and sheared in a standard

parallel-plate flow chamber. This procedure, which was repeated thrice for each biotinylated architecture and twice for each of 5k-2k and 2k, was also performed using DSPE- and OTS-coated substrates.

2.5 Results and Discussion

Fig.2-2 shows an example of a measured force vs distance profile, for the bimodal 5k-2kB mixture interacting with streptavidin. When the surface separation was much greater than the length of the tether ($D \gg 159 \text{ \AA}$), a screened electrostatic repulsion consistent with the buffer electrolyte concentration and known surface charge density was observed. As the surfaces approached, a discontinuity in the data was observed near the capture distance (D_B) where the surfaces “jumped” into adhesive contact, typically within ~ 1 s. The large attractive force that produced this movement can be attributed to specific bridging between the surfaces^{12,42}. Upon closer approach, a strong steric repulsion was measured as the polymer layers were compressed. Upon withdrawing the surfaces, a comparable steric repulsion was followed by a regime where once again the attractive (negative) bridging force dominated until the pull-off force (F_{adh}) was reached and the surfaces jumped apart. This pull-off force generally corresponded to a minimum (most negative) in the force profile, as exemplified in Fig.2-2.

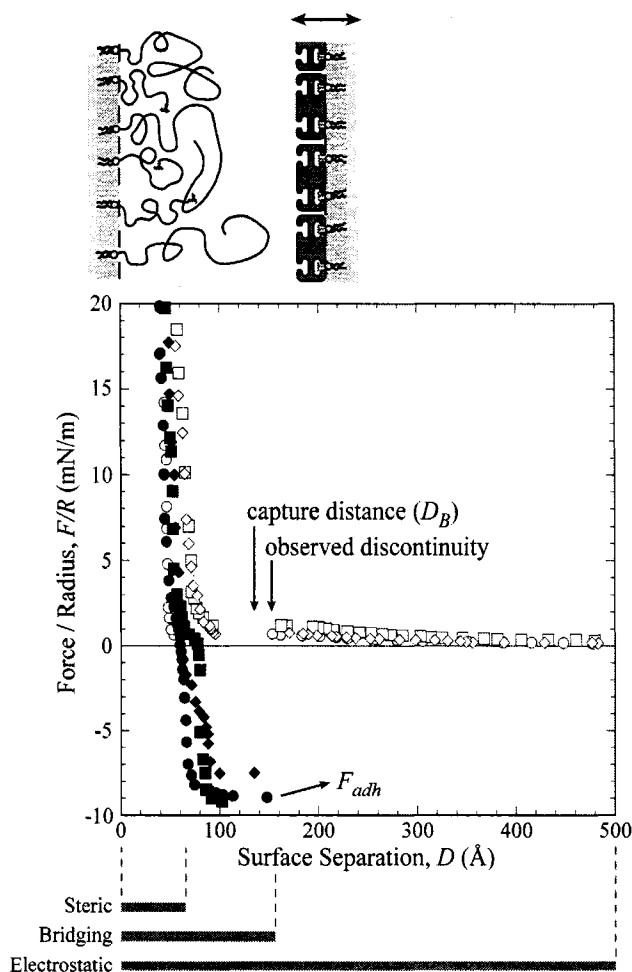


Figure 2-2. Examples of force vs distance profiles for a bimodal mixture of grafted PEG ligated with biotin (here 5k-2kB) interacting with a streptavidin-coated membrane. Shown are successive approaches (\circ , \square , \diamond) and withdrawals (\bullet , \blacksquare , \blacklozenge). Arrows mark discontinuities in the measurements due to instability of the cantilever spring. During approach, this measured discontinuity is always slightly greater than the actual capture distance (D_B) due to incremental stepping of the surface separation. During withdrawal, the force at the instability was defined as the adhesive pull-off force (F_{adh}). Above graph: Schematic of the ligated 5k-2kB bimodal surface (left) and movable receptor surface (right) used in these measurements. Below graph: Distance regimes over which each force is significant. For distances below D_B , both steric and bridging forces have significant magnitudes. Beyond D_B , electrostatic repulsion dominates the force landscape.

In contrast, Fig.2-3 shows an example of a force vs distance profile for a non-ligated bimodal architecture (5k-2k). Here no adhesion was observed, only electrostatic and steric repulsion as surfaces were approached and then compressed. However,

significant hysteresis in the force profile for 5k-2k was observed (Fig.2-3 inset); that is, the force during surface separation was less than that during approach for a given surface separation. A detailed explanation of this phenomenon is beyond the scope of this paper. Proposed explanations include hydrophobic or bridging interactions from protein unfolding, nonspecific adhesion of PEG to streptavidin, transformation of the PEG backbone into the less ordered gauche configuration, compression induced phase segregation, and electrostatic attraction between streptavidin and ions chelated by PEG^{31,61,62}.

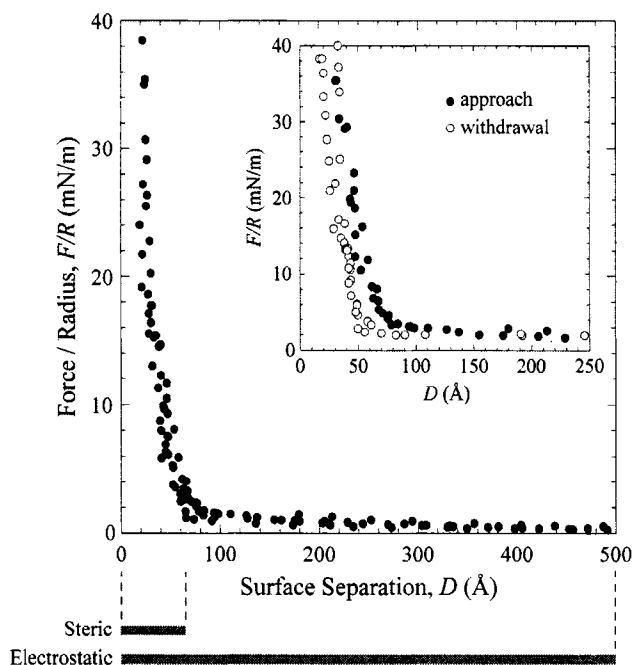


Figure 2-3. Example of a force vs distance profile for the compression of a non-ligated, bimodal mixture of grafted PEG (here 5k-2k) interacting with a streptavidin-coated membrane. The superimposed measurements of the force during approach show a consistent steric repulsion (positive force). The regime where this force dominates (marked below graph) is short-range compared to the electrostatic repulsion between opposing membranes. In contrast to the ligated surface shown in Fig.2-2, a bridging force was not observed. Inset: Superposition of examples of surface approach (●) and withdrawal (○), showing hysteresis during compression/decompression of the non-functionalized polymer layers.

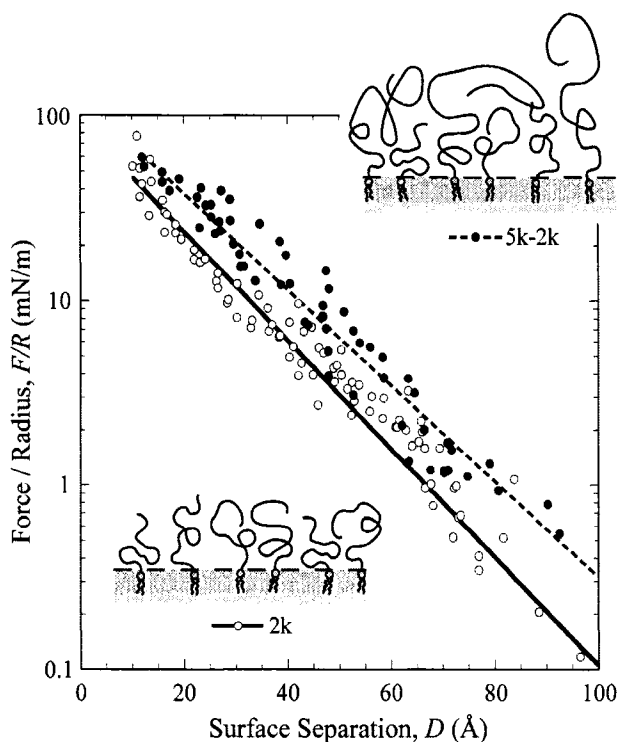


Figure 2-4. Compression of the bimodal polymer mixture (5k-2k, ●) compared to the monomodal mixture (2k, ○), after subtraction of electrostatic repulsion. Several repeated measurements of the same representative samples are shown superimposed in the graph. The measured compression of both 5k-2k and 2k is log-linear, as shown by the fits to the Dolan and Edwards exponential-decay form (lines, Eq.2-1, parameters in Table 2-3). The depictions of each architecture reflect the observation that the presence of the 5k chains increases the steric repulsive force.

Fig.2-4 compares the compression of the non-ligated bimodal 5k-2k and monomodal 2k layers. The presence of the longer 5k chains significantly increased the repulsion against the model receptor surface. For both architectures the force decays exponentially with distance ($R^2 \geq 0.95$). Thus, it is convenient to fit these data to an empirical form of the Dolan and Edwards theory for the compression of *monomodal* polymer mushrooms¹⁵:

$$F = 72\pi kTR\sigma\phi e^{-D/l} \quad \text{Eq.2-1}$$

where k is the Boltzmann constant, T is temperature, R is the effective intersurface radius, σ is the surface grafting density (chains/area), and D is the surface separation. Because Eq.2-1 is derived from scaling relations, it was necessary to simultaneously fit the prefactor, ϕ (expected to be on the order of 1), and the length scale l (expected to equal the polymer layer thickness). For dilute monomodal mushrooms, l has been shown to equal the polymer Flory radius (R_f)⁸. In our experiments, lateral crowding may extend l because the average distance between the anchors of neighboring chains was 29Å, less than either chain's R_f . This changes the equilibrium extension of the polymer layer, which for closely packed bimodal *brushes* is:

$$H \approx aN_2\sigma_T^{1/3} \left[1 + (N_1/N_2 - 1)x_1^{1/3} \right] \quad \text{Eq.2-2}$$

where N_1 and N_2 are the number of mers of the longer and shorter chains, respectively, and σ_T is a dimensionless surface concentration¹⁸. For the bimodal polymer *mushrooms* in our experiment, one might expect $R_{f,2} \leq l \leq H$, where $R_{f,2}$ is the Flory radius of the smaller chain.

As shown in Table 2-3, compression of the non-ligated surfaces reasonably fitted the form of Eq.2-1, but with significant deviation from expected values. For example, within experimental error there was no difference between the compression length scales of 5k-2k and 2k. Instead, the larger steric repulsion of 5k-2k was seen in a prefactor to Eq.2-1 that was nearly twice 2k's (statistically distinguishable). Further insight is provided by Sheth and Leckband³¹, who explored the compression of 2k chains against streptavidin using an SFA under experimental conditions nearly identical to our own and achieved similar results. Some of their observations included: 1) significant attraction between end-grafted PEG and streptavidin upon high compression ($F/R > 12$ mN/m) that

uprooted molecules from the interface and thickened the grafted layer; and 2) hysteresis in the measured force between successive approaches and withdrawals. Both phenomena were observed in our measurements of 2k and 5k-2k, further validating that the high compression of these PEG layers against streptavidin cannot be modeled as pure steric repulsion. Indeed, the Dolan and Edwards theory fails here in that both 2k and 5k-2k exhibited length scales that were significantly smaller than either chain's R_f . For brevity we omit fits to other models for polymer compression that also poorly represented these data, including blob theory³⁹, Flory mean field analysis³⁴, and de Gennes theory⁶³ for the compression of polymer mushrooms, and the theories of Milner, Witten, and Cates^{9,24} and Alexander and de Gennes^{10,64} for the compression of polymer brushes. To our knowledge, models have not yet been developed that accurately model the complex interactions of PEG with streptavidin reported here and elsewhere³¹.

Table 2-3. Parameters fit to Eq.2-1 for compression of the non-ligated polymer layers.

	coefficient, ϕ		length scale, l (Å)		R^2 ^a
	measured	predicted	measured	predicted	
5k-2k	1.3 ± 0.3	1	14 ± 2	88 ^b	0.95
2k	0.8 ± 0.3	1	15 ± 1	35 ^c	0.95

^a correlation coefficient from linear regression. ^b maximum value expected; with the *brush* model (Eq.2-2). ^c Flory radius, R_f (Table 2-1).

To test if the 5k chains interfere with specific ligand-receptor bond formation, the measured D_B values of the ligated architectures are compared in Table 2-4. Within experimental error there was no statistically significant difference in D_B among the three architectures. The average capture distance for all three cases was 124 ± 7 Å, about 80% of

the tether's contour length. This matches well with the 125 ± 5 Å reported for 2kB-coated surfaces and the 122 Å predicted for an isolated 2kB chain¹². This similarity between the three architectures' capture distances would be expected if near D_B the 5k chains neither interfered with the kinetics of bond formation nor significantly repulsed the particles. To quantify these effects, we have predicted D_B for each architecture using numerics described elsewhere⁴³. In short, *a priori* estimates were made of the repulsive steric and electrostatic forces and of the attractive bridging and van der Waals forces, which were used to predict D_B ⁵⁹. For the steric force, Eq.2-1 was used with the parameters in Table 2-3. As shown in Table 2-4, the predicted D_B increased when the steric repulsion was reduced (cf. 5k-2kB to 2k-2kB), or when the ligand density was increased (cf. 2k-2kB to 2kB). Both of these effects increased D_B slightly because stable cross-bridges were able to form at slightly farther chain extensions. However, these subtle distinctions are hardly significant considering that all three predicted D_B values are identical within ± 1 Å. That the experimentally measured capture distances are statistically identical to the three D_B values predicted from estimates of equilibrium forces suggests that the 5k chains did not interfere with the kinetics of bond formation near the surface separation D_B within the measurement time frame of ~ 1 s.

The similarity in capture distances is further explained through a simple geometrical argument. For 2kB, we estimate that the discontinuity that marks spontaneous adhesion occurs when an estimated $\sim 11,000$ chains have formed specific cross-bridges. At this extension the bridging force averages ~ 52 pN per chain (calculated from Monte Carlo data reported elsewhere¹²). It is easy to show geometrically that bringing the surfaces 1 Å closer will bring into range another $\sim 36,000$ tethers at roughly

the same extent of stretching (~ 50 pN per chain), quadrupling the bridging force. Thus, the attractive bridging force near D_B is very sensitive to D . In comparison, repulsive electrostatic and steric forces near D_B are much weaker and change slowly with distance (Figures 2-3 and 2-4). Consequently, the capture distance occurs abruptly in all cases.

Table 2-4. Measured properties of bond formation and rupture for the biotinylated architectures.

	capture distance, D_B (Å)		average decohesion force, F_{adh}	average maximum compression	average contact time	n_s ^c	n_r ^d
	measured	predicted ^a	(mN/m) ^b	(mN/m)	(min)		
5k-2kB	127 ± 22	123.3	-6 ± 4	45 ± 11	3.6 ± 1.5	5	13
2k-2kB	131 ± 11	124.4	-14 ± 9	33 ± 8	4.2 ± 2.1	2	5
2kB	115 ± 27	125.1	-12 ± 6	17 ± 11	2.5 ± 0.9	4	13

^a *A priori* estimates; method described elsewhere⁴³. ^b Negative signs indicate attractive forces. ^c Number of independently prepared samples. Prior to each measurement, samples were repositioned to allow interaction of regions of the samples that had not previously contacted, allowing multiple measurements per sample. ^d Number of independent force profiles (runs) used to calculate the decohesion force.

To compare how the presence of 5k chains influences bond rupture, Table 2-4 reports the average force required to decohere each architecture (F_{adh}). Although the reported uncertainties arising from variation between measurements cannot be discounted, it seems plausible that the generally lower adhesion strength measured for 5k-2kB arose from steric repulsion from the 5k chains. Even while in contact, increased steric repulsion would tend to hold the surfaces farther apart, where fewer bonds would be able to form within the experimental time frame⁴³. This is because the rate of tethered ligand-receptor bond formation decreases exponentially with increased surface

separation¹²⁻¹⁴. The combination of greater steric repulsion and a reduced attractive bridging force would decrease the measured decohesion force.

Variation in the duration and amount of compression may also lead to variation in the number of bound chains. Higher amounts of compression of the polymer layer bring the surfaces closer together, bringing more receptors into range of the ligated chains across the surfaces' curved landscape. A further uncertainty in these decohesion measurements is that either the ligand-receptor bond or the lipid anchor-membrane bond may be broken⁶⁵. Although the effects of the amount of compression, contact time, and lipid pullout cannot be discerned quantitatively from these data, it is clear that the presence or absence of the 5k chains plays a dominant role in determining the decohesion force. Through steric repulsion between surfaces, the 5k chains likely destabilize the anchored ligand-receptor bonds, and would increase the rate that mimetic liposomes would detach from targeted cells⁶⁶. Last, the decohesion forces of 2kB and 2k-2kB were statistically indistinguishable despite their ligand densities differing by a factor of 2.5. This is likely due to saturation of the streptavidin receptors, which had a smaller areal density ($4.4 \times 10^4 \mu\text{m}^{-2}$) than either of the ligands in 2kB ($1.2 \times 10^5 \mu\text{m}^{-2}$) or 2k-2kB ($4.8 \times 10^4 \mu\text{m}^{-2}$).

In the flow adhesion assay, none of the controls (5k-2k-, 2k-, DSPE-, or OTS-coated substrates) arrested the functionalized microspheres. However, all biotinylated architectures showed robust adhesion to the microspheres, with loss of less than 50% of the bound microspheres at shear rates between 16 and 500 s^{-1} . Thus, we found that the 5k chains did not prevent specific adhesion to the model receptor surface under either static or dynamic fluid conditions.

Our results contrast with findings that adhesion fails if the ligand is mounted inside the polymer layer. Blume et al. observed that liposomes targeted with ligands on a $\sim 10\text{\AA}$ spacer beneath a canopy of 6.8 mol % PEG₅₀₀₀ bound to *in vitro* targets up to 7 times less frequently than when ligands were mounted on the distal ends of the PEG⁵, suggesting that the magnitude of their polymer bridging force was smaller than in our experiments. Similarly, Kim et al. showed in a force microscopy experiment that adhesion failed when biotin ligands were tethered to a membrane by a $\sim 12\text{\AA}$ aminohexanoyl spacer beneath a canopy of PEG₁₇₆₀ (40 mers, $R_f = 32\text{\AA}$, $\sigma = 2.5 \times 10^5$ chains/ μm^2)²². In both cases, the spacer was significantly shorter than the equilibrium thickness of the polymer layer (R_f), dictating that specific binding could only occur when opposing membranes were separated by $\sim 10\text{--}12\text{\AA}$ apart. Using Eq.2-1, we estimate that compressing the polymer layer into a 10\AA gap would induce a repulsive force on the order of $\sim 80\text{ mN/m}$. At that range, the maximum attractive force that would evolve from specific bridging can be estimated to be a mere -11 mN/m (numerics described elsewhere⁴³). Although these are perhaps crude estimates of the forces involved, they likely explain why adhesion was not observed.

What is different in our study is that ligands were mounted onto PEG chains that can form cross-bridges at distances up to 125\AA , or about 80% of their contour length—well beyond our largest estimate for the equilibrium height of the bimodal mushroom layer (88\AA). Thus, cross-bridge formation can occur far away from the polymer layer, where the polymer chains are not compressed. At a distance 10\AA closer than D_B (at $D = 114\text{\AA}$) the steric repulsion is still only on the order of $\sim 1.5\text{ mN/m}$ while the estimated bridging force is $\sim -7\text{ mN/m}$, inducing a long-range net attraction between the surfaces

on the order of ~ -5.5 mN/m. Thus, we observe rapid and strong adhesion among all three architectures. Consistently, Gabizon et al. observed with cancer cells overexpressing folate receptor that liposome attachment frequencies were enhanced when folic acid (FA) ligands were extended beyond the polymer corona by a longer tether (PEG₃₃₅₀-FA vs PEG₂₀₀₀)⁷. For such an architecture, repulsive steric forces that antagonize ligand-receptor bonds are minimized and ligand accessibility is enhanced.

2.6 Conclusions

We have measured the compression of bimodal and monomodal mixtures of grafted polymers and the effect of their structure on the specific adhesion of tethered ligands. The presence of a longer 5k chain significantly increased the steric repulsion of these layers and lessened their adhesion to model receptor surfaces. Still, all the ligated structures adhered to receptors under both static and dynamic fluid flow conditions. Their capture distances were experimentally indistinguishable, which agrees with our theoretical predictions. It is clear from comparison to other studies that ligand accessibility plays a dramatic role in the efficacy of specific adhesion in these architectures. However, ligands need not be grafted on the exterior of the PEG layer to observe adhesion. Ligands grafted by shorter chains can escape from the mushroom layer and form cross-bridges to opposing receptors at distances far beyond the equilibrium thickness of the bimodal mushroom layer. Our observations suggest a guideline for designing targeted liposomes, namely, that the length of the tether be greater than the equilibrium thickness of the bimodal mushroom layer. This work should be useful to those designing targeted liposomes and nanoparticles, bioassays, nonimmunogenic coatings, and self-assembled biomimetic nanostructures.

2.7 Acknowledgements

We thank Dennis J. Mulder for assistance with the electronics for the SFA, Melodi King, Danny Nou, Bertha Kuo, and Prof. A.I. Barakat for performing companion flow cell studies, and Carlos Marques for furnishing the Monte Carlo data. This work was supported by NSF Grant DMR-0606564.

2.8 References & Footnotes

- (1) Nobs, L.; Buchegger, F.; Gurny, R.; AlleMann, E. *J. Pharma Sci.* **2004**, 93(8), 1980–1992.
- (2) Vyas, S.P.; Singh, A.; Sihorkar, V.; *Crit. Rev. Ther. Drug Carrier Syst.* **2001**, 18(1), 1–76.
- (3) Lasic, D.D.; Needham, D. *Chem. Rev.* **1995**, 95(8), 2601–2628.
- (4) Cattell, L., Ceruti, M.; Dosio, F. *Tumori*, **2003**, 89(3), 237–249.
- (5) Blume, G., Cevc, G.; Crommelin, M.D.J.A.; Bakker-Woudenberg, I.A.J.M., Kluft, C.; Storm, G. *Biochim. Biophys. Acta*, **1993**, 1149, 180–184.
- (6) Chen, C.-C.; Dormidontova, E.E. *Langmuir* **2005**, 21, 5605–5615.
- (7) Gabizon, A.; Horowitz, A.T.; Goren, D.; Tzemach, D.; Mandelbaum-Shavit, F.; Qazen, M.M.; Zalipsky, S. *Bioconjugate Chem.* **1999**, 10, 289–298.
- (8) Kuhl, T. L.; Leckband, D. E.; Lasic, D. D.; Israelachvili, J. N. *Biophys. J.* **1994**, 66, 1479–1488.
- (9) Kenworthy, A.K.; Hristova, K.; Needham, D.; McIntosh, T. J. *Biophys. J.*, **1995**, 68, 1921–1936.
- (10) deGennes, P.G. *Adv. Colloid Interface Sci.* **1987**, 27, 189–209.
- (11) Szleifer, I.; Carignano, M.A. *Adv. Chem. Phys.* **1996**, 94, 165–260.
- (12) Jeppesen, C.; Wong, J.Y.; Kuhl, T.L.; Israelachvili, J.N.; Mullah, N.; Zalipsky, S.; Marques, C.M. *Science* **2001**, 293, 465–468.
- (13) Moreira, A.; Jeppesen, C.; Tanaka, F.; Marques, C. *Europhys. Lett.* **2003**, 62(6), 876–882.
- (14) Moreira, A.G.; Marques, C.M. *Biophys. J.* **2004**, 120(13), 6229–6237.
- (15) Israelachvili, J. N. *Intermolecular & Surface Forces*, 2nd ed; Academic Press: San Diego, 1992; Chapters 12 and 14.
- (16) Torchilin V.P.; Omelyanenko, V.G.; Papisov, M.I.; Bogdanov, A.A.; Trubetsky, V.S.; Herron, J.N.; Gentry, C.A. *Biochim. Biophys. Acta - Biomembranes.* **1994**, 1195(1), 11–20.

- (17) Satulovsky, J.; Carignano, M. A.; Szleifer, M. A. *Proc. Natl. Acad. Sci. U.S.A.* **2000**, 97(16), 9037–9041.
- (18) Dhoot, S.; Watanabe, H.; Tirrell, M. *Colloids Surf. A.* **1994**, 86, 47–60.
- (19) Kilbey II, S.M.; Watanabe, H.; Tirrell, M. *Macromolecules* **2001**, 34, 5249–5259.
- (20) Dan, N.; Tirrell, M. *Macromolecules* **1993**, 26, 6467–6473.
- (21) Currie, E.P.K.; Wagemaker, M.; Cohen Stuart, M. A.; van Well, A. A. *Macromolecules* **1999**, 32, 9041–9050.
- (22) Kim, D.H.; Klibanov, A.L.; Needham, D. *Langmuir* **2000**, 16(6), 2808–2817.
- (23) Tirrell, M.; Parsonage, E.; Watanabe, H.; Dhoot, S. *Polym. J.* **1991**, 23, 641–649.
- (24) Milner, S.T.; Witten, T.A.; Cates, M.E. *Macromolecules* **1989**, 22, 853–861.
- (25) Drobek, T.; Spencer, N.D.; Heuberger, M. *Macromolecules* **2005**, 38(12), 5254–5259.
- (26) Currie, E.P.K.; Wagemaker, M.; Cohen Stuart, M. A.; Fleer, G.J. *Macromolecules* **1999**, 32, 487–498.
- (27) McLean, S.C.; Lioe, H.; Meagher, L.; Craig, V.S.J.; Gee, M.L. *Langmuir* **2005**, 21, 2199–2208.
- (28) Carignano, M.A.; Szleifer, I. *Interface Sci.*, **2003**, 11(2), 187–197.
- (29) Grest GS. *Adv. Polym. Sci.* **1999**, 138, 149–183.
- (30) Efremova, N.V.; Bondurant, B.; O'Brien, D.F.; Leckband, D.E. *Biochemistry* **2000**, 39, 3441–3451.
- (31) Sheth, S. R.; Leckband, D. *Proc. Natl. Acad. Sci. U.S.A.* 1997, 94, 8399–8404.
- (32) Needham, D.; Kim, D.H. *Colloids Surf. B: Biointer.* **2000**, 18, 183–195.
- (33) Kuhl, T.L.; Leckband, D.E.; Lasic, D.D.; Israelachvili, J.N. In *Stealth[®] Liposomes*; Lasic, D.; Martin, F., Eds.; CRC Press: Boca Raton, 1995; pp 73–91.
- (34) Hristova, K.; Needham, D. *J. Colloid Interface Sci.* **1994**, 168, 302–314.
- (35) Steels, B.M.; Leermakers, F.A.M.; Haynes, C.A. *J. Chromatogr. B* **2000**, 743, 2000, 31–40.
- (36) Cloud, T.D.; Rajagopalan, R. *J. Colloid Interface Sci.* **2003**, 266, 304–313.
- (37) Subramanian, G.; Williams, D.R.M.; Pincus, P.A. *Europhys. Ltrrs.* **1995**, 29(4), 285–290.
- (38) Edvinsson, T.; Elvingsson, C. *J. Chem. Phys.* **2002**, 116(21), 9510–9517.
- (39) Williams, D.R.M.; MacKintosh, F.C. *J. Phys. II France* **1995**, 5, 1407–1417.
- (40) Marsh, D.; Bartucci, R.; Sportelli, L. *Biochim. Biophys. Acta* **2003**, 1615, 33–59.
- (41) Sain, A.; Wortis, M. *Phys. Rev. E.* **2004**, 70, 031102.
- (42) Wong, J.Y.; Kuhl, T.L.; Israelachvili, J.N.; Mullah, N.; Zalipsky, S. *Science* **1997**, 275, 820–822.

- (43) Moore, N.W.; Kuhl, T.L. *Biophys. J.*, 91(5), 1675-1687.
- (44) Longo, G.; Szleifer, I. *Langmuir*, **2005**, 21(24), 11342–11351.
- (45) The entanglement molecular weight of PEG depends on the concentration, but has been reported by Kuhl et al. to be 17600⁴⁶ and by Wool et al. to be 4400⁴⁷.
- (46) Kuhl, T.L.; Guo, Y.; Alderfer, J.L.; Berman, A.D.; Leckband, D.E.; Israelachvili, J.N.; Hui, S.W. *Langmuir*, **1996**, 12, 3003–3014.
- (47) Wool, R. P. *Polymer Interfaces: Structure and Strength*; Hunser Publishers: Munich, 1995; p 102.
- (48) Florin, E.L.; Moy, V.T.; Gaub, H.E. *Science* **1994**. 264(5157), 415–417.
- (49) Helm, C.A.; Knoll, W.; Israelachvili, J.N. *Proc. Natl. Acad. Sci. U.S.A.*, **1991**, 88(18), 8169–8173.
- (50) Leckband, D.E.; Mueller, W.; Schmitt, F.J.; Ringsdorf, H.; *Biophys. J.* **1995**, 69(3), 1162–1169.
- (51) Yuan, C.B.; Chen, A.; Kolb, P.; Moy, V.T.; *Biochemistry* **2000**. 39(33), 10219–10223.
- (52) Torchilin, V.P. *Nat. Rev. Drug Discovery* **2005**. 4(2), 145–160.
- (53) Leckband, D.E.; Schmitt, J. F.-J.; Israelachvili, J.N.; Knoll, W. *Biochemistry* **1994**, 33, 4611–4624.
- (54) Ghaghadaa, K.B.; Sauld, J. Natarajanb, J.V.; Bellamkondad, R.V.; Annapragadaa, A.V. *J. Controlled Release* **2005**, 104, 113–128.
- (55) Gabizon, A.; Shmeeda, H.; Horowitz, A.T.; Zalipsky, S. *Adv. Drug Delivery Rev.* **2004**, 56, 1177–1192.
- (56) Israelachvili, J. *J. Colloid Interface Sci.* **1973**, 44, 259–272.
- (57) Israelachvili, J.; Adams, G. *J. Chem. Soc. Faraday Trans. I.* 1978, 74, 975–1001.
- (58) Heuberger, M.; Luengo, G.; Israelachvili, J. *Langmuir*, **1997**, 13(14), 3839–3848.
- (59) Vinogradova, O.I.; Horn, R.G. *Langmuir* **2001**, 17, 1604–1607.
- (60) Grabbe, A. *Langmuir* **1993**, 9, 797–801.
- (61) Kuhl, T.L.; Berman, A.D.; Hui, S.W.; Israelachvili, J.N. *Macromolecules* **1998**, 31, 8258–8263.
- (62) Halperin, A.; Leckband, D.E.; *Comptes Rendus de L'Academie des Sciences Serie IV Physique Astrophysique* **2000**, 1(9), 1171–1178.
- (63) de Gennes, P.G. *Scaling Concepts in Polymer Physics*; Cornell University Press: New York, 1979.
- (64) Alexandar, S. *J. Phys. (Paris)*, **1977**, 38, 983–987.
- (65) Wieland, J.A.; Gewirth, A.A.; Leckband, D.E. *J. Phys. Chem. B.* **2005**, 109, 5985–5993.

(66) Bell, G.I. *Science* **1978**, 200(4342), 618–627.

Chapter 3: Weak Ligand-Receptor Interactions Probed with an Automated Surface Forces Apparatus

3.1 Abstract

We present rare, direct force measurements of a small, low-affinity ligand extracted from a receptor. Specifically, we have used an automated Surface Forces Apparatus (SFA) to explore the specific adhesion between two curved surfaces bridged by an ensemble of tethered ligand and receptor molecules. Such architectures are commonly used for targeted therapeutic carriers, biosensors, and self-assembling nanostructures. Two streptavidin-binding ligands tethered to PEG were compared: biotin ($K_D \sim 10^{-15}$ M) and (2-(4-hydroxyphenylazo) benzoic acid) (or HABA), whose affinity approaches typical antibody-antigen interactions ($K_D \sim 10^{-6}$ M). With the HABA ligand, less surface damage (lipid pullout) occurred during decohesion than when the biotin ligand was used in otherwise identical experiments. Instead, we are able to show from our data that HABA-streptavidin bonds ruptured and reformed on a timescale on the order of ~ 1 – 100 ns in the slow pulling regime (loading rate ~ 0.1 pN/s). Importantly, we show that the timescale for bond equilibration is fast compared to experimental and biological timescales, which complicates the analysis of bond rupture forces under the slow pulling regime. Also, with the weaker, tethered HABA ligand, the probability of cross-bridge formation—and hence the specific bridging force between surfaces—was significantly reduced. Last, we show using thermodynamic arguments that moderate levels of

polydispersity of the PEG tether (P.I. < 1.2) has little influence on the magnitude of the force between particles bridged by many tethered ligands and receptors.

3.2 Introduction

The forces of interaction between specific ligand and receptor pairs control many biologically important events, including cell adhesion and communication (1–3). As discussed in Chapters 1 and 2, understanding ligand-receptor interactions is also critical to many commercial endeavors, including the design of drug delivery vehicles and self-assembling nanostructures, as well as for understanding bridging forces in colloidal and biological systems. When a ligand is attached to a surface by a flexible polymer tether, the tether's mechanical properties alter the force landscape between the tethered ligand and a complementary receptor protein in certain predictable ways (2, 4–6). This synergy is frequently harnessed to elucidate the strengths of biomolecular bonds, for example (7–8). Shorter tethers, such as PEG oligomers, are also frequently used in interfacial biochemical assays to immobilize specific receptors to surfaces (8).

The rupture forces between ligand-receptor bonds have been studied extensively through dynamic force microscopy applied with the atomic force microscope (AFM), optical traps, and other mechanical transducers (for reviews see refs. (9–11)). Many of these mechanical studies concern the rupture of bonds with a dissociation constant less than 2×10^{-8} M, so that more than $\sim 18 k_B T$ of thermal energy is required for their separation (Appendix 3-A). The best characterized is the streptavidin-biotin bond, which requires an enormous $35 k_B T$ to dissociate ($K_d \sim 10^{-15}$ M)(12–15). In the absence of external forces, such “strong” bonds appear irreversible to the experimentalist. It is in this regime that many of the theories relating to bond rupture forces have been developed (5,

6, 16, 17), since the bond can be assumed to be formed before the application of an external force.

Nature, however, seems to have chosen a much lower regime of bond energies in which to facilitate life—one that is centered on $14.7 k_B T$ (Appendix 3-A). According to Kramer's reaction-diffusion theory (17a, 17b), the intrinsic lifetime of a bond with that energy would be ~ 3 ms, enabling rich kinetic interactions even when external forces are not present. If pulled slowly (i.e. by an AFM tip), the ligand may unbind and rebind many times during a single measurement. Under very fast loading rates, the bond may appear to break very early along the rupture pathway. Thus, capturing such delicate interactions with force spectroscopy includes challenges such as enhancing single-molecule sensitivity, differentiating specific interactions from thermal noise, and decoupling the history of applied force from the intrinsic force landscape (18).

Here we explore this weaker-binding regime using 2-(4-hydroxyphenylazo) benzoic acid (or HABA)—a small ligand that is nearly the same size as biotin but which binds to streptavidin (SA) with an energy of only $9\text{--}12 k_B T$ ($K_d \sim 10^{-6}$ M) (14, 19, 20). We circumvent many of the aforementioned issues by using a Surface Forces Apparatus (SFA) to measure the interactions of $\sim 10^7$ weakly-binding tethered ligand receptor pairs in equilibrium, which ensures statistical significance with each measurement. Using automated interferometry and near-angstrom surface positioning, we are able to determine with high precision the probability that a weakly binding ligand-receptor pair forms a molecular cross-bridge between two opposing surfaces. The polymer cross-bridges exert a well-characterized force that can be related to the single-molecule kinetics by adapting the theoretical frameworks discussed in the previous chapters. Last,

implications are presented for the performance of biofunctionalized coatings used in targeted drug delivery vehicles, biosensors, and self-assembled nanostructures.

3.3 Methods

3.3.1 Materials

The following high purity lipids and lipid conjugates (>99%) were purchased from Avanti Polar Lipids (APL; Alabaster, AL) and Northern Lipids (NL; Vancouver, BritishColumbia, Canada): dipalmitoyl phosphatidyl ethanolamine (DPPE, Lot#160PE-81), dilauroylphosphatidyl ethanolamine (DLPE, Lot#120PE24), and distearoyl phosphatidyl ethanolamine(DSPE, Lot#180PE62). *N*-((6-(biotinoyl)amino)hexanoyl)-1,2-dihexadecanoyl*sn*-glycero-3- phosphoethanolamine, triethylammonium salt (biotin-X DHPE, Lot#45311) was purchased from Molecular Probes (Eugene, OR). Streptavidin was purchased from PierceBiotechnology (Rockford, IL) (Lot#GC94900). Salts (>99.5% purity) were purchased from Sigma-Aldrich (St. Louis, MO). Water was purified with a Millipore Milli-Q filtration system (Billerica, MA). HPLC grade methanol and chloroform were from Fisher Scientific (Pittsburgh, PA). The HABA-PEG-DSPE conjugate (Fig.3-1B) was synthesized using materials and methods described in a separate publication (29).

3.3.2 Preparation of Functionalized Bilayers

Supported lipid bilayers were prepared by Langmuir-Blodgett deposition (LB) using a Wilhelmy trough (Nima Technology Ltd., Coventry, UK) as described elsewhere (19). All preparations were carried out in a laminar flow box (Labconco, Kansas City, MO). Lipids were dissolved in 9:1 chloroform/methanol at a concentration of ~1 mg/ml.

Fig.3-1A shows a schematic of the receptor and ligand surfaces constructed for this study. A close-packed, solid phase inner monolayer of DPPE ($\sim 43 \text{ \AA}^2$ per molecule, $\Pi = 40 \text{ mN/m}$) was deposited onto molecularly smooth, back-silvered mica substrates glued onto silica disks by pulling the substrates up through a compressed DPPE monolayer at the air-water interface. Afterwards, the DPPE coated mica substrates were allowed to air-dry overnight. For the tethered ligand surface, a 5:95 mixture of HABA-PEG2000-DSPE and DSPE was then deposited by passing the DPPE coated substrates down through the monolayer film ($\sim 43 \text{ \AA}^2$ per molecule, $\Pi = 40 \text{ mN/m}$) to form the outer leaflet of the membrane. Subsequently, the membrane-coated surfaces were kept under water.

The preparation of oriented monolayers of streptavidin has been described previously (20, 21, 13). Briefly, streptavidin was assembled by specific adsorption onto a supported lipid bilayer where the outer leaflet was a mixture of DLPE and 5 mol% DHPE-X-biotin (a lipid conjugate where biotin is coupled to DHPE via a thirteen-carbon spacer, ($\sim 43 \text{ \AA}^2$ per molecule, $\Pi = 35 \text{ mN/m}$). After deposition of the mixed DLPE:DHPE-X-biotin outer leaflet, the membrane was removed underwater from the Wilhelmy trough and incubated with streptavidin at a concentration of 59 \mu g/ml ("high-SA" samples) or 0.59 \mu g/ml ("low-SA" samples) in phosphate buffer for a minimum of three hours. The coverage of streptavidin using this adsorption method for the high-SA samples has previously been determined to be $\sim 3600 \text{ \AA}^2$ per streptavidin, or 79% of the bilayer surface (22). This receptor grafting density was comparable to the ligand grafting density ($1.19 \cdot 10^5 / \mu\text{m}^2$), which is comparable to reported expressions of folate receptors on tumor cells (23, 24) and to grafting densities of targeted liposomes (25). For the low-SA samples, the 100-fold smaller streptavidin concentration may have decreased the

adsorption rate, resulting in a substantially lower grafting density of streptavidin on the receptor surface compared to the high-SA samples.

All measurements were conducted in phosphate buffer containing 0.5 mM Na⁺ at pH 7.2. The buffer was saturated with DSPE to prevent solubilization of the bilayer. Lateral diffusion of lipids was minimized by operating at $25 \pm 0.1^\circ\text{C}$, which is below the phase transition temperature of the lipid bilayers. In all cases, the duration of measurement was much smaller than the 1–10 h diffusion timescale estimated for gel-phase lipids (26) and observed for PEG-DSPE (27). The diffusion rate would also be decreased during surface contact due to obstruction from anchored cross-bridges (28).

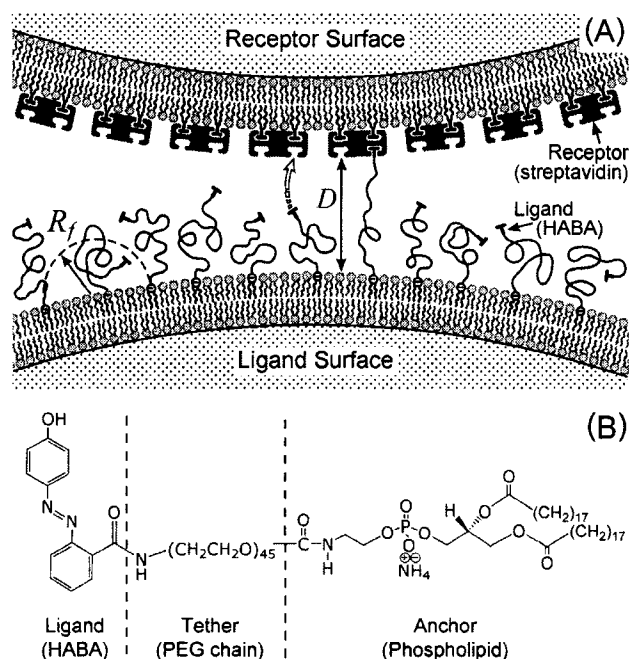


Figure 3-1. (A) Schematic of the experiments in the SFA. Shown as an example is a grafting of PEG ligated with HABA and positioned at a distance (D) from the receptor surface. Here the chains are grafted apart at a distance near their Flory radius (R_f). The receptor pockets of streptavidin are parallel to the upper supported membrane. The surface curvature is exaggerated for clarity (typically the interaction radius is ~ 1 cm). (B) Chemical structure of the HABA-PEG-DSPE conjugate synthesized by Moore et al. (29).

3.3.3 Computer-Assisted Force-Distance Measurements

The surface forces apparatus (SFA) technique has been used extensively to measure interaction forces between surfaces (30, 31). Here we only briefly describe the conventional technique and enhancements we have made to achieve high accuracy and precision. Both the conventional (“manual”) method and automated method were used to characterize the tethered HABA / streptavidin architecture. The latter is described below. Table 3-2 compares the procedural parameters used with each technique, as well as with manual measurements of an analogous tethered biotin / streptavidin architecture published elsewhere (32).

Table 3-1. Procedural Parameters used in the SFA studies*

SFA method	Biotin**	HABA	
	manual	automated	manual
Approach step size (ΔD), Å	17±7	3±1	34±10
Average approach rate near D_B , Å/s	2.4±0.7	0.6±0.1	17±5
Maximum compression, mN/m***	17±11	14±5	21±5
Contact time, m	3±1	12±1	3±1
Average withdrawal rate, Å/s	1.3±0.5	0.5±0.2	1±3
Loading rate (withdrawal, last stage), pN/s	0.3±0.1	0.13±0.05	0.3±0.7
Cycle time, m	5±2	35±4	4±1

* Reported uncertainties are standard deviations. ** (32). *** Data from first approaches.

In short, one surface (i.e. the ligated surface) was mounted on a fixed support while the other (i.e. the receptor surface) was mounted on a double cantilever spring, displaceable vertically by a motorized micrometer screw. The silver layer on each disk

partially transmits light directed normally through the surfaces but also constructively interferes such that distances between the surfaces can be measured by observation of the displacement of fringes of equal chromatic order (FECO) within a spectrometer (30–32). In the force-distance curves shown in this study, D was defined as the distance between the outer edge of the streptavidin receptor and the outer lipid leaflet on the opposing ligated surface as shown in Fig.3-1A. This reference frame was determined at the end of each experiment by draining the buffer from the SFA with the surfaces well separated, which removes the outer monolayers of the assembled bilayers. After draining, the surfaces were brought into contact and the thickness change measured with interferometry. Known thicknesses for DSPE, DLPE, and streptavidin allow the remainder to be ascribed to the PEG chains (27). The surfaces were then dried *in situ* with a stream of dry nitrogen or 0.2 μ m-filtered air and subsequently treated with UV light to vaporize the DPPE monolayers remaining on each surface. The surfaces were then re-contacted and the polymer thickness recalculated independently.

Samples were illuminated by a 100W quartz-tungsten halogen lamp reflected from a cold mirror and focused into and aligned normal to the sample by a liquid light guide (Oriel Instruments). Light transmitted from the SFA environmental chamber (Mark II) was polarized and aligned into a 750-mm spectrometer with a 600-line/inch diffraction grating (Acton). The spectrometer was controlled with WinSpec software version 2.5.16.2 (Roper Scientific) and our own custom software. FECO images were digitized using a 2048 \times 512 pixel CCD detector (Princeton Instruments) stabilized at -70°C to achieve a ~40% photon efficiency, yielding resolution of $\pm 0.25\text{\AA}$ in wavelength and $\pm 1\ \mu\text{m}$ in lateral distance across a sample surface.

Automated, high-resolution determination of FECO peak wavelengths were obtained to $\pm 0.5\text{\AA}$ with time resolution up to $\pm 1\text{s}$ as follows: 1) The region of the digital FECO image containing the FECO center (surface contact point) was binned over the central few pixels to produce a calibrated transmission spectrum of intensity (I) vs. wavelength (λ) at each point of data collection. 2) Spectra were smoothed using a five-term simple moving average linear transformation to filter transient noise. 3) Intensities below a moveable baseline were truncated to yield spectra with high signal-to-noise ratio. 4) The truncated spectra were interpolated with 2nd-order polynomials to minimize error from discretization of the true spectra. 5) Boundaries for the location and number of peaks were determined by comparing the signs of $dI/d\lambda$ at a variable number of wavelengths along the reduced spectrum. Two consecutive sampled wavelengths with positive and negative derivatives, respectively, indicated the presence of a peak between them and provided boundaries for a Newton's method search for the maximum intensity. Separate algorithms identified the contact fringe and measured the surface topography. The above computation was performed in Mathematica 5.0 (Wolfram) and the results input to a spreadsheet for automated calculation of the force-distance profiles, giving users rapid feedback during an experiment.

To minimize mechanical drift of the samples in the SFA chamber, the temperature of the sample and SFA mechanical train was stabilized to $\pm 0.05^\circ$ by enhancing convection inside a closed-circuit temperature-stabilized room. The SFA was allowed to re-equilibrate for 10 minutes after each user intervention. Further, stepping the surfaces in five-second intervals allowed the samples and the SFA mechanical drive train to fully equilibrate after each motor pulse. Under these conditions, undirected movement of the

surfaces (drift) averaged only $0.4\text{\AA} / \text{h}$. Fine control of surface movement ($\pm 0.5\text{\AA}$) was obtained from a digital timing circuit that delivered 1-ms pulses to an 8-rpm AC motor (Hurst), thus avoiding the need for expensive piezoelectric crystals.

The enhancements of the automated SFA permitted a more precise determination of the range of adhesion than has been previously reported (32–35). We define the capture distance, D_B , as the distance during surface approach at which surfaces jump into contact (32, 35). This mechanical instability occurs when the gradient of the interaction force exceeds the spring constant of the measuring spring in the SFA (36). It has been shown that D_B is a reasonable estimate of the extension at which cross-bridge formation becomes favorable for a single polymer tether (33, 35). This is because for a single tether the transition from the bound to the unbound state occurs over a very narrow range in the surface separation ($\sim 3\text{\AA}$ for PEG₂₀₀₀ bearing biotin against streptavidin)(33). For the range of parameters typically used in SFA, the measurement of D_B does not depend strongly on either the cantilever spring constant or the interaction radius of the substrates (Appendix 3-B). Conveniently, the capture distance should therefore represent the distance at which a targeted liposome or other particle will spontaneously adhere to its target. Two nonidealities in measuring the capture distance were accommodated as described previously (32). First, because the surfaces are approached with steps ΔD (typically $\sim 3\text{\AA}$), $\Delta D/2$ was subtracted from the measured discontinuity. Second, because surface damage may occur after surfaces have contacted (due to pullout of the lipid anchors, discussed later), only capture distances from the first approaches were averaged.

3.3.4 Statistical Methods

Each architecture was prepared and characterized in four independent experiments, with multiple force measurements made in different regions of each sample. Uncertainties in the absolute surface separation, D , were dominated by determination of the polymer layer thickness (± 6.2 – 8.1 \AA) and FECO peak wavelengths ($\pm 0.5 \text{ \AA}$), and surface vibration ($\pm 0.5 \text{ \AA}$ near contact). Uncertainties in capture distances also contain error attributed to stepping the surface separation ($\pm 1.5 \text{ \AA}$). Uncertainties in the measured forces ($\pm 4\%$) were dominated by determinations of the cantilever spring constant ($\pm 3\%$) and surface interaction radii ($\pm 0.3\%$) (Appendix 3-C). Except where noted, reported uncertainties represent 95% confidence intervals from the student-t distribution propagated through calculation in the usual way. Uncertainties in theoretically derived quantities incorporate uncertainties from any experimentally determined parameters used in the calculations.

3.4 Results and Discussion

We now present direct measurements of the interaction forces between the weakly-binding ligand-receptor pair, HABA-streptavidin.

3.4.1 Force-Distance Profiles

Fig.3-2 shows an example of a measured force vs. distance profile for the tethered HABA interacting with streptavidin during several successive approaches. When the surface separation was much greater than the length of the tether ($D \gg 159 \text{ \AA}$), a screened electrostatic repulsion consistent with the buffer electrolyte concentration and known surface charge density was observed (27). As the surfaces approached, a

discontinuity in the data was observed near the capture distance (D_B) where the surfaces “jumped” into adhesive contact, completing the traverse in ~ 10 s. The attractive force that produced this movement can be attributed to specific bridging between the surfaces^{12,42}. The observed capture distance of $D_B = 92 \pm 9 \text{ \AA}$ for the high-SA architecture was substantially smaller than the $125 \pm 7 \text{ \AA}$ measured elsewhere for biotin architectures (32, 33) and is consistent with the known weaker bond strength of HABA-SA (14). After the initial capture, a strong repulsion was measured as the polymer layer was compressed. No long-range adhesion was observed for the low-SA architecture.

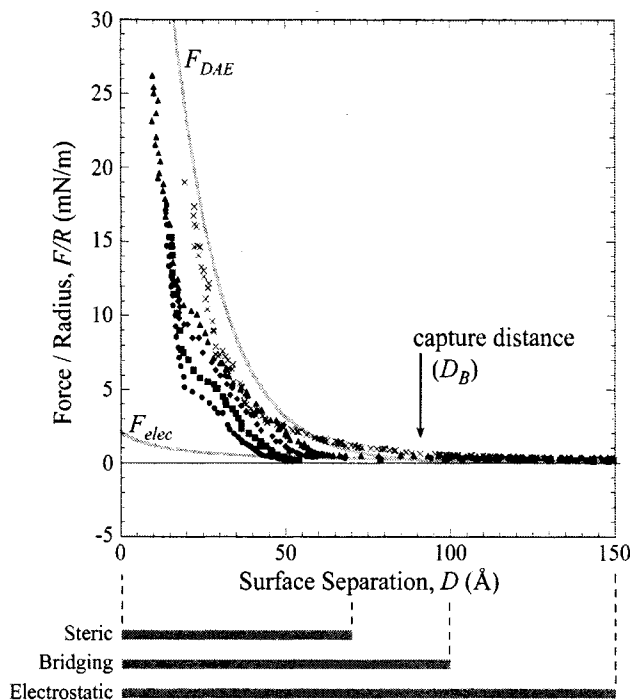


Figure 3-2. Example force profiles measured during surface approach for the high-SA surface (consecutive approaches marked by ●, ■, ◆, and ▲, respectively) and the low-SA surface (crosses; for clarity shown is an average of two independent measurements of the same sample, first approaches only; electrostatics subtracted for comparison). During approach of the high-SA surfaces, a discontinuity in the measured force is correlated to the capture distance (D_B) by accounting for the incremental stepping of the surface separation. Below graph: the distance regimes over which each force is significant. For distances below D_B , both bridging and steric forces have significant magnitudes. The latter is estimated from a parameterization of

Dolan and Edwards theory (line marked F_{DAE} ; Eq.3-7). Beyond D_B , electrostatic repulsion dominates the force landscape (line marked F_{elec} ; Eq.3-6). Together, these comparisons demonstrate the presence of an attractive bridging force between the surfaces for the high-SA surface. Within experimental error, the presence of bridging for the low-SA surface cannot be identified. The abscissa is just shorter than the length of the PEG tethers (159Å).

During the first three approaches the surfaces were compressed to 14 ± 5 mN/m to minimize structural changes in the PEG layer at higher compression (22, 25). During the fourth approach, the surfaces were compressed to 28 ± 2 mN/m. From these controlled measurements several compressive regimes are clear. Following the initial long-range bridging by the polymer tethers near ~ 90 Å, the surfaces equilibrated to a separation of 49 ± 7 Å. Compressing the surfaces steadily and slowly (0.3 Å/s for $20 < D < 50$ Å) evidenced a transition in the measured force near $D = 32$ Å that was observed in $\sim 85\%$ of the approaches. This transition roughly corresponds to compression of the grafted polymer chains below their Flory radius, R_f , of 35 Å (37), below which the compression of polymer mushrooms produces significant repulsive force (for a review, see ref. (38)). The repulsive force before and after this transition increased uniformly with the number of times the surfaces had contacted—a phenomenon observed elsewhere (22, 26, 32, 33) that we discuss later in more detail.

Compressing below 20 Å at a rate of 0.05 Å/s yielded a compressive force that was linear with respect to D and independent of the number of times the surfaces had been in contact. There the bridging force changed little with respect to D (35), while steric repulsion is generally believed to increase exponentially with decreased distance (39) but could appear quasi-linear over the range 10 Å $< D < 20$ Å (c.f. the slope of the predicted steric force in Fig.3-2). Also, the compression may force any extracted tether-anchoring

lipids to reinsert into the membrane, so that osmotic forces arising from the confinement of material between the surfaces would be independent of the number of times surfaces had contacted. Although to our knowledge the kinetics of lipid reinsertion has not been fully explored, this may not be unrealistic considering the relatively slow compression/decompression cycle time of ~ 11.5 min.

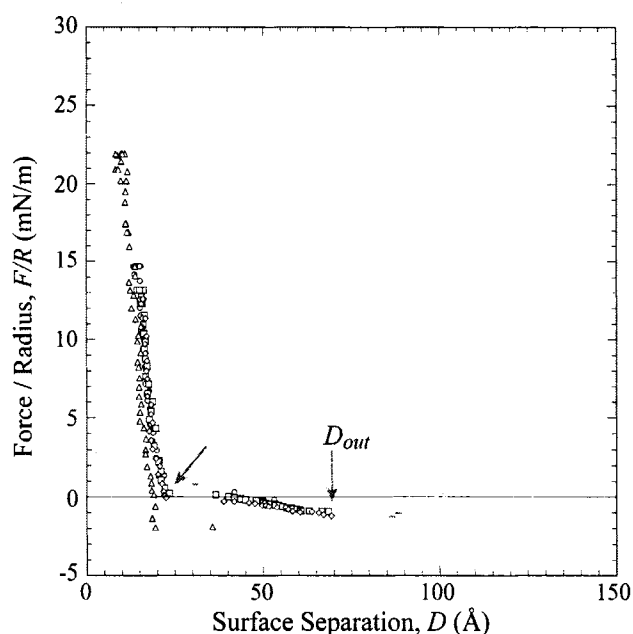


Figure 3-3. Example force profiles measured during four consecutive withdrawals (\circ , \square , \diamond , and \triangle , respectively). Forces measured during the first three withdrawals were coincident. Higher compression preceding the fourth withdrawal increased the depth of the force well. Arrows mark discontinuities in the force profile, which were observed consistently during each withdrawal. The second discontinuity is the “jump out” distance (D_{out}) corresponding to the adhesive pull-off force (F_{adh}). Dashes mark data captured by the automated SFA while surfaces moved beyond these points of instability. The abscissa is just shorter than the length of the PEG tethers (159\AA).

During surface withdrawal, an initially steep force gradient corresponding to decompression of the PEG chains was followed by a relatively shallow gradient, corresponding to the rupture of many ligand-receptor and/or lipid-membrane bonds across the curved interfacial landscape (Fig.3-3)(33, 34). Between these two distance

regimes ($\sim 20\text{\AA} < D < 40\text{\AA}$) exists a discontinuity in the measured force profile, which we observed in all measurements. This discontinuity, which likely stems from a shallow secondary minimum in the force profile, has not been observed in otherwise identical experiments with the more strongly-binding biotin ligands (32–35). Upon further separation, a mechanical instability was observed where the force gradient exceeded the cantilever spring constant. Just before this discontinuity surfaces moved more quickly with each motor step, resulting in a lower data density. This last stable point defined the adhesive pull-off force, F_{adh} , and the critical “jump out” distance, D_{out} , beyond which the surfaces rapidly separated to a distance of $\sim 1000\text{\AA}$ within 5–10 s (Appendix 3-D).

At close separations ($D < 20\text{\AA}$), the force during withdrawal decayed roughly exponentially, corresponding to decompression and slow relaxation of the polymer chains. Also noteworthy is that the force gradient was steeper during withdrawal than during approach, as observed and discussed elsewhere (22, 32, 40, 41). In short, it has been shown that compressing grafted PEG against streptavidin can induce non-specific attractive forces between the polymer and the protein (Sheth&Leckband PNAS 1997). Also, higher compression of the surfaces brings more tethered ligands into range of receptors, which allows more polymer cross-bridges to form. Consistently, the first three withdrawals gave coincident force profiles, while the fourth withdrawal—following compression to nearly twice the force—exhibited stronger adhesion and a steeper force gradient.

3.4.2 Bond Rupture Forces

One unique feature of these measurements is the small adhesive pull-off force, F_{adh} , of -1.6 ± 0.4 mN/m ($n = 54$), or almost equivalently, -1.4 ± 0.9 mN/m when only first

withdrawals are considered ($n = 13$). For comparison, in otherwise identical experiments with biotin ligands, F_{adh} was -12 ± 6 mN/m (32) due to the higher biotin-streptavidin bond strength. The measured pull-off force was roughly double that measured for a PEG adhering non-specifically to streptavidin after similar compression (22). Further, in the control experiment with low streptavidin coverage no adhesion was observed. Thus, we believe the long-range adhesion shown in Fig.3-3 originates from the specific adhesion of tethered HABA to streptavidin.

We now calculate the average rupture force per bond and show that it depends intimately on the surface geometry. During withdrawal the surfaces separated spontaneously when the nominal distance between surfaces was $D_{out} = 74 \pm 4$ Å. A comparable average of $D_{out} = 74 \pm 15$ Å was obtained from data from the first withdrawals. However, due to surface curvature the average surface separation around the contact area was always somewhat larger, given by:

$$\langle h \rangle \approx (D + l_B) / 2 \quad \text{Eq.3-1}$$

Eq.3-1 is accurate to better than $\pm 2\%$ for any $0 \leq D \leq l_B$ when $R \geq 10 l_B$. This approximation accounts for the fact that the interaction area for tethered ligand-receptor architectures becomes smaller as the surface separation increases (35). Importantly, the average surface separation approaches D only as $D \rightarrow l_B$. In adhesion studies with SFA, the average surface separation is often approximated as D ; however, Eq.3-1 shows that for a contact at $D = 0$ the average surface separation is ~ 50 Å for $R \sim 1$ cm and $l_B \sim 100$ Å, and over the range of interest h ranges from 0–100 Å. Using the spring model for the tether stretching force (Eq.3-1-7), the ratio of the average force against a tethered bond compared to the nominal force at the contact center is:

$$f(\langle h \rangle) / f(h) \approx (h + l_B - 2l_{eq}) / (2h - 2l_{eq}) \quad \text{Eq.3-2}$$

with $H > l_{eq}$. At our measured D_{out} , the average surface separation was $\langle h \rangle = 87 \pm 2 \text{ \AA}$ ($87 \pm 10 \text{ \AA}$ based on first withdrawals). At these distances, the ratio in Eq.3-2 is ~ 1.1 . Thus, at these far extensions all bonds have experienced roughly the same stress. At this distance, Monte Carlo data proffers a bond force of $17 \pm 1 \text{ pN}$ ($17 \pm 5 \text{ pN}$ for the first withdrawals) as the force that each bond would experience if a cross-bridge were formed (33). However, normalizing the measured force at D_{out} by the estimated $(4.8 \pm 0.7) \times 10^6$ receptors within range of the tethered surface at that distance would suggest that each tether actually contributed $2.4 \pm 0.4 \text{ pN}$ to the total measured force. The ratio of the forces calculated with these two approaches suggests that at any instant in time only $14 \pm 3\%$ of the tethered HABA ligands formed cross-bridges to the opposing surface. The lower propensity of the tethered HABA ligand to form cross-bridges is a unique feature of this weakly-binding streptavidin ligand.

In contrast, when the same analysis is repeated on the otherwise identical measurements with biotin ligands, we found that the stronger ligand-receptor bond resulted in all or most of the biotin ligands being bound to streptavidin receptors during the last stage of surface separation. Specifically, we found that $D_{out} = 85 \pm 14 \text{ \AA}$ where $\langle h \rangle = 93 \pm 7 \text{ \AA}$, $f(\langle h \rangle) / f(h) \approx 1.1$, and there were $\sim 2.8 \times 10^6$ chains bound (32). Then based on the stretching potential of PEG, the force per bond that would be expected to evolve if all tethers in the interaction area formed cross-bridges is $20 \pm 4 \text{ pN}$. Within experimental error, this force is in good agreement with the $23 \pm 11 \text{ pN}$ corresponding to the measured force of the tethered biotin ensemble normalized by the number of receptors, confirming that a high fraction of biotin ligands were bound preceding the

surfaces' jump out. These results demonstrate that the bond's relative propensity to rebind after dissociation plays a dominant role in the outcome of force spectroscopy—a phenomenon not observable with strongly-binding ligands (i.e. biotin) due to their low rate of dissociation.

It is also insightful to compare the measured bond decohesion forces with the 19 ± 3 pN measured for a HABA-streptavidin bond by Leckband et al., also using a Surface Forces Apparatus (14). In their experiment, the rupture force was calculated by assuming that all HABA ligands within range of a streptavidin receptor would have formed a bond. Consistently, their estimate for the HABA-streptavidin rupture force is comparable to the 17 ± 1 pN we estimated above by assuming 100% binding. However, the rupture force that will be measured for a weakly-binding ligand-receptor bond depends intimately on the probability of cross-bridge formation, which may be much less than unity even under equilibrium conditions.

Another difficulty in comparing our results to Leckband's measurements is the marked difference in the loading rate applied to the bonds (9). In both SFA experiments force was transduced to each ligand-receptor through PEG tethers; consequently, the loading rate was independent of the surface geometry; viz., $\partial F / \partial t = k_{\text{effective}} |dD/dt|$, where $k_{\text{effective}} = (k_{\text{cantilever}}^{-1} + k_{\text{PEG}}^{-1})^{-1}$ (6). In our experiments, $k_{\text{PEG}} \approx 2.6 \times 10^{-3}$ N/m for PEG (35), much less than the SFA measuring spring's $k_{\text{cantilever}} = 328 \pm 11$ N/m, so $k_{\text{effective}} \approx k_{\text{PEG}}$. Thus, the loading rate was ~ 0.1 pN/s in our study, well within the limits of the equilibrium regime (5). In contrast, in Leckband's experiments the PEG tethers were oligomers (4 mers), for which the molecular stiffness is known to increase sharply with decreased length. A lower bound for the molecular stiffness of a 4-mer PEG chain can be

gleaned from molecular dynamics simulations of a 6-mer PEG chain in water (41a). In the low extension regime we calculate from the simulations an effective spring constant on the order of ~ 0.15 N/m. (In justification, the binding range for the 6-mer PEG would be $l_B \approx l_{eq} + (W_{LR}/k)^{1/2}$ (35), or about 15\AA , where the force extension curve is still quasi-linear.) For an upper bound, we consider a structurally similar 10-carbon, planar poly(ethylene) chain, which has a calculated stiffness on the order of ~ 10 N/m (42). Then, assuming a comparable rate of separation, the loading rate in Leckband's measurements may have been in the range $\sim 6\text{--}400$ pN/s, which would dramatically increase the rupture force compared to our experiments (5, 15).

3.4.3 Repeated Compression and Withdrawal

To determine the effect of repeated compression and withdrawal on the surfaces' adhesivity, Fig.3-4 shows the pull-off force as a function of the number of times surfaces had contacted prior to separation (cycle #). Shown is a superposition of measurements with both the automated SFA ($\sim 40\%$ of trials) and the manual method, which had statistically indistinguishable results. The HABA-ligated surfaces typically remained adhesive for up to eight repetitions of compression and withdrawal, in contrast to analogous experiments with biotin ligands where surfaces lost specificity after three to four repetitions due to extraction of lipid anchors with each withdrawal (32–35). It is an unusual result that the surfaces retained adhesivity (Fig.3-4) despite an increase in the net repulsion with each cycle at small separations (Fig.3-2). To explain this discrepancy, we briefly quantify how each force might have been altered by repeated compression and withdrawal.

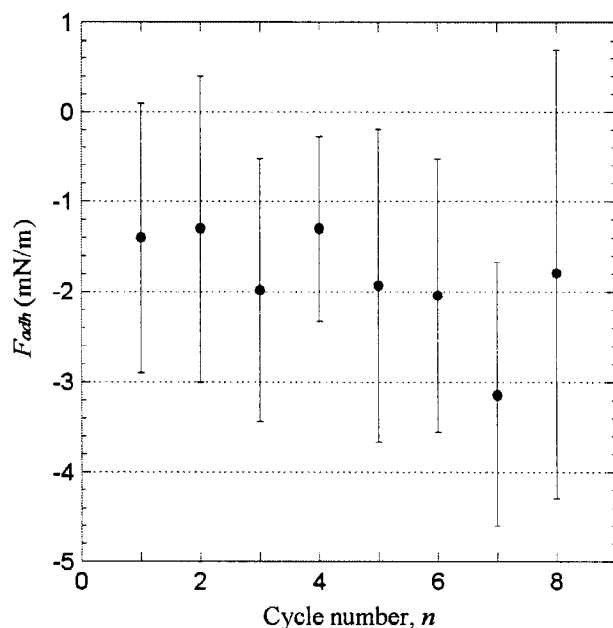


Figure 3-4. Measured decohesion force (F_{adh}) as a function of the number of times surfaces had contacted (cycle #). Error bars are standard deviations of 2–13 measurements among four independently prepared samples.

According to estimations elsewhere (32), at $D = 25\text{\AA}$ (for example) the electrostatic force likely was on the order of ~ 1 mN/m, which is not significantly smaller than the 4.4 ± 0.2 mN/m measured at that distance during the first approach. The lipids anchoring PEG carry a 1- charge; however, they outnumber the streptavidin receptor sites on the opposing surface by a factor of ~ 3 . For example, removal of 50% of bridged tethers would only reduce the surface charge of the tether-anchoring membrane by $\sim 17\%$. According to solution of the non-linear Poisson Boltzmann equation for our experimental parameters (43), this decrease in surface charge would decrease the electrostatic forces by an average of 5% over the range $5\text{\AA} < D < 100\text{\AA}$. Thus, the electrostatic force should not be significantly altered by the extent of lipid pullout.

As for the steric force, it has been shown that when PEG is compressed above 12 mN/m against oriented streptavidin monolayers the range of the steric force decreases

due to attraction between PEG (22, 25). The apparent attraction has also been attributed to structural changes in the PEG layer, which can exhibit relaxation times of > 3 h (22). In contrast, our experiments show an increase in the measured force with each cycle.

A more plausible explanation for the increased repulsion between compression cycles may be that a fraction of lipid anchors were uprooted from the membrane with each cycle after ligands bound to a receptor. (The kinetics of this process is discussed in Section 3.4.6). Because of the low binding affinity of the HABA-streptavidin bond, tethers grafted to the receptor surface by the HABA-streptavidin bond would frequently dissociate and become “free” in solution, while the contractility of the polymer tether would minimize the rate of rebinding. The high tether density, large radius of surface curvature, and the small surface separations maintained throughout the experiment would minimize diffusion of “free” tethers away from the intersurface gap. Consequently, such unbound tethers would make a larger contribution to the measured repulsion than bound tethers due to the presence of the uprooted lipid in the intersurface gap. However, the bridging force would not decrease until $> 2/3$ of the tethers desorbed, since tethered ligands outnumbered receptors by a factor of ~ 3 . This proposed mechanism is consistent with the coincidence of the measured force profiles during surface separation at far distances (Fig.3-3), since there the distances may have been sufficiently large as to render the steric repulsion of any extracted lipids negligible with respect to the other, longer-range forces.

To relate the measured force to the extent of lipid pullout, we assume that the probability that a tether bridging the two surfaces will remain attached to the lipid-anchoring membrane between successive cycles is $\phi = 1 - \phi_{\text{uprooted}} + \phi_{\text{reinserted}}$, where

$\phi_{uprooted}$ and $\phi_{reinserted}$ are the probabilities that the tether's lipid anchor is uprooted from or reinserted into the anchoring membrane, respectively. The slow timescale of these experiments may allow both processes to occur during either surface approach or withdrawal. Also, due to their additivity, $\phi_{uprooted}$ and $\phi_{reinserted}$ cannot be determined uniquely from these measurements. In the simplest view, the measured force includes contributions from the forces of specific bridging, electrostatic repulsion and van der Waals attraction (DLVO), polymer compression, and the osmotic confinement of any lipids extracted from the membrane; in order, these forces are summed as:

$$F_{total}(D) = F_{bridging}(D) + F_{DLVO}(D) + F_{steric,polymer}(D) + F_{osmotic,lipid}(D) \quad \text{Eq.3-3}$$

For this particular analysis, we assume that at any distance the first three terms in Eq.3-3 are constant with respect to repeated compression and withdrawal. The force arising from osmotic confinement of any extracted lipids should be proportional to the fraction of uprooted lipids; viz.,

$$F_{osmotic,lipid}(D) = C(D)(1 - \phi^{n-1}) \quad \text{Eq.3-4}$$

where n is the cycle number and $C(D)$ is constant with respect to n . Combining Eq.3-3 and Eq.3-4, the measured force has the empirical form:

$$F_{total}(D, n) = F^*(D) + C(D)\phi^{n-1} \quad \text{Eq.3-5}$$

The three fitting parameters are ϕ (assumed constant), and F^* and C (both distance dependant). We have fit Eq.3-5 to the approaching force profiles in Fig.3-2 for 20 distance values over the range $17 < D < 36\text{\AA}$, where the shift in the measured force was the most clearly discernable between runs. Because it was necessary to linearly interpolate the profiles to perform the comparison, only the results from the majority 75%

of the fits are considered. As an example of a typical fit, Fig.3-5 shows the fit at $D = 30\text{\AA}$, which shows excellent agreement between the data and the form of Eq.3-5.

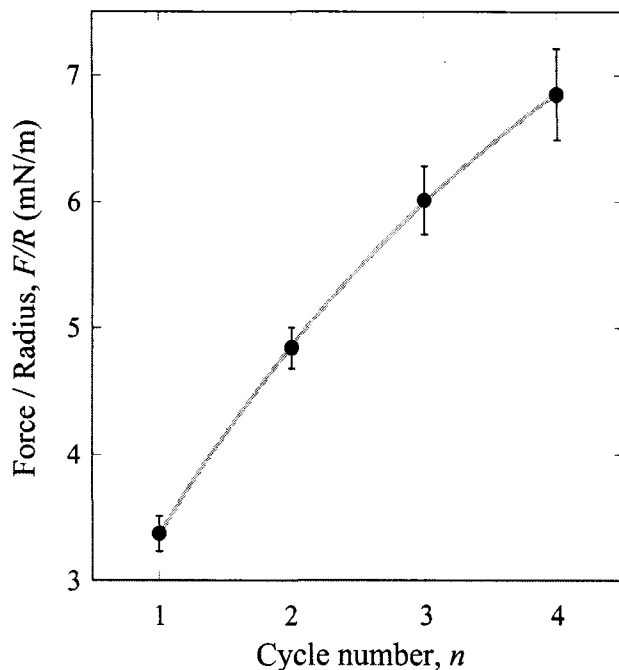


Figure 3-5. Example fit (line) of Eq.3-5 to the force measured during surface approach (circles) as a function of the cycle number at $D = 30\text{\AA}$.

The fits to Eq.3-5 gave an average of $\phi = 0.79 \pm 0.12$ for the fraction of bridged tethers remaining anchored in the membrane between successive cycles. The measured ϕ is a lower bound for the probability of lipid pullout, since $\phi_{reinserted}$ is unknown. If $\phi_{reinserted}$ is negligible, then this result suggests that during each withdrawal $\sim 21\%$ of lipids anchoring bound tethers were extracted from the outer leaflet of the ligated membrane. Because of the excess of tethers to receptors, the surfaces should begin to lose adhesivity when $n = -\ln(3)/\ln(0.79) \approx 5$ (cycles). Unfortunately, the large scatter in these measurements, possibly owing to variation in the amount and time of compression, may obfuscate any reduction in the measured adhesion after 5 cycles.

3.4.4 Extraction of Bridging Forces from the Force Profiles

To characterize the specific bridging force, steric and electrostatic forces were subtracted from the measured force profiles. To model the electrostatic force, we have fit the measured force profiles over the range $200\text{\AA} < D < 900\text{\AA}$ to an empirical approximation of the electrostatic force,

$$F_{elec} = \left(\pi R \sigma_e^2 / \epsilon \epsilon_0 \kappa \right) e^{-\kappa D} \quad \text{Eq.3-6}$$

where σ_e is the surface charge density (assumed constant), κ^{-1} is the Debye length, ϵ is the permittivity, and ϵ_0 is the permittivity of vacuum (44). Eq.3-6 represents the electrostatic forces accurately to better than $\pm 10\%$ over the entire distance regime, as compared to solving the nonlinear Poisson-Boltzmann equation using code kindly provided by Alexis Grabbe (43). For the steric force we use the form of Dolan and Edward's theory (39),

$$F_{steric} = 72\pi k_B T R \sigma_t \varphi e^{-D/\lambda} \quad \text{Eq.3-7}$$

where $k_B T$ is the thermal energy, σ_t is the surface grafting density of tethers, R is the surface interaction radius, and the empirical parameters λ and υ are the decay length and a correction factor to Dolan & Edwards scaling theory for the compression of polymer mushrooms, respectively (32). For a conservative estimate, fitting the low-SA data to Eq.3-7 over the range $25\text{\AA} < D < 100\text{\AA}$ gave the parameters $\varphi = 0.48 \pm 0.01$ and $\lambda = 16.8 \pm 0.2 \text{\AA}$, in close agreement with parameters reported for the compression of PEG2000 against streptavidin (shown by the gray line in Fig 1) (32). The bridging force was then extracted by subtracting the electrostatic and steric forces. The bridging forces were then linearly interpolated and smoothed using a moving average filter to minimize propagation of error when derivatizing the force profiles in subsequent analysis. Due to

the high data density achieved with the automated SFA, these transformations reduced the numerical accuracy of the data by $< 5\%$. Although in principle this method could be applied to the forces measured during all approaches or withdrawals, we omit this comparison because: 1) the origin of the change in forces measured during approach between cycles has not been fully explored (Section 3.4.3); and 2) the first three withdrawals gave coincident results (note coincident force profiles in Fig.3-3), while the fourth withdrawal (following double the compression) exhibited an insufficient data density for $D > 25\text{\AA}$ due to more rapid withdrawal of the surfaces.

Using these methods, we have extracted the bridging forces from the forces measured during the first approach and withdrawal, for the data shown in Fig.3-2 and Fig.3-3. The results of this calculation are shown in Fig.3-6. At larger distances, the bridging force measured during the approach appears to follow the same trend as the bridging force measured during surface separation. After the approach the bridging force increased in magnitude by $\sim 35\%$. This effect was only seen at closer distances ($D < 25\text{\AA}$), and may originate from providing tethers near the periphery of the contact area more time to form cross-bridges, or from allowing any uprooted lipid anchors to reinsert into the membrane. In all cases, the magnitude of the bridging force tended to increase as the surfaces approach, as suggested elsewhere (35).

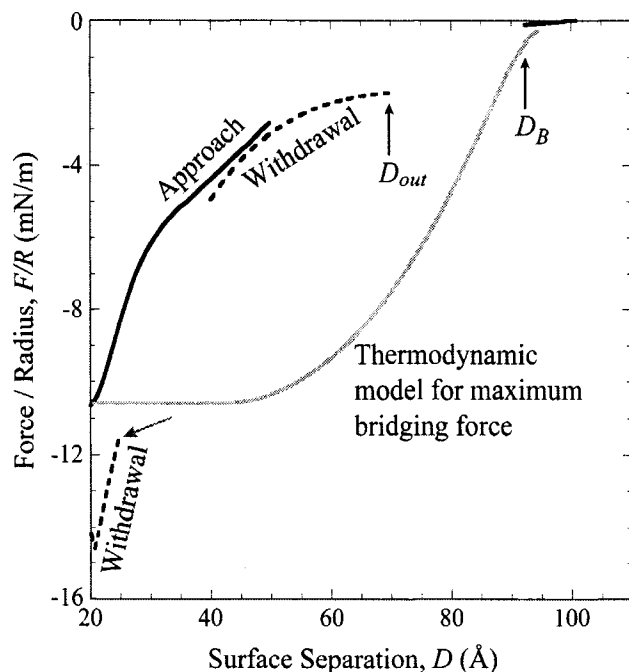


Figure 3-6. Bridging forces extracted from the force profiles in Fig.3-2 and Fig.3-3 as measured during the first surface approach (solid black) and first withdrawal (dashed). Arrows mark discontinuities arising from mechanical instabilities that produced gaps in the measured forces during approach (at D_B) and during withdrawal ($D \sim 25\text{\AA}$, and at D_{out}). These discontinuities precluded calculation of the bridging force over the entire distance range. In all cases, the bridging force extracted from the data is smaller in magnitude than what is predicted by the thermodynamic model (gray line, Eq.3-10, discussed in Section 3.4.5).

3.4.5 Thermodynamic Model for the Bridging Force

In this and the next section we evaluate two competing models for the bridging force between tethered ligand-receptor architectures, based on thermodynamic and kinetic arguments, respectively.

It has previously been shown using otherwise identical experiments with biotin ligands that many important features of the bridging force could be accurately described using an equilibrium model developed from thermodynamic arguments (32, 35). In short, a priori estimates were made of the repulsive steric and electrostatic forces and of the attractive bridging and van der Waals forces. In that model, lipid anchors were assumed

to be permanently bound within the membrane, so the probability of cross-bridge formation at a given tether extension, l , was:

$$\phi_{CB}(l) = e^{\frac{[W_{LR}-U(l)]}{k_B T}} / \left(1 + e^{\frac{[W_{LR}-U(l)]}{k_B T}}\right) \quad \text{Eq.3-8}$$

where W_{LR} is the bond energy of the ligand-receptor pair, $U(l)$ is the energy required to stretch the tether a distance l , and $k_B T$ is the available thermal energy (45, 46). Eq.3-8 is sigmoidal with a steep transition between bound and unbound states for most tethers and ligand/receptors of interest in biophysical research (35). The inflection in Eq.3-8 is defined as the tether's binding range, l_B , and can be used to provide a reasonable estimate of the maximum (or equilibrium) bridging force between two opposing, curved surfaces bridged by tethered ligands / receptors according to:

$$F_{bridging} = -\pi R k \sigma (l_B - D) (D + l_B - 2l_{eq}) \quad \text{Eq.3-9}$$

where k and l_{eq} are the tether's effective spring constant and equilibrium extension, respectively, R is the surface interaction radius (35). Here σ is the areal density of streptavidin receptor pockets ($3.9 \times 10^{16} \text{ m}^{-2}$), which is smaller than the ligand density ($1.2 \times 10^{17} \text{ m}^{-2}$). For short PEG tethers, the critical binding range, and consequently the bridging force, has been hypothesized to be independent of the approach velocity for $dD/dt < 10^4 \text{ \AA/s}$ (45, 46)—a condition that is generally true in SFA experiments. Although, Eq.3-9 is a very practical form, in this work we calculate the maximum bridging force more precisely using

$$F_{bridging}(D) = \int_{r=0}^{r=r_p} 2\pi r \sigma f(h) \cdot \phi(h) \cdot \alpha(h) dr \quad \text{Eq.3-10}$$

where $f(h)$ is the polymer stretching force based on Monte Carlo simulations reported elsewhere (33), $\sphericalangle(h) \approx 1$ is an operator that accounts for bridging at angles away from the surface normal, $h(r)$ is the gap height that varies along the in-plane radial distance, r , according to $h = D + R - (R^2 - r^2)^{1/2}$, and r_L is the radius of the contact area in the surface plane (Fig.1-1)(32, 35).

Here we improve this previous thermodynamic model by allowing tether-anchoring lipids to be uprooted from the membrane. Appendix 3-E explicitly shows that the polydispersity of the PEG tethers used in this study and for moderate levels of polydispersity (i.e. < 1.2) has only a miniscule effect on the binding range of individual tethers, and therefore should not significantly affect either the ensemble capture distance (D_B) or the resulting bridging force between surfaces; thus, we subsequently ignore polydispersity. To account for the uprooting of lipid anchors, we also use Boltzmann statistics for the equilibrium probabilities of attaining the following states, which are depicted in Fig.3-7: I) tether bound to lipid-anchoring membrane only (ϕ_{lipid}); II) cross-bridge formed between membranes (ϕ_{CB}); III) tether bound to receptor membrane only (ϕ_{LR}); and IV) neither lipid nor ligand bound. Mathematically,

$$\phi_{lipid}(l) = e^{W_{lipid}/k_B T} / Q(l), \quad \text{Eq.3-11}$$

$$\phi_{CB}(l) = e^{[W_{lipid} + W_{LR} - U(l)]/k_B T} / Q(l), \quad \text{Eq.3-12}$$

$$\phi_{LR}(l) = e^{W_{LR}/k_B T} / Q(l), \quad \text{Eq.3-13}$$

where $Q(l) = 1 + e^{W_{lipid}/k_B T} + e^{W_{LR}/k_B T} + e^{[W_{lipid} + W_{LR} - U(l)]/k_B T}$. In the thermodynamic limit the probability of both tether ends disjoining, $Q(l)^{-1}$, is small compared to the other states.

Further, numerical exploration of Eq.3-12 shows that the probability of cross-bridge formation is dominated by the weaker bond; that is, Eq.3-8 and Eq.3-12 are indistinguishable when the weaker bond energy is used in Eq.3-8 except when

$$|W_{lipid} - W_{LR}| < 1 k_B T.$$

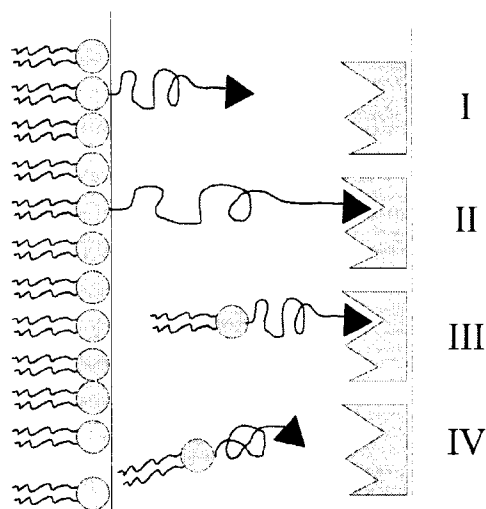


Figure 3-7. Four hypothesized configurations illustrating anchoring of a tether to: I) the ligated surface only (initial state), II) both surfaces via cross-bridge formation, III) the receptor surface only via lipid pullout, and IV) neither surface via dissociation of the ligand-receptor bond during state III. All tethers are presumed to be in state I at the experiment start but may “switch sides” to state III through the intermediary state II during repeated compression and withdrawal cycles. Given sufficient time (an open question), the lipids may reinsert (transition from state III to II) to achieve a more thermodynamically favorable environment.

We now compare the predictions of the thermodynamic model to three metrics in our experiment: the capture distance (D_B), the bridging force ($F_{bridging}$), and the jump out distance (D_{out}). The latter is discussed in Appendix 3-D.

Assuming that lipids are permanently bound within the membrane ($W_{lipid} \rightarrow \infty$) as in Eq.3-8 suggests a capture distance for the HABA architecture of $101 \pm 3 \text{ \AA}$, which is within the experimental uncertainty of the measured $92 \pm 9 \text{ \AA}$. If lipid anchors are instead

assumed removable, Eq.3-10 predicts the same D_B within $\pm 0.2\text{\AA}$ when $W_{lipid} > W_{HABA}$. Estimates of PEG-DSPE's anchor energy vary considerably depending on the measurement method: $13\pm 1 k_B T$ from CMC data of PEG2000-DSPE (47–50), $26 k_B T$ from single-molecule force spectroscopy of gel-phase DMPC (26) extrapolated for the longer length of DSPE, and $36\pm 4 k_B T$ from CMC data of a variety of phospholipids (51). However, all estimates give $W_{lipid} > (W_{HABA} = 10.5\pm 1.5 k_B T)$. Consistently, the measured D_B can be used as input to Eq.3-10 (with Eq.3-12) to back-calculate that the measured D_B could only be produced by $W_{lipid} \geq 9\pm 6 k_B T$. Thus, a wide range of lipid-membrane bond energies can be used to explain the measured capture distance of the tethered HABA architecture, as suggested by the lack of a term representing bond strength in the approximation for D_B derived in Appendix 3-B. This coincidence is somewhat remarkable given that the measured bridging forces are only marginally represented by the equilibrium model (Fig.3-6).

Similarly, Eq.3-10 and Eq.3-12, predict that the capture distance of the biotinylated tethers should be quite sensitive to W_{lipid} . Because biotin and streptavidin have one of the highest known ligand-receptor bond energies of $35 k_B T$ (52), Eq.3-10 predicts that a smaller lipid-membrane bond energy will dominate the probability of cross-bridge formation. The estimates of D_B for the biotinylated architecture range from $97\text{--}125\text{\AA}$ for $9 k_B T \leq W_{lipid} \leq 36 k_B T$, respectively. Mapping Eq.3-10 and Eq.3-12 to the measured D_B of the biotinylated architecture suggests that $W_{lipid} \geq 25 k_B T$. Mapping Eq.3-12 the ϕ measured from the model of repeated compression and withdrawal (Eq.3-5) along with the known HABA-streptavidin bond energy estimates that the lipid-membrane bond energy was $\geq 12\pm 1 k_B T$, in good agreement with the $13\pm 1 k_B T$ estimated from the

CMC of PEG-DSPE (47–50). Consequently, the biotin experiments provide a more accurate way to estimate the lipid-membrane bond energy. Though, both experiments give lower bounds for W_{lipid} , since similar results could be obtained for higher bond energies under non-equilibrium conditions (discussed in Section 3.4.6).

Fig.3-6 shows the bridging force expected from the thermodynamic model for the maximum bridging force (Eq.3-10 and Eq.3-12). The apparent plateau in the predicted bridging force for $D < l_{eq}$ evolves from a balance between tethers near the contact center exhibiting no force extension and tethers in the contact's periphery coming into range as D is decreased. The bridging force of ~ -10.5 mN/m at close contact ($D \sim 20\text{\AA}$) measured during the first approach is accurately predicted by the *a priori* thermodynamic model. These results do not invalidate the thermodynamic model as an estimate of the *maximum* bridging forces as a function of the surface separation. Indeed, the prediction in Fig.3-6 was made *a priori*—and deviated by less than a factor of 3 at all distances. And the thermodynamic model accurately predicted both the jump-in and jump-out distances, which depend intimately on tether properties. But clearly a more complex model is needed to fully account for the rich behavior of tethered HABA-streptavidin interactions, which was not evident in the biotin-streptavidin experiments due to the much stronger ligand-receptor bond strength.

3.4.6 Kinetic Model for the Bridging Force

For new insight we briefly develop a kinetic model of tethered ligand-receptor interactions and use the high-resolution data captured with the automated SFA to compute the rates of bond formation. As mentioned previously, the events that may dynamically affect the adhesion and decohesion include: ligand-receptor bond formation

and reformation, lipid pullout and reinsertion, and biased diffusion of the ligand on the flexible polymer tether. This diffusion rate is estimated from scaling arguments according to:

$$k_p(h) = U(h) e^{-U(h)} / 1.43 \tau_z, \quad \text{Eq.3-14}$$

where τ_z is the chain's Zimm relaxation time, as described fully elsewhere (33, 37, 45, 46). This diffusion rate ranges from $10^3 - 10^7 \text{ s}^{-1}$ over the distance regime of interest, and is therefore fast compared to the experimental timescale. Moreira et al. show using an adaptation of Kramer's kinetics for the escape of a particle over a potential barrier that a single ligand-receptor pair tethered by a 100-mer PEG chain should exhibit equilibrium bond kinetics for surface approach or withdrawal speeds $< 10^4 \text{ \AA/s}$ for $W \sim 10 k_B T$ (45, 46)—conditions that are met here.

To quantify the rate of lipid pullout, we have estimated the impact of the known forces on the lifetimes of the ligand-receptor and lipid-membrane “bonds”. To a first approximation, ligand-receptor and lipid-membrane bond lifetimes have been shown to depend on the force, f , applied to the bond according to $\tau = \tau_0 e^{-fx/k_B T}$, where x is the effective bond length as first proposed by Bell (2) and discussed by others in the context of lipid extraction (14, 26, 53). Although the Bell model lacks predictive precision in many situations, it is nonetheless sufficiently accurate to semi-quantitatively compare the timescales relevant to this study (6, 16). Because the anchoring DSPE lipid is long (28.9 \AA) (51) compared to the force length scale ($l_B - l_{eq} \approx 50 \text{ \AA}$), the polymer extension force that is applied to the lipid-membrane bond changes dramatically as the lipid is pulled out from the membrane. Therefore, we calculate an average dissociation time, viz.,

$$\tau_{bond} = (\tau_0/x) \int_0^{x'} e^{-f x'/k_B T} dx' \quad \text{Eq.3-15}$$

which is significantly longer than if the lipid length were ignored. For the intrinsic lifetime of a DSPE-membrane bond we use the empirical observation that samples prepared and characterized in the SFA exhibit negligible loss of adhesion for up to ~3 days, suggesting a natural timescale for the spontaneous transfer of ligated PEG-DSPE from the membrane to the solvent. Similarly, liposomes protected by a layer of PEG2000-lipid are able to circulate in vasculature for several days (i.e. ref 54), suggesting a comparable timescale for PEG-lipid / membrane dissociation. For the lifetime of the ligand-receptor bond, we use the Bell model to calculate $\tau = 1/k_{off}$ along with a harmonic function for the lifetime of the unstressed bond; viz., $\tau_0 = (1/\nu) e^{-W_{LR}/k_B T}$ and $x = 4\text{\AA}$, the length of a hydrogen bond, where $\nu \sim 10^9 \text{ s}^{-1}$ is the damped vibrational frequency of the bonded ligand in an aqueous (viscous) environment (17a, 17b).

Table 3-2 shows the predicted lifetimes for single HABA-streptavidin, biotin-streptavidin, and DSPE-membrane bonds as a function of the gap height. For first-order continuum processes, the system timescale is dominated by the slowest internal mechanism. As shown in Table 3-2, the controlling timescale depends intimately on h and therefore varies across the curved interfacial landscape of the SFA surfaces. Considering just the center of the interaction area ($h = D$), when tethers are stretched near their binding range ($\sim 100\text{\AA}$), cross-bridges would be expected to dissociate rapidly through breakage of HABA-streptavidin bonds and slowly through lipid-membrane bonds. Likewise once the surfaces had pulled themselves into a close adhesive contact where bonds are largely unstressed ($h \approx 50\text{\AA}$), separating up to the jump out distance ($h \approx$

90Å) would primarily break HABA-streptavidin bonds. Away from the contact center ($h > D$), bonds within range ($h < l_B$) would experience nearly the same history of approach and withdrawal, $h(t)$, and similar rates of dissociation would be expected during surface movement. However, while the surfaces were in contact, typically for ~12 min., tethers in the periphery of the contact area where $h \approx 100 \text{ Å}$ might be expected to rapidly form cross-bridges and occasionally pullout lipids. However, in all cases the rate of HABA-streptavidin dissociation is very fast compared to the timescale of lipid pullout, and we expect the decohesion to be principally governed by the breakage of ligand-receptor bonds. Lipid reinsertion, if present, would be inconsequential if lipids had a small probability of leaving the membrane. Only for the biotin experiments would lipid pullout be expected to significantly contribute to the decohesion due to the long lifetime of the biotin-streptavidin bond.

Table 3-2. Predicted lifetimes of bonds stressed by PEG2000 tethers for various tether extensions, h .

“Bond”	τ_0 (bond unstressed)	τ (bond stressed)		
	$h = l_{eq}$	$h = 50 \text{ Å}$	$h = 90 \text{ Å}$	$h = 100 \text{ Å}$
HABA-streptavidin *	37 μ s	31 μ s	6 μ s	3 μ s
biotin- streptavidin *	19 d	14 d	3 d	38 h
Lipid-membrane	3 d **	62 h	8 m	34 s

* $W_{HABA} = 10.5 k_B T$; $W_{biotin} = 35 k_B T$. ** from experimental observation.

Therefore, as a first approximation we assume negligible rates of lipid pullout and lipid reinsertion, so the fraction of tethers forming cross-bridges at a given gap height is:

$$\partial\phi_{CB}/\partial t = k_{on}(h)(1 - \phi_{CB}) - k_{off}\phi_{CB} \quad \text{Eq.3-16}$$

where in general $\phi_{CB} = \phi_{CB}(h(t))$. In the slow-approach regime of our experiments, the equilibrium probability of cross-bridge formation is:

$$\phi_{CB}(h) = k_{on}(h)/(k_{on}(h) + k_{off}(h)). \quad \text{Eq.3-17}$$

Although the initial rate of ligand-receptor association is governed by the diffusion timescale of the tethered PEG (~ 1 ms near D_B) (33, 34, 45, 46), the re-association rate may be dramatically faster because the relatively sluggish movement of the polymer chain may allow many more attempt frequencies than if a polymer chain recoiled completely after breaking a ligand-receptor bond. Here we calculate k_{on} from the presumed bridging forces using Eq.3-17. For this computation, the bridging forces inferred from surface withdrawal were used, since the data spanned a more useful range than the forces measured during surface approach (Fig.3-2 and Fig.3-3). The probability of cross-bridge formation was deciphered by inverting Eq.3-10 with $\angle(h) = 1$; viz.,

$$\phi_{CB}(D) = (\partial(F/R)/\partial D)/(2\pi\sigma f(D)). \quad \text{Eq.3-18}$$

Fig.3-8 shows that the probability of cross-bridge formation measured for tethered HABA-streptavidin was always much less than that predicted by the thermodynamic model (Eq.3-12). Both approach 1 and 0 at near and far distances, respectively, but differ significantly at intermediary distances. During the first three withdrawals, the calculated ϕ_{CB} curves were coincident within $\pm 5\%$; of these withdrawals only the first is shown for clarity. Although Eq.3-18 properly accounts for the curved interfacial geometry, it nonetheless is an area-weighted average, which precludes a more precise description of its origin. Another limitation is that Eq.3-18 is less accurate at close distances because it

divides two values close to zero, and is therefore very sensitive to noise in the data. Consequently, the calculated probabilities of cross-bridge formation were not bounded by 1. Also, values within 4\AA of D_{out} could not be determined due to truncation of the dataset from the smoothing filter. However, back-substitution of the calculated ϕ_{CB} curves into the numerical solution for the bridging force (Eq.3-10) produce reasonable agreement to the measured results (omitted for brevity).

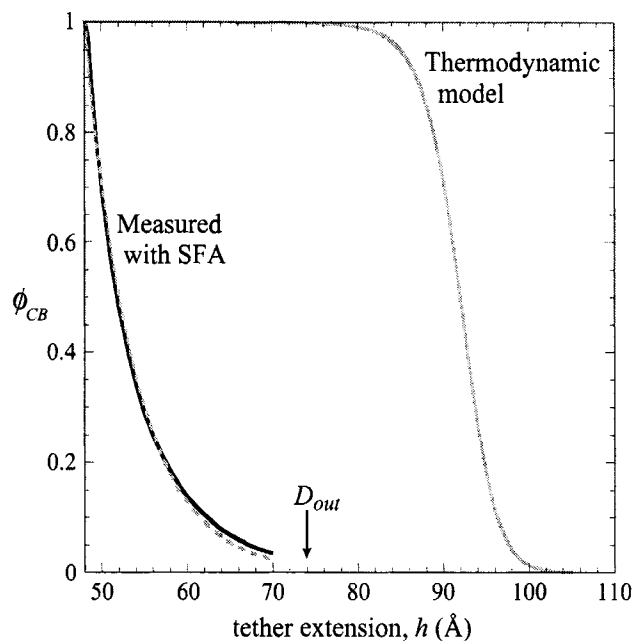


Figure 3-8. Probability of a single tether forming a cross-bridge as a function of the distance, h , between the tether anchor and a complementary receptor on an opposing surface. The thermodynamic model (solid gray, Eq.3-12) overestimates the probability of cross-bridge formation for the weakly binding HABA-streptavidin tethered interaction, compared to that measured during the first surface withdrawal (solid black, Eq.3-18). The latter decays exponentially, as shown by the fit to Eq.3-19 (dashed gray).

The binding probability curve shown in Fig.3-8 coincided with the form,

$$\phi_{CB} = \nu e^{-(h-\delta)/\Lambda} \quad \text{Eq.3-19}$$

for $h \geq \delta$. The fitted parameters are $\delta = 48 \pm 1 \text{ \AA}$, $\nu = 0.97 \pm 0.05$, and $\Lambda = 5.84 \pm 0.03 \text{ \AA}$. Although empirical in origin, the exponential dependence of ϕ_{CB} on D is expected from the form of Eq.3-12. The probability of cross-bridge formation decays towards zero as the receptor is moved farther away from the anchor of the tethered ligand. This result is also seen by repeating the same analysis on the forces measured during the first approach, for which ϕ_{CB} can only be calculated over the range $D_B < h < L$ due to discontinuities in the data (Fig.3-2). Although this is a fairly narrow range of distances and the numerical uncertainty is significant, we nonetheless found that there ϕ_{CB} also diminished towards zero as $h \rightarrow L$, in agreement with the form of Eq.3-19.

Using the fit to Eq.3-19 for the probability of cross-bridge formation, we have extrapolated the probability curve shown in Fig.3-8 beyond the measured range to estimate the k_{on} for the tethered HABA-SA reaction over the entire distance regime via Eq.3-17. Fig.3-9 compares the measured rates of HABA-streptavidin association against the presumed rates of dissociation as a function of the gap height, h . As with the binding probability curves (Fig.3-8), the calculated association rates are area-weighted averages, which precludes precise interpretation; however, several important features are clear. The rate of association decreased by nearly two orders of magnitude over a distance of just 50 \AA , while the predicted dissociation rate increased by only one order of magnitude. Both rates are influenced by the tether properties. For the dissociation rate, this was an assumption of the Bell model, as the tether pulls against the bond (2). For the initial association rate, the role of the tether's stretching potential is implicit in Eq.3-14. The

characteristic timescale for re-association is of the order $1/k_{on} \sim 100 \mu\text{s}$, which is typically superiorly faster than the characteristic diffusion rate of the distal end of a PEG tether (Fig.3-9). Thus, we infer that the preference of the polymer chain to return to its relaxed state biases the diffusion of its distal end but not strongly enough to remove the ligand from the vicinity of the receptor surface. This comparison may suggest a more universal result; namely, that for a single tethered ligand-receptor a large difference in timescales may exist between the first and subsequent bridging events.

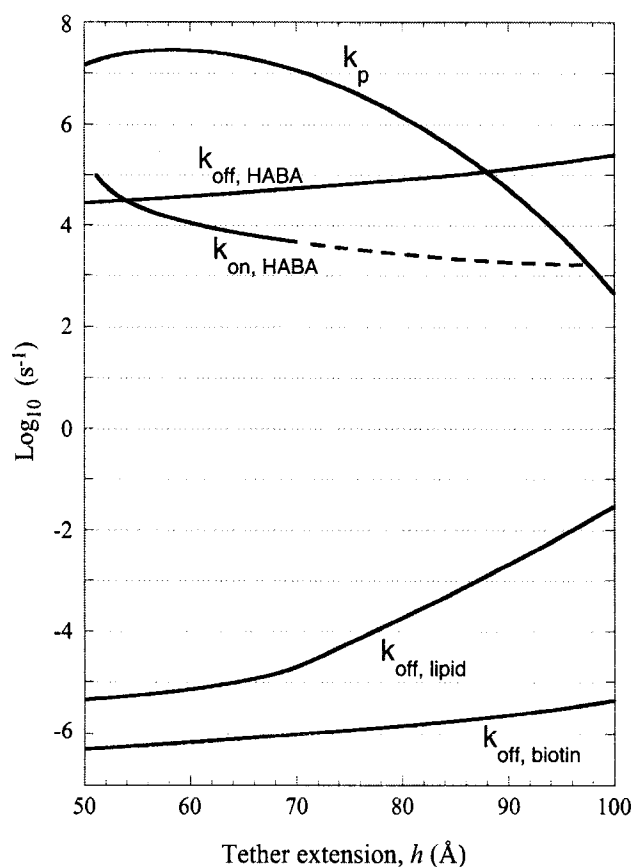


Figure 3-9. Kinetic parameters of the tethered HABA-streptavidin interactions. The interaction distance, h , is defined as the distance between the tether anchor and a complementary receptor on an opposing surface. In SFA experiments, h varies across the curved substrates (Fig.1-1). The rate of association between tethered HABA and streptavidin ($k_{on, HABA}$) is shown as a solid line over the measured region. Beyond the measured region, $k_{on, HABA}$ was determined by extrapolating the measured cross-bridge probability using Eq.3-19 and thus has considerable uncertainty (dashed line). The

bond dissociation rates of tethered HABA-streptavidin ($k_{off, HABA}$) and of tethered biotin-streptavidin ($k_{off, biotin}$) are derived from the Bell model (2). For the measurements with HABA, over most of the distance regime the kinetic rates are much slower than the polymer sampling rate (k_p , Eq.3-14) but much faster than the rate of lipid pullout ($k_{off, lipid}$), justifying the quasi-steady state assumption used to derive Eq.3-18.

With these kinetic effects in mind, it is both remarkable and convenient that the equilibrium framework discussed in Section 3.4.5 accurately predicts the capture distances for both the HABA and biotin architectures. However, it is uncertain from where this coincidence arises. Although all experiments were performed within the slow velocity regime, and with loading rates slower than most reported in the literature (Table 3-1)(6, 16), there are clear non-equilibrium effects, such as a persistence of lipid anchors between successive cycles of approach and withdrawal despite low thermodynamic probabilities of retention.

However, one significant limitation of the equilibrium model is that it does not account for molecular structure. The pull of a tether may bias the trajectory of a ligand leaving a binding site, which could dramatically alter the bond kinetics by defining a new energy landscape along the reaction coordinate (17, 18, 55). Thus, the energy of the HABA-SA bond under directed stress could be lower than the 9–12 $k_B T$ reported from solution thermodynamics (14, 19, 20). A decrease in bond energy would shift the inflection of the sigmoidal binding-probability curve towards shorter distances, which is consistent with our observations (Fig.3-8).

Also, Martin et al. showed that a reduction in the mobility of ligands or receptors within their anchoring planes could decrease ϕ_{CB} substantially (11). In our experiments, there is one receptor pocket per $\sim 1800 \text{ \AA}^2$ of surface, which along with the lateral

diffusion rate of the lipids anchoring tethers (Section 3.3.2), suggests that the relevant diffusion timescale is of the order of ~ 1 ms, which is fast enough that this effect is unlikely to be significant. Importantly, though, Martin et al. suggested that the probability of cross-bridge formation is significantly reduced when tethered ligands outnumber receptors due to competition and exclusion effects (11). Such occlusion, which is not accounted for by our thermodynamic model, would also decrease the probabilities of cross-bridge formation.

3.5 Conclusions

We have characterized the binding frequency of a weak ligand-receptor bond using an automated Surface Forces Apparatus (SFA). The use of PEG to tether the ligands deconvoluted the curved geometry of the SFA by simultaneously applying the same loading rate to several million bonds. Along with the control and precision afforded by our automated SFA, this has enabled the weakly-binding HABA-streptavidin bond to be characterized with a precision and statistical validity that is not usually available with other force spectroscopies. Primary advantages of using HABA instead of biotin as a ligand towards streptavidin include: 1) less surface damage (lipid pullout) occurs during decohesion; and 2) the binding affinity is similar to the average encountered in nature, making studies more generalizable to the vast array of biological interactions.

Results from this experiment with HABA ligands interacting with streptavidin receptors were compared to otherwise identical experiments with biotin ligands. The probability of cross-bridge formation—and hence the specific bridging force between surfaces—was significantly smaller when HABA was used as the ligand. We have shown that for weakly-binding tethered ligands and receptors the intrinsic off-rate and

subsequent on-rate may be significant on the experimental or biological timescales, which complicates the analysis of bond rupture forces under the slow pulling regime. However, the thermodynamic model for specific bridging (Eq.3-10) still provides an order-of-magnitude estimate for the maximum bridging force between the surfaces as a function of their separation. The thermodynamic model also reasonably estimates the surface capture distance and jump-out distance when corrections are made for the pullout of lipid anchors and tether polydispersity. The latter is shown to have only a small effect on the range and magnitude of the adhesion.

Continued research into the behavior of weakly-binding ligands and receptors should foster enhanced performance of biofunctionalized coatings used in targeted drug delivery vehicles, biosensors, and self-assembled nanostructures.

3.5 Appendix 3-A: Survey of Ligand-Receptor Bond Energies and Molecules Selected for Force Spectroscopy

It is insightful to compare the energies of dissociation for ligand and receptor pairs used in dynamic force spectroscopy (DFS), shown in Table 3-3. Although this list is not exhaustive and not all energies are known by the author as of the date of this publication, an attempt has been made to represent work that in our opinion has been pivotal to the progress of the technique. Note that there is significant overlap between the entries in Table 3-3 and those in Table 1-1, as many of the ligands and receptors of broad interest have been explored with DFS.

Table 3-3. Selected ligands and receptors studied with DFS.

Molecular pair	Bond energy* ($k_B T$)	K_d (nM)*	Technique(s) used for force transduction **	Refs
biotin / (strept)avidin	35	10^{-6}	BFP, AFM, SFA	(5, 12–15, 22, 26, 32–35, 56, 57, 64a–64i)
lipids (various) / membrane	20–23	0.55	AFM	(26)
anti-fluorescein / Fab' (including mutants)	17–24	0.04–39	SFA, AFM	(65–67b)
neural cell adhesines	19–21	0.8–6	AFM	(68)
sialyl Lewis X / selectin	18–24	0.04–20	AFM	(61–64)
Ferritin / antiferritin Ab	20	13	AFM	(68a–68b)
MUC1 / scFv	18.5	9	AFM	(60)
Recombinant P-selectin / P- selectin glycoprotein ligand- 1 (PSGL-1)	17	55	AFM	(68c)
Anti-HSA / HSA	14	830	AFM	(68d)
carbohydrate / L-lectin	---	---	BFP	(4)
concanavalin A / alpha-D- mannose	---	---	AFM	(69)
mannuronan C-5 epimerase AlgE4 and its polymer substrate	---	---	AFM	(70)
digoxigenin / antibody	---	---	AFM	(71)
IgG—Ab / protein G	---	---	AFM	(71a)
Anti-intercellular adhesion molecule-1 (ICAM-1) / ICAM-1	---	---	AFM	(71b)
Actin / actin in actin	---	---	AFM	(64f)
Cell adhesion proteoglycans	---	---	AFM	(71c)
Insulin/insulin	---	---	AFM	(71d)
Two protein substrates citrate synthase or β - lactamase / E.coli chaperonin GroEL	---	---	AFM	(71e)
Mylein basic protein / lipid bilayers	---	---	AFM	(71f)
DNA, various lengths	---	---	AFM, OT	(71g–71k)

* When only one of W or K_d was reported the other was estimated: $K_d = \exp(-W/k_B T)$ (2). ** BFM = biomembrane force probe; AFM = atomic force microscopy; SFA = surface forces apparatus; OT = optical trapping.

Also, in Chapter 1 it was stated that the average bond energy for the 2,276 biological ligand-receptor complexes listed in the PDBbind database v.2004 was $14.7 k_B T$ (monomodal with standard deviation $4.9 k_B T$) (72, 72). Now that the latest version of this database (v.2005) has grown substantially, now encompassing 2,756 entries from the protein databank, it is worth re-examining. The average bond energy calculated from dissociation constants reported in this newer database is $14.6 k_B T$ (standard deviation of $4.8 k_B T$), in good agreement with the value reported in Chapter 1. A plot of the calculated bond energies in Fig.3-10 shows that the distribution of bond energies for biologically occurring ligand-receptor complexes roughly follows a gaussian distribution centered around $14.6 k_B T$.

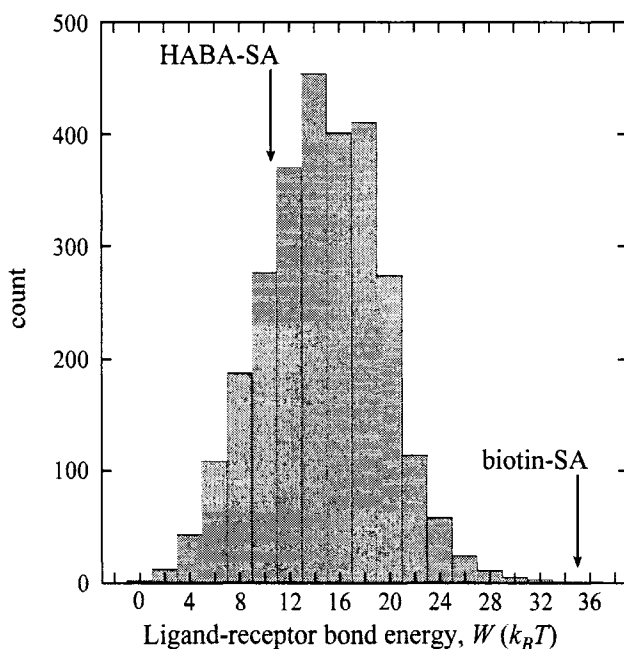


Figure 3-10. Distribution of biologically occurring ligand-receptor bond energies, calculated from dissociation constants reported in the PDBbind database v.2005 (72, 72) via $W = -k_B T \ln(K_d)$ (2). Arrows mark the estimated energy of the HABA-SA bond (left) and the biotin-SA bond (right).

3.6 Appendix 3-B: Analytical Solution For the Capture Distance

It can be shown that the capture distance during surface approach is relatively insensitive to variation in $k_{cantilever}$, R , and σ , as shown numerically elsewhere (35), when $l_{eq} \gg k_{cantilever}/2k\pi R\sigma$, giving the approximation:

$$D_B \approx l_{eq} + \kappa^{-1} \Upsilon \left[\left(\sigma_e \kappa e^{-\kappa l_{eq}} / 2k\sigma\epsilon\epsilon_0 \right) \right] \quad \text{Eq.3-20}$$

where σ_e is the surface charge density, ϵ and ϵ_0 are the permittivity of solvent and vacuum, and κ^{-1} is the solvent Debye length—giving $D_B \approx 90\text{\AA}$ for this study (see also Eq.3-6). Although this value coincides with the measured D_B of $92 \pm 9\text{\AA}$, Eq.3-20 should underestimate D_B because it assumes that each tether's binding range is discrete; consequently, D_B is always slightly extended beyond l_B , as shown elsewhere numerically (35).

3.7 Appendix 3-C: Measuring Interaction Radii with a CCD

Although the use of a CCD camera to record FECO fringes during an SFA experiment is gaining wider acceptance, it is worth noting that it produces considerably smaller error in measuring the interaction radius compared to the 10–20% usually reported (74–77). This is because in conventional (manual) SFA technique, the interaction radius is measured by repeatedly measuring the relative positions of only three or a few points along the shape of the FECO fringe; therefore, the sphericity of the contacting surfaces must be assumed. In contrast, digitization of the FECO fringes allows 100–200 points along the path of each FECO fringe to be fit simultaneously. Here the error in measuring either a normal or cross radius was typically $\pm 0.1\%$ (95% CI), which propagates to $\pm 0.3\%$ in the effective R . Because all the forces of interest scale linearly

with R (78), including the specific bridging force (35), this reduction in the uncertainty of R significantly improves the precision in determining the intersurface forces.

3.8 Appendix 3-D: Analytical Solutions for Jump Out Distance

To posit how decohesion may have involved the breakage of lipid-membrane bonds, we briefly develop several expressions that relate the critical distance of decohesion (D_{out}) to physical properties of the tether architecture. The analysis is based on the thermodynamic model, which we have shown provides a reasonable estimate of the bridging forces for strongly-binding tethered ligands (Section 3.4.5). At present, derivations based on the kinetic model for weakly-binding tethered ligand-receptor pairs (Section 3.4.6) have not yet been developed.

As with the capture distance, the jump out distance occurs from a mechanical instability at the distance where the derivative of the force profile exceeds the stiffness of the measuring cantilever ($k_{cantilever}$) (36). In general, it may be predicted by solving:

$$dF_{total}/dD \approx d[F_{steric}(D_{out}) + F_{bridging}(D_{out})]/dD = k_{cantilever}. \quad \text{Eq.3-21}$$

For the steric force we use the form of Dolan and Edward's theory (Eq.3-7). For the bridging force we use the thermodynamic model (Eq.3-9). Then the jump out distance is:

$$D_{out} \approx l_{eq} + \frac{k_{cantilever}}{2\pi kR\sigma} + \lambda \Upsilon \left(\frac{36\nu k_B T}{k\lambda^2} \text{Exp} \left[- \left(2l_{eq} + \frac{k_{cantilever}}{\pi kR\sigma} \right) / 2\lambda \right] \right) \quad \text{Eq.3-22}$$

where Υ is the Lambert W-function applied to the parenthetical terms (79). Eq.3-22 shows that to a first approximation the jump out distance does not depend on l_B (or by implication on the bond strengths), but instead is related to the balance between compressive and elastic properties of individual tethers. Consequently, D_{out} is also relatively insensitive to the surface from which the tether disjoins.

Eq.3-22 predicts $D_{out} = 51.8\text{\AA}$. which is slightly larger than the 45\AA obtained from subtracting the length of a DSPE lipid (28.9\AA) from the measured D_{out} . This discrepancy likely results from the inadequacy of the thermodynamic model to capture the complex interactions of the weakly-binding HABA-SA conjugate. The extrinsic measurement conditions ($k_{cantilever}$, R , σ) are inconsequential when $l_{eq} \gg k_{cantilever}/2k\pi R\sigma$, as in our measurements. In such cases,

$$D_{out} \approx l_{eq} + \lambda\Upsilon\left(36\nu k_B T e^{-l_{eq}/\lambda} / k\lambda^2\right) \quad \text{Eq.3-23}$$

or 51.7\AA for the architecture in this study. The value l_{eq} is a lower bound for D_{out} and is reached in the limit $F_{steric} \rightarrow 0$. Due to the relative weakness of the measuring cantilever used (328 ± 11 N/m), D_{out} can also be accurately estimated from the location of maximal adhesive force, D_{F^*} . Solving $d(F_{steric} + F_{bridging})/dD = 0$ for D gives a positive second derivative in the force profile, and the minimum (most negative) force occurs at:

$$D_{F^*} \approx \lambda\Upsilon\left(36k_B T \nu \lambda^{-2} e^{l_{eq}/\lambda}\right) - l_{eq} \quad \text{Eq.3-24}$$

or 51.7\AA . To test these analytical solutions, we use the numerical model Eq.3-10 with Eq.3-12 to locate where the force gradient equals $k_{cantilever}$. In agreement with the analytical solutions, the D_{out} predicted with this numerical method changed by less than 1% over an enormous range of cantilever spring constants ($0-10^6$ mN/m) and surface interaction radii ($0.1 \text{ cm} \rightarrow +\infty$) for the parameters of interest. When the lipid length is added, the jump out distances predicted by both the numerical and analytical solutions agree with the measured D_{out} within $\pm 2\text{\AA}$ over a wide range of ligand-receptor and lipid-membrane bond energies ($W_{lipid} \sim 9-36 k_B T$, $W_{LR} \sim 10.5-35 k_B T$), showing that lipid pullout is a major component of the decohesion mechanism. The insensitivity of D_{out} to

the bond energies is expected from the analytical solutions for D_{out} (Eqs.22, 23, and 24) for the parameters of interest.

Eqs.22, 23, and 24 show that to a good approximation the distance of maximal adhesive force between curved surfaces bridged by many tethered ligand-receptors is not a strong function of the binding ranges or bond strengths, but is more closely related to the balance between compressive and elastic properties of individual tethers. This insensitivity likely explains why the thermodynamic still provides reasonable estimates for D_{out} and D_B (Appendix 3-B).

3.9 Appendix 3-E: Polydispersity Effects

To examine the role of polydispersity on specific cross-bridge formation, we first consider the binding probability of an ensemble of tethered ligand / receptors averaged over a gaussian distribution of chain lengths; viz.,

$$\langle \phi(h) \rangle = \int_0^{\infty} \phi_N(h) P_N dN \quad \text{Eq.3-25}$$

where N is the chain length in mers, where $\phi_i(h)$ is Eq.3-12 with the tether stretching energies interpolated from Monte Carlo data (33), and P_N is a gaussian distribution with center, $\langle N \rangle$, and standard deviation, $s.d.$ Fig.3-11 plots Eq.3-25 for several levels of polydispersity. Expectedly, the transition between bound and unbound states becomes less discrete with respect to distance as the width of the distribution increases. However, the predicted inflection point, l_B , changed by less than 0.03\AA over a wide range of parameters relevant to this study ($\langle N \rangle = 45$ mers, $1 \text{ mer} < s.d. < 15$ mers, and $W = 10.5 k_B T$). Because the thermodynamic model shows that the bridging force (Eq.3-9) is

correlated to the binding range of individual tethers (l_B), we intuit that the bridging force should not be very sensitive to tether polydispersity.

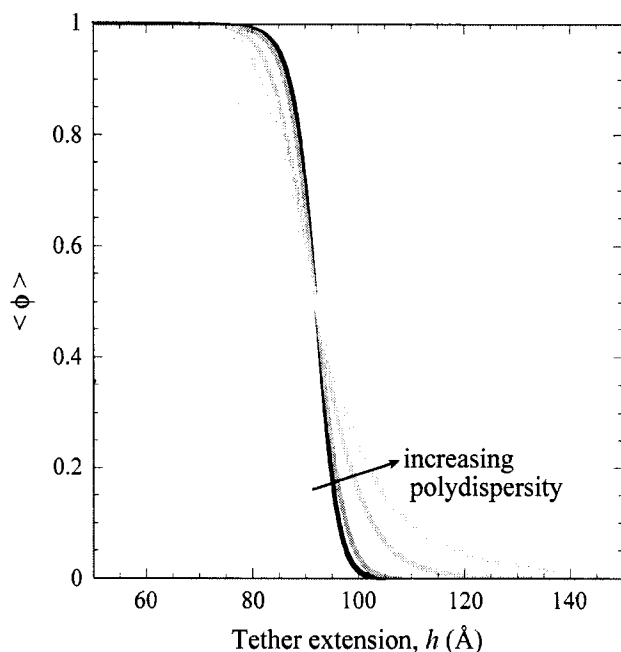


Figure 3-11. Ensemble-averaged probability of cross-bridge formation between plane-parallel interfaces bearing PEG-ligand / receptor architectures for various levels of polydispersity (Eq.3-25). The arrow marks the direction of increasing polydispersity of the PEG tether; left to right: $s.d. = 0$ (PI = 1), $s.d. = 4.2$ (PI = 1.008), $s.d. = 10$ (PI = 1.04), $s.d. = 15$ (PI = 1.1). In all cases the average polymer length is $\langle N \rangle = 45$ mers and the ligand-receptor bond energy of $10.5 k_B T$ corresponds to HABA / SA.

To test this hypothesis, we calculated the bridging force expected for both a mono- and poly-disperse mixture of PEG tethers using the thermodynamic model; viz.,

$$F_{bridging}(D) = \int_{r=0}^{r=r_i} 2\pi r \int_0^{\infty} \sigma_N f_N(h) \cdot \phi_N(h) \cdot \zeta_N(h) dN dr \quad \text{Eq.3-26}$$

where the functions $f(h)$, $\phi(h)$, $\zeta(h)$, and the constant σ , have been explicitly written as functions of the polymerization index. The known distribution of the length of the

HABA-PEG-DSPE conjugate used in these studies was used to determine each σ_N ($\langle N \rangle = 45$ mers, $s.d. = 4.2$ mers, or polydispersity index (PI) = 1.008 (29)). For the stretching forces and energies, the Monte Carlo data were interpolated as before.

Expectedly, the bridging force was reduced by less than a few percent over the entire distance range when the effect of polydispersity was considered. As the width of the chain length distribution increases, the bridging force decreases due to a balance between shorter and longer chains exhibiting more or less elasticity, extent of stretching at a given distance, and frequency of bond formation. The predicted capture distance (D_B) was only 0.5\AA smaller than that of the monomodal distribution. At close distances where the effect of polydispersity is greatest, the predicted jump-out distance (D_{out}) was 1.9\AA larger than in the monodisperse case. For an enormous standard deviation of 20 mers (PI = 1.18), the model predicts a reduction of F_{adh} by only 2 mN/m.

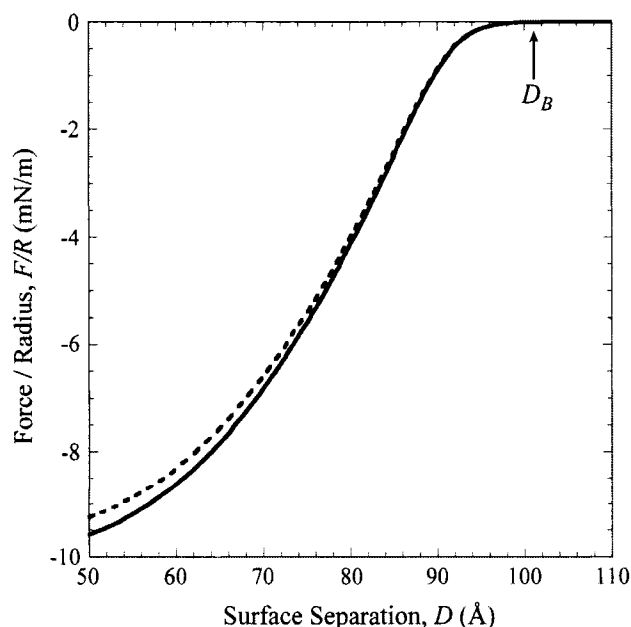


Figure 3-12. Ensemble-averaged bridging force between spherically-curved surfaces bearing PEG-ligand / receptor architectures, predicted using the thermodynamic model for monodisperse (solid line, Eq.3-10) and polydisperse (dashed, Eq.3-12, $s.d.$

= 4.2 mers) PEG2000 tethers wielding HABA against a field of streptavidin receptors ($\langle N \rangle = 45$ mers, $W_{LR} = 10.5 k_B T$).

3.10 Acknowledgements

We thank Anthony Delacruz for helping synthesize the HABA-PEG-DSPE conjugate, Dennis Mulder and Kaki Cheung for writing the spectrometer control software, D.M. for assistance with the SFA electronics, Carlos Marques for kindly providing the Monte Carlo data, Alexis Grabbe for furnishing the electrostatics program, and Volkmar Heinrich, Igal Szleifer, and Stephen Boyles for useful discussions. This work was supported by NSF DMR-0606564.

3.11 References

1. Alberts, B. et al. 1994. *Molecular Biology of the Cell*, 3rd ed. Garland, New York.
2. Bell, G.I. 1978. Models for the Specific Adhesion of Cells to Cells. *Science* 200: 618–627.
3. Hammer, D.A. and M. Tirrell. 1996. *Annu. Rev. Mater. Sci.* 26:651–691.
4. Evans, E.B. 1999 Looking inside molecular bonds at biological interfaces with dynamic force spectroscopy. *Biophys. Chem.* 82(2-3):83–97.
5. Merkel, R, P. Nassoy, A. Leung, et al. 1999. Energy landscapes of receptor-ligand bonds explored with dynamic force spectroscopy. *Nature.* 397(6714):50–53.
6. Hummer G. and A. Szabo. 2003. Kinetics from nonequilibrium single-molecule pulling experiments. *Biophys. J.* 85 (1):5–15.
7. Gabai, R., L. Segev, and E. Joselevich. 2005. Single polymer chains as specific transducers of molecular recognition in scanning probe microscopy. *J. Am. Chem. Soc.* 127(32):11390–11398.
8. Larsen, K., M.B. Thygesen, F. Guillaumie, et al. 2006. Solid-phase chemical tools for glycobiology. *Carbohydr. Res.* 341(10):1209–1234.
9. Evans E. 2001. Probing the relation between force - Lifetime - and chemistry in single molecular bonds. *Annu. Rev. Biophys. Biomol. Struct.* 30:105–128.
10. Hinterdorfer, P. and Y.F. Dufrene. 2006. Detection and localization of single molecular recognition events using atomic force microscopy. *Nat. Methods.* 3(5): 347–355.

11. Martin, J.I., C.Z. Zhang, Z.G. Wang. 2006. Polymer-tethered ligand-receptor interactions between surfaces. *J. Polym. Sci., Part B: Polym. Phys.* 44(18):2621–2637.
12. Florin, E.L., V.T. Moy, and H.E. Gaub. 1994. *Science*. 264(5157):415–417.
13. Helm, C.A., W. Knoll, and J.N. Israelachvili. 1991. *Proc. Natl. Acad. Sci. U.S.A.* 88(18):8169–8173.
14. Leckband, D., W. Müller, F.J. Schmitt, and H. Ringsdorf. 1995. Molecular mechanisms determining the strength of receptor-mediated intermembrane adhesion. *Biophys.J.* 69(3):1162–1169.
- 14a. Torreggiani, A. and G. Fini. 1998. *Biospectroscopy*. 4(3):197–208.
15. Yuan, C.B., A. Chen, P. Kolb, and V.T. Moy, V.T. 2000. Energy Landscape of Streptavidin-Biotin Complexes Measured by Atomic Force Microscopy. *Biochemistry*. 39(33):10219–10223.
16. Olga K. Dudko,¹ Gerhard Hummer,² and Attila Szabo². 2006. Intrinsic Rates and Activation Free Energies from Single-Molecule Pulling Experiments. *Phy. Rev. Lett.* 96(10):108101-1–108101-4 (2006).
17. Raible, M., M. Evstigneev, P. Reimanna, et al. 2004. Theoretical analysis of dynamic force spectroscopy experiments on ligand–receptor complexes. *J. Biotechnol.* 112:13–23.
- 17a. Kramers, H. A. 1940. Brownian motion in a field of force and the diffusion model of chemical reactions. *Physica (Utrecht)*. 7:284–304.
- 17b. Hänggi, P., P. Talkner, and M. Borkovec. 1990. Reaction Rate Theory: Fifty Years After Kramers. *Rev. Mod. Phys.* 62:251–342.
18. Marshall, B.T., K.K. Sarangapani, J.H. Lou, et al. 2005. Force history dependence of receptor-ligand dissociation. *Biophys.J.* 88(2):1458–1466.
19. Hofstetter, H. M. Morpurgo, O. Hofstetter, E.A. Bayer, and M. Wilchek. 2000. A labeling, detection, and purification system based on 4-hydroxyazobenzene-2-carboxylic acid: an extension of the avidin-biotin system. *Anal. Biochem.* 284:354–366.
19. Kuhl, T. L., D.E. Leckband, D.D. Lasic, and J.N. Israelachvili. 1994. *Biophys. J.* 66:1479–1488.
20. Leckband, D.E., J.N. Israelachvili, F.J. Schmitt, and W. Knoll. 1992. Long-range attraction and molecular rearrangements in receptor-ligand interactions. *Science* 255:1419–1992.
20. Weber, P.C., J.J. Wendoloski, M.W. Pantoliano, and F.R. Salemme. 1992. Crystallographic and thermodynamic comparison of natural and synthetic ligands bound to streptavidin. *J. Am. Chem. Soc.* 114:3197–3200.
21. Schmitt, F.-J., R. Blankenburg, L. Häußling, et al. 1992. Biological Interfaces: Specific Protein Binding to Functionalized Interfaces. In *Synthetic Microstructures in Biological Research* (Schnur, J.M., & Peckerar, M., Eds.), Plenum Press, New York.
22. Sheth, S.R. and D.E. Leckband. 1997. Measurements of attractive forces between

- end-grafted poly(ethylene glycol) chains. *Proc. Natl. Acad. Sci. U.S.A.* 94:8399–8404.
23. Ghaghadaa, K.B., J. Sauld, J.V. Natarajanb, et al. 2005. *J. Controlled Release*. 104:113–128.
 24. Gabizon, A. H. Shmeeda, A.T. Horowitz, and S. Zalipsky. 2004. *Adv. Drug Delivery Rev.* 56:1177–1192.
 25. Efremova, N.V., S.R. Sheth, and D.E. Leckband. 2001. Protein-induced changes in poly(ethylene glycol) brushes: Molecular weight and temperature dependence. *Langmuir* 17(24):7628–7636.
 26. Wieland, J.A., A.A. Gewirth, and D.E. Leckband. 2005. Single-molecule measurements of the impact of lipid phase behavior on anchor strengths. *J.Phys.Chem.B* 109(12):5985–5993.
 27. Leckband, D.E., F.-J. Schmitt, J.N. Israelachvili, and W. Knoll. 1994. Direct Force Measurements of Specific and Nonspecific Protein Interactions. *Biochem.* 1994. 33:4611–4624.
 28. Manghia, M. and M. Aubouy. 2003. Mobile polymer connectors. *Eur. Phys. J. E* 11:243–254.
 29. Moore, N.W., A.D. Delacruz, K.S. Lancaster, T. Diekmann, and T.L.Kuhl. Synthesis of a Reversible Streptavidin Binder for Biomimetic Assemblies. Submitted to *Aus.J.Chem.*
 30. Israelachvili, J. J. Thin Film Studies Using Multiple Beam Interferometry. *Colloid Interface Sci.* 1973, 44, 259–272.
 31. Israelachvili, J.N. and E. Gayle. 1978. Measurement of Forces between Two Mica Surfaces in Aqueous Electrolyte Solutions in the Range 0-100 nm. *J. Chem. Soc., Farad. Trans. 1*, 74:975–1001.
 32. Heuberger, M., G. Luengo, and J. Israelachvili. 1997. Topographic Information from Multiple Beam Interferometry in the Surface Forces Apparatus. *Langmuir.* 13:3839–3848.
 32. Moore, N.W. and T.L. Kuhl. 2006. Bimodal Polymer Brushes: Compression and Specificity towards Receptor Surfaces. *Langmuir.* 22(20):8485–8491.
 33. Jeppesen, C., J.Y. Wong, T.L. Kuhl, et al. 2001. Impact of Polymer Tether Length on Multiple Ligand-Receptor Bond Formation. *Science.* 293:465–468.
 34. Wong, J.Y., T.L. Kuhl, J.N. Israelachvili, N. Mullah, and S. Zalipsky. 1997. Direct Measurement of a Tethered Ligand-Receptor Interaction Potential. *Science* 275:820–822.
 35. Moore, N.W. and T.L. Kuhl. The Role of Flexible Tethers in Multiple Ligand-Receptor Bond Formation between Curved Surfaces. 2006. *Biophys. J.*, 91(5):1675–1687.
 36. Vinogradova, O.I. and R.G. Horn. 2001. Attractive Forces between Surfaces: What Can and Cannot Be Learned from a Jump-In Study with the Surface Forces

- Apparatus? *Langmuir* 17:1604–1607.
37. De Gennes, P. 1979. Scaling concepts in Polymer Physics. Cornell Univ. Press, Ithaca.
 38. Szleifer I. Polymers and proteins: Interactions at interfaces. 1997. *Current Opinion In Solid State & Materials Science*. 2(3):337–344.
 39. Dolan, A. and F. Edwards, F. 1974. Theory of the stabilization of colloids by adsorbed polymer. *Proc. R. Soc. London* 337:509–516.
 40. Reference deleted in proof.
 41. Halperin, A. and D.E. Leckband. 2000. From ship hulls to contact lenses: repression of protein adsorption and the puzzle of PEO. *Comptes Rendus de L'Academie des Sciences Serie IV Physique Astrophysique*. 1(9):1171–1178.
 - 41a. Bedrova, D. and G.D. Smith. 2003. The role of local conformations in the stretching of a poly(ethylene oxide) chain in solution. *J. Chem. Phys.* 118(14):6656–6663.
 42. Lim, T.-C. 2003. Spring constant analogy for estimating stiffness of a single polyethylene molecule. *J. Math. Chem.* 34(3–4):151–161.
 43. Grabbe, A. 1993. Double Layer Interactions between Silylated Silica Surfaces. *Langmuir*. 9:797–801.
 44. Israelachvili, J. N. 1992. *Intermolecular & Surface Forces*, 2e. Academic Press, San Diego.
 45. Moreira, A.G. and Marques, C.M. 2004. The role of polymer spacers in specific adhesion. *J. Chem. Phys.* 120(13): 6229–6237.
 46. Moreira, A.G., C. Jeppesen, F. Tanaka, and C.M. Marques. 2003. Irreversible vs reversible bridging: when is kinetics relevant for adhesion? *Europhys. Lett.* 62(6):876–882.
 47. Ashok, B., L. Arleth, R.P. Hjelm, I. Rubinstein, and H. Önyüksel. 2004. In Vitro Characterization of PEGylated Phospholipid Micelles for Improved Drug Solubilization: Effects of PEG Chain Length and PC Incorporation. *Pharma. Sci.* 93(10):2476–2487.
 48. Chen, T., L.R. Palmer, D.B. Fenske, A.M.I. Lam, K.F. Wong, and P.R. Cullis. 2004. Distal Cationic Poly(Ethylene Glycol) Lipid Conjugates in Large Unilamellar Vesicles Prepared by Extrusions Enhanced Liposomal Cellular Uptake. *J. Liposome Res.* 14(3&4): 155–173.
 49. Lukyanov, A.N., G. Zhonggao, L. Mazzola, and V.P. Torchilin. 2002. Polyethylene Glycol-Diacyllipid Micelles Demonstrate Increased Accumulation in Subcutaneous Tumors in Mice. *Pharm. Res.* 19(10):1424–1429.
 50. Uster a, P.S., T.M. Allen, B.E. Daniel, C.J. Mendez, M.S. Newman, and G.Z. Zhu. 1996. Insertion of poly(ethylene glycol) derivatized phospholipid into preformed liposomes results in prolonged in vivo circulation time. *FEBS Lett.* 386(2–3):243–246.
 51. Cevc, G. and D. Marsh. 1987. *Phospholipid Bilayers. Physical Principles and Models.*

John Wiley & Sons, New York, pp.19–23.

52. Holmberg, A., A. Blomstergren, O. Nord, et al. 2005. *Electrophoresis*. 26(10):501–503.
53. Evans, E. and F. Ludwig. 2000. Dynamic strengths of molecular anchoring and material cohesion in fluid biomembranes. *J. Phys.: Condens. Matter*. 12:A315–A320.
54. Allen, T.M. 1991. Liposomes containing synthetic lipid derivatives of poly(ethylene glycol) show prolonged circulation half-lives in vivo. *Biochim. et Biophysica Acta*. 1066(1):29–36.
55. Strunz, T., K. Oroszlan, I. Schumakovitch, et al. 2000. Model Energy Landscapes and the Force-Induced Dissociation of Ligand-Receptor Bonds. *Biophys. J.* 79(3):1206–1212.
56. Lo, Y.S., Y.J. Zhu, and T.P. Beebe. 2001. Loading-rate dependence of individual ligand-receptor bond-rupture forces studied by atomic force microscopy. *Langmuir* 17(12):3741–3748.
57. Zhang, X.H., and V.T. Moy. 2003. Cooperative adhesion of ligand-receptor bonds. *Biophys. Chem.* 104(1):271–278.
60. Sulchek, T. R.W. Friddle, and A. Noy. 2006. Strength of Multiple Parallel Biological Bonds. *Biophys. J.* 90(12): 4686–4691.
61. Zhang, X.H., D.F. Bogorin, and V.T. Moy. 2004. Molecular basis of the dynamic strength of the sialyl Lewis X-selectin interaction. *Chem. Phys. Chem.* 5(2):175–182.
62. Shao, J.Y. and R.M. Hochmuth. 1999. Mechanical Anchoring Strength of L-Selectin, b2 Integrins, and CD45 to Neutrophil Cytoskeleton and Membrane. *Biophys. J.* 77:587–596.
63. Evans, E., A. Leung, D. Hammer, and S. Simon. 2001. Chemically distinct transition states govern rapid dissociation of single L-selectin bonds under force. *Proc. Natl. Acad. Sci. U.S.A.* 98(7):3784–3789.
64. Fritz, J., A.G. Katopodis, F. Kolbinger, and D. Anselmetti. 1998. Force-mediated kinetics of single P-selectin/ligand complexes observed by atomic force microscopy. *Proc. Natl. Acad. Sci. U.S.A.* 95:12283–12288.
- 64a. Chilkoti, A., T. Boland, B.D. Ratner, and P.S. Stayton. 1995. The relationship between ligand-binding thermodynamics and protein-ligand interaction forces measured by atomic force microscopy. *Biophys. J.* 69:2125–2130.
- 64b. Dammer, U., M. Hegner, D. Anselmetti, et al. 1996. Specific antigen/antibody interactions measured by force microscopy. *Biophys. J.* 70:2437–2441.
- 64c. Lee, G.U., D.A. Kidwell, and R.J. Colton. 1994. Sensing discrete streptavidin-biotin interactions with atomic force microscopy. *Langmuir* 10:354–357.
- 64d. Lo, Y.-S., N. D. Huefner, W. S. Chan, F. Stevens, et al. 1999. Specific interactions between biotin and avidin studied by atomic force microscopy using the Poisson statistical analysis method. *Langmuir*. 15:1373–1382.
- 64e. Ludwig, M., W. Dettmann, and H. E. Gaub. 1997. Atomic force microscope imaging

- contrast based on molecular recognition. *Biophys. J.* 72:445–448.
- 64f. Moy, V.T., E.-L. Florin, E.-L. and H.E. Gaub. 1994. Intermolecular forces and energies between ligands and receptors. *Science* 266:257–259.
- 64h. Takeuchi O, Miyakoshi T, Taninaka A, et al. Dynamic-force spectroscopy measurement with precise force control using atomic-force microscopy probe. *J. Applied Phys.* 100(7): Art. No. 074315.
- 64i. Wong, S.S., E. Joselevich, A.T. Woolley, et al. 1998. Covalently functionalized nanotubes as nanometre-sized probes in chemistry and biology. *Nature.* 394:52–55.
65. Leckband, D.E., T.L. Kuhl, H.K. Wang, et al. 1995. 4-4-20-Anti-Fluorescyl IGG Fab' Recognition of Membrane-Bound Hapten — Direct Evidence For The Role of Protein and Interfacial Structure. *Biochem.* 34(36):11467–11478.
66. Leckband, D.E., T.L. Kuhl, H.K. Wang, et al. 2000. Force probe measurements of antibody-antigen interactions. *Methods* 20(3):329–340.
67. Ros, R., F. Schwesinger, D. Anselmetti, et al. 1998. Antigen binding forces of individually addressed single-chain Fv antibody molecules. *Proc. Natl. Acad. Sci. U.S.A.* 95:7402–7405.
- 67a. Schwesinger, F., R. Ros, T. Strunz, D. Anselmetti, H.-J. Güntherodt, A. Honegger, L. Jermutus, L. Tiefenauer, and A. Plückthun. 2000. Unbinding forces of single antibody-antigen complexes correlate with their thermal dissociation rates. *Proc. Natl. Acad. Sci. USA.* 97(18):9972–9977.
- 67b. Stuart, J.K., Hlady, V., 1995. Effects of discrete protein±surface interactions in scanning force microscopy adhesion force measurements. *Langmuir.* 11, 1368–1374.
68. Wieland, J.A., A.A. Gewirth, and D.E. Leckband. 2005. Single Molecule Adhesion Measurements Reveal Two Homophilic Neural Cell Adhesion Molecule Bonds with Mechanically Distinct Properties. *J.Biol.Chem.* 280(49):41037–41046.
- 68a. Allen, S., X. Chen, J. Davies, et al. 1997. Detection of antigen-antibody binding events with the atomic force microscope. *Biochem.* 36:7457–7463.
- 68b. Nymalm, Y. Z. Kravchuk, T. Salminen, et al. 2002. Antiferritin VL homodimer binds human spleen ferritin with high specificity. *J. Struct. Biol.* 138:171–186.
- 68c. Fritz, J., A.G. Katopodis, F. Kolbinger, et al. 1998. Force-mediated kinetics of single P-selectin ligand complexes observed by atomic force microscopy. *Proc. Natl. Acad. Sci. USA.* 95(21):12283–12288.
- 68d. Hinterdorfer, P., W. Baumgartner, H.J. Gruber, et al. 1996. Detection and localization of individual antibody-antigen recognition events by atomic force microscopy. *Proc. Natl. Acad. Sci. USA.* 93:3477–3481.
69. Ratto, T.V., R.E. Rudd, K.C. Langry, et al. 2006. Nonlinearly additive forces in multivalent ligand binding to a single protein revealed with force spectroscopy. *Langmuir* 22(4):1749–1757.
70. Ratto, T.V., K.C. Langry, R.E. Rudd, et al. 2004. Force spectroscopy of the double-tethered concanavalin-A mannose bond. *Biophys. J.* 86(4):2430–2437.

70. Sletmoen M., G. Skjak-Braek, and B.T. Stokke. 2004. Single-molecular pair unbinding studies of mannuronan C-5 epimerase AlgeE4 and its polymer substrate, *Biomacromolecules*. 5(4):1288–1295.
71. Neuert, G., C. Albrecht, E. Pamir, et al. 2006. Dynamic force spectroscopy of the digoxigenin-antibody complex, *FEBS Ltrrs*. 580(2):505–509.
- 71a. Moy, V.T., E.-L. Florin, H.E. Gaub, 1994. Adhesive forces between ligand and receptor measured by AFM. *Colloid Surf. A*. 93:343–348.
- 71b. Willemsen, O.H., M.M.E. Snel, K.O. van der Werf, et al. 1998. Simultaneous height and adhesion imaging of antibody-antigen interactions by atomic force microscopy. *Biophys. J.* 75(5):2220–2228.
- 71c. Dammer, U., O. Popescu, P. Wagner, et al. 1995. Binding strength between cell-adhesion proteoglycans measured by atomic-force microscopy. *Science* 267(5201):1173–1175.
- 71d. Yip, C.M., C.C. Yip, and M.D. Ward. 1998. Direct force measurements of insulin monomer-monomer interactions. *Biochem.* 37(16):5439–5449.
- 71e. Vinckier, A., P. Gervasoni, F. Zaugg, et al. 1998. Atomic force microscopy detects changes in the interaction forces between GroEL and substrate proteins. *Biophys.J.* 74(6):3256–3263.
- 71f. Mueller, H., H.J. Butt, and E. Bamberg. 1999. Force measurements on myelin basic protein adsorbed to mica and lipid bilayer surfaces done with the atomic force microscope. *Biophys. J.* 76(2):1072–1079.
- 71g. Boland, T. and B.D. Ratner. 1995. Direct measurement of hydrogen bonding in DNA nucleotide bases by atomic force microscopy. *Proc. Natl. Acad. Sci. USA* 92:5297–5301.
- 71h. Cluzel, P., A. Lebrun, C. Heller, et al. 1996. DNA: an extensible molecule. *Science* 271:792–794.
- 71i. Lee, G.U., L.A. Chrisey, and R.J. Colton. 1994. Direct measurement of the forces between complementary strands of DNA. *Science* 266:771–773.
- 71j. Noy, A., D.V. Vezenov, J.F. Kayyem, et al. 1997. Stretching and breaking duplex DNA by chemical force microscopy. *Chem. Biol.* 4:519–527.
- 71k. Smith, S.B., Y. Cui, and C. Bustamante. 1996. Overstretching B-DNA: the elastic response of individual double-stranded and single-stranded DNA molecules. *Science*. 271:795–799.
72. Wang, R., X. Fang, Y. Lu, and S. Wang. 2004. The PDBbind Database: Collection of Binding Affinities for Protein-Ligand Complexes with Known Three-Dimensional Structures. *J. Med. Chem.* 47, 2977–2980.
72. Wang, R., X. Fang, Y. Lu, C.-Y. Yang, and S. Wang. 2005. The PDBbind Database: Methodologies and Updates. *J. Med. Chem.* 48:4111–4119.
74. Grünewald, T. and C.A. Helm. 1996. Computer-Controlled Experiments in the Surface Forces Apparatus with a CCD-Spectrograph. *Langmuir*. 12:3885–3890.

75. Stewart, A.M. 1995. Measuring the Radii of Curvature of the Surfaces in a Surface Force Apparatus. *J.Am.Chem.Soc.* 117:287–289.
76. Heuberger, M. 2001. The extended surface forces apparatus. Part I. Fast spectral correlation interferometry. *Rev. Sci. Instrum.* 72(3):1700–1707.
77. Zäch, M. and M. Heuberger. 2000. Statistical and Systematic Errors of the Surface Forces Apparatus. *Langmuir.* 16:7309–7314.
78. Derjaguin, B.V. 1934. Friction and adhesion. IV. The theory of adhesion of small particles. *Kolloid Zeits.* 69:155–164.
79. Abramowitz, M. and I. Stegun. 1972. Handbook of Mathematical Functions. Dover.

Chapter 4: Synthesis of a Reversible Streptavidin Binder for Biomimetic Assemblies

Submitted to the Australian Journal of Chemistry, August 30, 2006, under the same title, with authors (in order): Nathan W. Moore, Anthony R.C. Delacruz, Katherine S. Lancaster, Thorsten Dieckmann, and Tonya L. Kuhl.

4.1 Abstract

The biotin/streptavidin ligand/receptor pair is used extensively in biotechnology. However, less is known about HABA, (2-(4-hydroxyphenylazo) benzoic acid), which binds to streptavidin with a bond energy and dissociation constant that more closely mimics antibody/antigen interactions. In this work we demonstrate some of HABA's useful properties that may make it a good substitute for biotin in a broad range of biochemical research. Specifically, we investigate its ease of conjugation to an anchoring pegylated lipid, characterization with MALDI, NMR, and VIS spectroscopies, and incorporation into lipid vesicles and membranes.

4.2 Introduction

Biotin and the proteins avidin or streptavidin are used extensively as biomimetic ligand/receptor pairs in research whose applications include drug targeting, membrane adhesion, and biomimetic nanoassembly.^[1-9] Their bond strength is relatively insensitive to pH and the protein receptor can be readily incorporated onto vesicles, supported bilayers, and other surfaces.^[10,11] However, the dissociation energy between biotin and avidin is $35 k_B T$ —the strongest biological noncovalent interaction known, with a remarkable dissociation constant of 10^{-15} M.^[12] In contrast, a recent survey found that a typical bond dissociation energy is of the order of $10-20 k_B T$ for antigen/antibody and

other ligand/receptor interactions more commonly occurring phenotypically, including those used in drug targeting.^[13] This survey included 2,276 biological ligand-receptor complexes listed in the PDBbind database v.2004 (Wang et al. 2004, Wang et al. 2005), for which the average bond energy was estimated as $14.7 k_B T$ (monomodal with standard deviation $4.9 k_B T$), corresponding to a dissociation constant of 4.1×10^{-7} M (Moore and Kuhl 2006). Thus, to make full use of streptavidin's robust physical and chemical properties, what is needed is a ligand that complexes streptavidin with a bond energy that is comparable to those encountered phenotypically.

2-(4-hydroxyphenylazo) benzoic acid, or HABA 1, is one of several commercially available streptavidin ligands, including also lipoic acid, 2'imino biotin, desthiobiotin, and biotin methyl ester. All have molecular masses from 214–258 D and together cover a range of dissociation energies with streptavidin from 5–35 $k_B T$.^[10,16] Because HABA's dissociation energy with streptavidin of 9–12 $k_B T$ is typical of many biological ligand-receptor pairs, using HABA as a ligand with streptavidin in biomimetic research may more accurately model ligands encountered biologically.^[16,17] Unlike the biotin/streptavidin bond, HABA binds to streptavidin with an estimated dissociation constant of 10^{-6} M that is low enough to permit significant dissociation rates^[18]. It also binds with an energy comparable to that anchoring lipids into bilayers; thus, vesicles wielding HABA ligands may be less susceptible to destruction upon decohesion from receptor surfaces.^[18–23]

Further, HABA's optical properties may facilitate the quantification of vesicle targeting, competitive adsorption, and dissociation kinetics. Its bright orange color acts as a convenient label, with an absorbance peak at 356 nm (near UV) that shifts to 500 nm

(bluish-green) after conjugating with streptavidin.^[18,25,25] Of particular interest for drug targeting and surface functionalization are conjugations between such ligands and lipids like 1,2-distearoyl-SN-glycero-3-phosphoethanolamine (DSPE) **2** that form vesicles capable of retaining crystallized drug, and between polymers such as 2000-D poly(ethylene glycol) (or PEG) **3** that are capable of sterically stabilizing vesicles and other surfaces from nonspecific protein adsorption.^[26-28] Thus, due to the broad interest in such conjugates that is likely to increase, we demonstrate a simple route to conjugating the weakly binding streptavidin ligand **1** to PEG-DSPE **4** and its incorporation into lipid vesicles. We hope that this method will serve as a useful pattern for others researching liposomal drug delivery, membrane adhesion, biomimetic self-assembly, and other biochemical research.

4.3 Materials

Amino-poly(ethylene glycol) (2000)-1, 2-distearoyl-SN-glycero-3-phosphoethanolamine (NH₃-PEG(2000)-DSPE, MW=2788.78D) **5**, 1,2-dioleoyl-SN-glycero-3-phosphocholine (DOPC) **6**, and fluorescent 1,2-dioleoyl-SN-glycero-3-phosphoethanolamine-NBD (DOPC-NBD) **7** were purchased from Avanti Polar Lipids, Inc. (Alabaster, AL). Obtained from Fluka (Buchs, Switzerland) were 2-(4-hydroxyphenylazo) benzoic acid (HABA, MW=242.23D, >99.5%) **1**, N,N'-dicyclohexylcarbodiimide (DCC, MW=206.33D, >99%) **8**, and N-(3-Dimethylaminopropyl)-N'-ethylcarbodiimide hydrochloride (EDC, ≥97%) **9**. Pyridine (>99.9%, MW=79.1D) and ninhydrin were purchased from Sigma-Aldrich (Saint Louis, MO). Avidin (Neutravidin Protein) was from Molecular Probes (Eugene, OR). Water was obtained from a Barnstead NANOpure ultra pure water system (Dubuque, Iowa). 10mL

dialysis tubes (1000D MWCO) were purchased from Spectrum Laboratories, Inc. (Rancho Dominguez, CA). All other reagents were of analytical grade.

4.4 Synthesis of HABA-PEG-DSPE 10

With the carboxylic group on **1** and the amine on **5**, carbodiimide chemistry provides a convenient route to conjugation using initiators **8** and **9** for the organic- and aqueous-phase reactions, respectively (Fig.4-1s). The formation of an unstable intermediate (o-acylisourea) occurs when the initiator is introduced to a carboxylic group.^[29] When the nucleophile (i.e. the amine of **5**) is introduced to this intermediate, the product **10** is formed and the dicyclohexyl urea byproduct **11** precipitates. The reaction scheme for the aqueous synthesis is analogous to the organic reaction (Fig.4-1s) if **8** is replaced by the water-soluble carbodiimide **9**. Both syntheses yield products with identical structure, and the initiator forms an ureal byproduct identical to the respective initiator except with both nitrogens protonated and the central carbon oxidized.

For both the organic and aqueous syntheses, all glassware was washed with a NaOH solution, rinsed, dried *in vacuo*, rinsed in the solvent to be administered, and dried with anhydrous nitrogen (purity 99.997%). Much of the work was conducted in a Class 100 laminar flow hood to maintain purity and cleanliness.

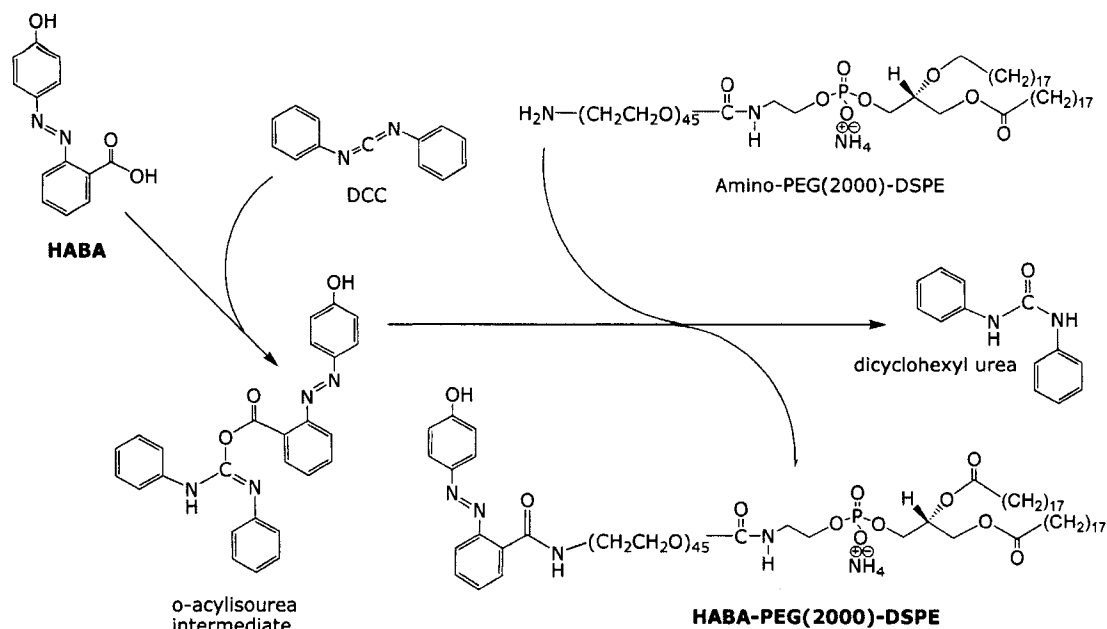


Figure 4-1s. Reaction mechanism and pathways used for the organic phase synthesis.

4.4.1 Organic-phase synthesis

For the organic-phase synthesis, 60 mg (22 μmol) of **5** was added to a 2-mL tapered vial and dissolved in 307 μL pyridine and 614 μL of DMSO was added. Between each addition of organic solvent the vial was sonicated for 10 min. The mixture was then agitated via micro-magnetic stirring rod, dosed with 9.08 mg (37 μmol) of **1**, and sonicated again for 10 min. **1** has a solubility in DMSO ≥ 0.2 M and is bright orange. 19.98 mg (97 μmol) of **8** was then added to initiate the reaction. Thus, at the start of the reaction the mixture contained 0.024 M of **5**, 0.041 M of **1**, and 0.107 M **8**. The mixture was rapidly agitated for 4 hours at 22°C. After about 2 h into the reaction the solution was appreciably darkened to orange-brown, presumably due to formation of water and the insoluble byproduct **11**.^[30] To quench the reaction, the solution was placed in a vacuum oven at 35°C for 30 min to remove the bulk of the pyridine. 6 mL of water was

added and **10** was removed by centrifugation. The solution was then dialyzed (1000D MWCO) in water for 40 h. The solution was again centrifuged to remove potential traces of insoluble byproduct or other trace contaminants prior to lyophilization into a dry, orange powder.

4.4.2 Aqueous-phase synthesis

For the aqueous-phase synthesis, 25 mg (9 μmol) of **5** was agitated in 1.4 mL of water with a micro-magnetic stirring rod for 10 min. 26.04 mg (108 μmol) of **1** was then added and sonicated for 10 min. To this mixture, 108 μL of 1 M NaOH was added to fully dissolve **1**. Sodium phosphate buffer (644 μL , pH 6, 1 M) was added to favor deprotonation of the amine terminus of **5**. The mixture was sonicated for 10 min prior to adding 19.2 μL (108 μmol) of **9** to start the reaction. Thus, at the start of the reaction the mixture contained 0.017 M of **5**, 0.05 M of **1**, and 0.05 M of **9**. The mixture was rapidly agitated for 12 hours at 22°C. The solution darkened with time but did not yield precipitate upon the addition of the 3.85 mL of H₂O to dilute the mixture and quench the reaction. The supernatant was dialyzed for 30 h to remove unreacted reagents and then lyophilized.

4.5 Characterization

4.5.1 MALDI

Product masses were characterized using Matrix Assisted Laser Desorption / Ionization (MALDI), performed on an IonSpec (Lake Forest, CA) Fourier transform mass spectrometer instrument equipped with an external multisample plate source and an actively shielded 7 T magnet. One μL of sample was spotted on a stainless steel probe

followed by 1 μL of matrix. The matrix used was 0.1 M 2,5-dihydroxybenzoic acid (DHB) (Sigma). The sample was air dried at room temperature and then ionized with a Nd:YAG laser ($\lambda = 226 \text{ nm}$). As a further test for the presence of unreacted **5** (viz., the presence of unreacted amines), ninhydrin (2M in ethanol) was applied to a TLC sheet treated with the conjugate solution and allowed to dry.

4.5.2 $^1\text{H-NMR}$

All NMR spectra were collected on Bruker DRX-600 or DRX-500 spectrometers equipped with a HCN triple resonance, triple-axis PFG probe. The 600 MHz system was outfitted with a cryogenic probe. Quadrature detection for the indirect dimensions in multidimensional experiments was achieved using the States-TPPI method.^[31] Two-dimensional DQF-COSY was conducted at 293K using NMR samples in methanol.^[32] All spectra were processed using the XWIN-NMR 2.6 software package (Bruker Inc.) and analyzed using XEasy on a Silicon Graphics O2 workstation.^[33] ^1H chemical shifts were referenced to an external standard of DSS.

4.5.3 Absorption Spectroscopy

VIS-spectrometry was performed at $24.0 \pm 0.1^\circ\text{C}$ using a 750-mm spectrometer with a 600 line/inch diffraction grating (Acton, Acton, Massachusetts). Spectrum digitization was achieved using a CCD detector (Princeton Instruments, Trenton, New Jersey) stabilized at -70°C to achieve a $\sim 40\%$ photon efficiency. The spectrometer was controlled with WinSpec software version 2.5.16.2 (Roper Scientific, Acton, New Jersey) and our own custom software. Sample solutions held in quartz cuvettes (Fisher Scientific, Pittsburg, Pennsylvania) were illuminated by a 100W quartz-tungsten halogen lamp

reflected from a cold mirror and focused into and aligned normal to the sample by a liquid light guide (Oriel Instruments). For each wavelength, transmittance was calculated as $(1 / L) (I_{\text{sample}} - I_{\text{background}}) / (I_{\text{solvent}} - I_{\text{background}})$, where L is the cuvette thickness and I are the wavelength-dependant intensities incident on the CCD, and the subscripts sample, solvent, and background refer respectively to light transmitted through the sample solution, an identical quartz cuvette filled with the same solvent, and ambient sources.

4.5.4 Vesicle Preparation

Vesicles were prepared with a mixture of **10**, **6**, and **7** with molar ratios 86:4.5:9.5, respectively, which was solvated in chloroform, dried *in vacuo* at 40°C for 72 h and reconstituted with a 35 mM sucrose solution to a final lipid concentration of 50 μ M. A small aliquot of the vesicle solution was dispersed in a 35 mM glucose solution to aid vesicle settling and was wicked between two glass slides separated by a 2-mm spacer to minimize fluid motion during microscopy. The vesicles (9.9 nM lipids, 0.45 nM **1**) were then incubated *in situ* with an excess of avidin (5.7 nM) for 18 h at 23°C and re-imaged. Fluorescence microscopy was performed on a Nikon Measurescope MM-11 equipped with a Hg lamp, FITC HQ filter cube, 20x & 50x long working-distance objectives (Nikon USA, Florham Park, NJ), CoolSNAP-Pro cf monochrome CCD camera (Media Cybernetics, Silver Spring, MD), and Simple PCI data acquisition software (Compix Inc., Lake Oswego, OR).

4.6 Results & Discussion

The following demonstrate the formation of the new conjugate **10** via the organic-phase synthesis in Fig.4-1s.

MALDI spectra from both the organic and aqueous syntheses are shown in Fig. 4-1. For the organic synthesis (Fig. 4-1A), a peak at 3,044 D, corresponding to the expected molecular mass of the desired conjugate **10** (3,029 D), suggests its formation. However, due to fragmentation of the heat labile lipid tails during laser ionization, a more dominant peak is observed at 2,300 D, which coincides with the molecular mass of the ligand **1** conjugated to the reactant **5** less the molecular mass of the lipid **2** ($3,029 \text{ D} - 748 \text{ D} = 2,281 \text{ D}$). Some of **1** may also have been lost from fragmentation. Nonetheless, two major series of peaks sculpt a definitive bell shaped curve that reflects the polydispersity of the polymer **3**. Within each series, the spacing between adjacent peaks is 44.031D, corresponding to the mass of the polymer unit (44.054 D). The two series differ by 18.006 D, suggesting that water crystallized onto the hygroscopic **3** when the sample was cooled before ionization.

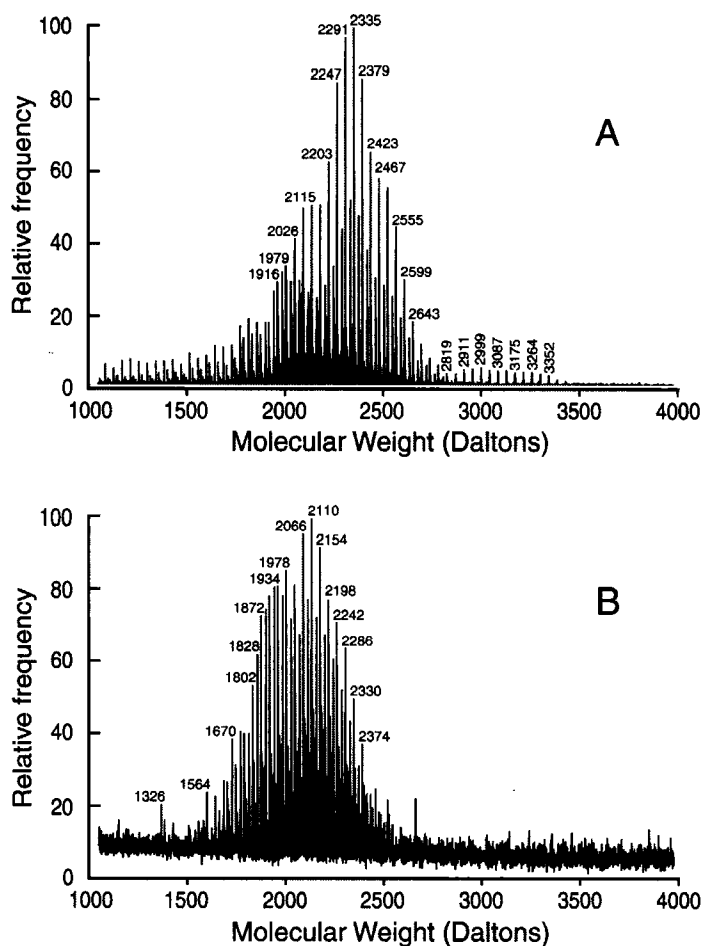


Figure 4-1. MALDI spectra of products separated from organic (A) and aqueous (B) syntheses of HABA-PEG-DSPE **11**. The interval between isotopic clusters of signals is 44 m/Z, corresponding to the polymer repeat unit. Not all peaks labeled for clarity.

In contrast, the aqueous synthesis yielded only a broad series of peaks centered on a mass of 2,044 D (Fig. 4-1B). This peak coincides with the difference in molecular masses of **5** and the lipid **2** (2,789 D – 748 D = 2,041 D), suggesting that the reactant **5** (and not the desired product **10**) was present before fragmenting into **2** and NH₂-PEG **12**. The lack of a peak near the molecular mass of **10** (3,029 D) also suggests that the aqueous synthesis did not yield a significant amount of product despite both syntheses having comparable concentrations of **5** and of the initiators **8** or **9**, and the aqueous synthesis having thrice the reaction time. Although a detailed analysis is beyond the

scope of this paper, it is likely that the *o*-acylisourea intermediate hydrolyzes rapidly compared to the diffusive timescale of the PEG-lipid, which may have had reduced collision frequency from micellization, as its CMC of 1–20 μM was comparable to the reaction conditions.^[22,23,34]

To further validate the conjugation of **1** to **5** via the organic-phase synthesis, high resolution NMR spectroscopy (2D-DQF COSY) of the reactant **5** and product **10** are shown in Figs. 4-2A and 4-2B, respectively. The spectrum of **5** shows all resonances at the expected chemical shifts.^[28] The spectra of the product **10** displays additional aromatic signals from the HABA **1** moiety between 6.8 and 8.5 ppm, as well as a new signal at 8.95 ppm. This signal has one cross peak at 3.75 ppm in the DQF-COSY spectrum and can be assigned to the NH group linking **1** and **5**, showing covalent conjugation of these two compounds.

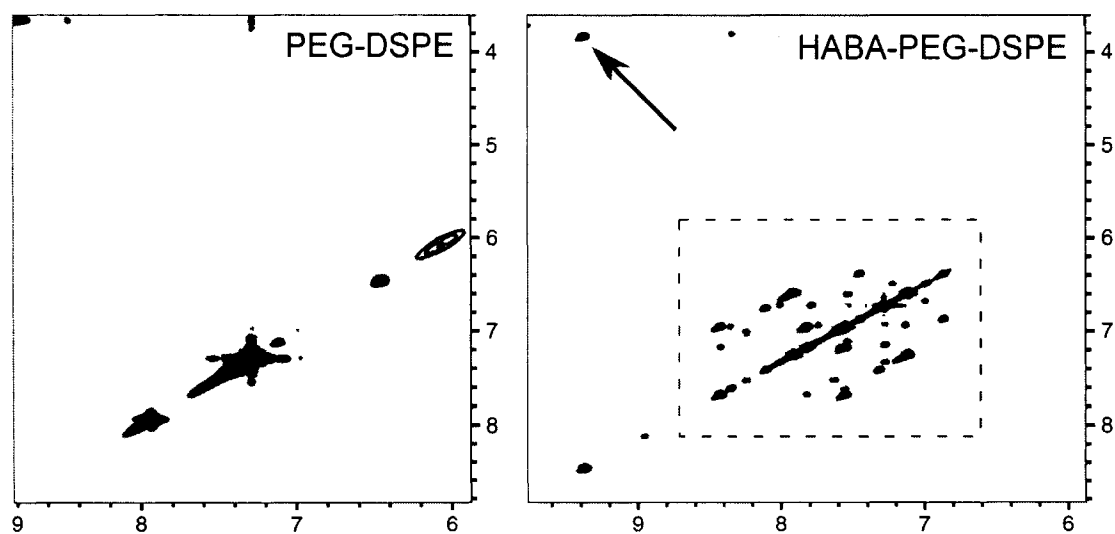


Figure 4-2. 600 MHz ^1H 2D DQF-COSY spectra of the aromatic/NH region of the reactant **5** and product **11**. All axes are ppm. The dashed box marks the signals originating from the conjugated moiety **1**. The arrow marks the cross peak between the linking amide NH and the PEG **3** protons.

The VIS transmittance of **1** dropped significantly over the range 500–650 nm, as expected from the orange appearance of **1** and its absorption frequency of 356 nm.^[18] At a wavelength of 550 nm the transmittance was 50% and the molar absorptivity was 19.5 M⁻¹ cm⁻¹. The transmittance (T) of **1** had the greatest sensitivity to its molarity (C) at a wavelength of 525 nm, which scaled as $-\log(T) = 358C + 9 \times 10^{-5}$ ($R^2=0.9994$, $0.1 < C < 1.6 \mu\text{M}$). Because neither chloroform nor aqueous solutions of the pegylated lipid **5** portion of the product were absorbing, we were able to use absorbance to calculate the product yield for the organic phase synthesis of **10** after purification to be $\geq 97 \pm 3\%$. In agreement, ninhydrin tested negative for the presence of unreactive amines of **5** in the product, indicating a substantial extent of conjugation.

As further validation, Fig. 4-3 shows vesicles prepared with the product **10** before and after the addition of an avidin linker. Before addition, vesicles were numerous and polydisperse, freely diffusing throughout the solution, as exemplified in Fig. 4-3A. However, after adding avidin ~5% of the visible vesicles adhered to another vesicle, as exemplified by the vesicles in Fig. 4-3B, which rotated and translated together. The relatively low yield of coupling is likely from the large molar excess of free avidin oversaturating the vesicle's ligands **1**. Nonetheless, Fig. 4-3 demonstrates that **10** was synthesized and shows its ability to stabilize vesicles and to cross-link them in the presence of avidin. Further, adhesion measurements with a Surface Forces Apparatus demonstrated that supported membranes incorporating **10** exhibited specificity towards complementary streptavidin membranes (to be published elsewhere). Bond formation between **1**- and streptavidin- functionalized surfaces was weaker and more easily reversible than when biotin was used in otherwise identical experiments.

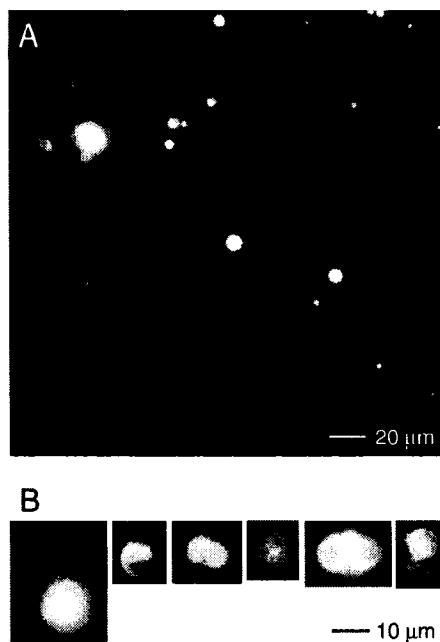


Figure 4-3. Fluorescence micrographs of vesicles functionalized with the sterically stabilizing HABA conjugate **11**. A) In the absence of the avidin linker, vesicles were non-adhering throughout the entire sample. The few vesicles that appear coincident moved independently in different focal planes and were not coupled. Larger vesicles appear flared due to limited depth of field. B) A collage of adherent vesicles after the addition of avidin. Left to right: clusters of 2, 2, 2, 3, 3, and 4 vesicles.

4.7 Conclusions

We have demonstrated the synthesis of a functionalized PEG-lipid **10** with a more biomimetic binding affinity to streptavidin than biotin. MALDI, NMR, and VIS spectroscopy cooperatively confirm that **10** was synthesized in the organic-phase reaction and purified to $\geq 97\%$. This same synthetic route may be utilized with other streptavidin-binding ligands, all of which display carboxylic groups except for biotin methyl ester. In contrast, synthesis in aqueous media proved ineffective. This new streptavidin binder, which can be easily incorporated into lipid vesicles and supported membranes and provides steric stabilization, should promote research into tethered ligand/receptor interactions that are more biomimetic than when biotin is used.

4.8 Acknowledgments

We thank Jordan Kopping, Philip J. Costanzo, and Tim E. Patten for useful discussions, Jeff de Ropp for assistance with NMR, Kaki Cheung and Dennis J. Mulder for writing the spectrometer control software, and Yanto Yanto for help making vesicles. This work was supported by NSF Grant NER DMII-0404457.

4.9 References

- [1] W.T. Phillips, R. Klipper, B. Goins, *J.Pharmacol. Exp. Ther.* **2000**, 295, 309.
- [2] V.P. Torchilin, *Nature Rev.* **2005**, 4, 145.
- [3] J.J. Lin, J.A. Silas, H. Bermudez, V.T. Milam, F.S. Bates, D.A. Hammer, *Langmuir* **2004**, 20, 5493.
- [4] D.H. Kim, A.L. Klibanov, D. Needham, *Langmuir* **2000**, 16, 2808.
- [5] J.Y. Wong, T.L. Kuhl, J.N. Israelachvili, N. Mullah, S. Zalipsky, *Science* **1997**, 275, 820.
- [6] S. Brown, *Nano Lett.* **2001**, 1(7), 391.
- [7] S. Connolly, S.N. Rao, R. Rizza, N. Zaccheroni, D. Fitzmaurice, *Coord. Chem. Rev.* **1999**, 185–186, 277.
- [8] A.L. Hiddessen, S.D. Rodgers, D.A. Weitz, D.A. Hammer, *Langmuir* **2000**, 16, 9744.
- [9] O.D. Velev, E.W. Kaler, *Langmuir* **1999**, 15(11), 3693.
- [10] A. Torreggiani, G. Fini, *Biospectroscopy* **1998**, 4(3), 197.
- [11] L. Nobs, F. Buchegger, R. Gurny, E. Allemann, *J. Pharma. Sci.* **2004**, 93(8), 1980.
- [12] A. Holmberg, A. Blomstergren, O. Nord, M. Lukacs, J. Lundeberg, M. Uhlén, *Electrophoresis* **2005**, 26, 501.
- [13] N. W. Moore, T.L. Kuhl., *Biophys.J.* **2006**, 91(5),1675.
- [14] R. Wang, X. Fang, S. Wang, *J. Med. Chem.* **2004**, 47, 2977.
- [15] R. Wang, X. Fang, Y. Lu, C.-Y. Yang, S. Wang, *J. Med. Chem.* **2005**, 48, 4111.
- [16] D. Leckband, W. Muller, F.J. Schmitt, H. Ringsdorf, *Biophys.J.* **1995**, 69, 1162.
- [17] P.C. Weber, J.J. Wendoloski, M.W. Pantoliano, F.R. Salemme, *J. Am. Chem. Soc.* **1992**, 114, 3197.
- [18] H. Hofstetter, M. Morpurgo, O. Hofstetter, E.A. Bayer, M. Wilchek, *Anal. Biochem.* **2000**, 284, 354.
- [19] S.J. Marrink, O. Berger, P. Tieleman, F. Jähnig, *Biophys.J.* **1998**, 74, 931.
- [20] P.S. Uster, T.M. Allen, B.E. Daniel, C.J. Mendez, M.S. Newman, G.Z. Zhu, *FEBS*

- Ltrs.* **1996**, 386(2–3), 243.
- [21] J.A. Wieland, A.A. Gewirth, D.E. Leckband, *J. Phys Chem B* **2005**, 109, 5985.
- [22] B. Ashok, L. Arleth, R.P. Hjelm, I. Rubenstein, H. Önyüksel, *Pharama. Sci.* **2004**, 93(10), 2476.
- [23] T. Chen, L.R. Palmer, D.B. Fenske, A.M.I. Lam, K.F. Wong, P.R. Cullis, *J. of Liposome Research* **2004**, 14(3&4), 155.
- [24] K.K.-W. Lo, W.-K. Hui, *Inorg. Chem.* **2005**, 44, 1992.
- [25] O. Livnah, E.A. Bayer, M. Wilchekb, J.L. Sussman, *FEBS* **1993**, 328(1,2), 165.
- [26] O. Garbuzenko, Y. Barenholz, A. Priev, *Chem. Phys. Lipids* **2005**, 135, 117.
- [27] S. Zalipsky, *Bioconj. Chem.* **1993**, 4, 296.
- [28] S. Zalipsky in *Stealth Liposomes* (Eds. D. Lasic, F. Martin) **1995**, Ch.9, pp.93–102 (CRC Press: Boca Raton).
- [29] G.T. Hermanson, *Bioconjugate Techniques* **1996**, pp. 170–180 (Academic Press: San Diego).
- [30] L. Yet, *Albany Molecular Research, Technical Reports* **1999**, 4(1), 1.
- [31] D. Marion, M. Ikura, A. Bax, *J. Magn. Reson.* **1989**, 84, 425.
- [32] U. Piantini, O.W. Sørensen, R.R. Ernst, *J. Am. Chem. Soc.* **1982**, 104, 6800.
- [33] C. Bartels, T.H. Xia, M. Billeter, P. Guntert, K. Wuthrich, *J. Biomol. NMR* **1995**, 6, 1.
- [34] A. Priev, S. Zalipsky, R. Cohen, Y. Barenholz, *Langmuir* **2002**, 18, 612.